



Fluids and Combustion Facility: Fluids Integrated Rack Modal Model Correlation

Mark E. McNelis and Vicente J. Suarez
Glenn Research Center, Cleveland, Ohio

Timothy L. Sullivan, Kim D. Otten, and James C. Akers
Analex Corporation, Brook Park, Ohio

The NASA STI Program Office . . . in Profile

Since its founding, NASA has been dedicated to the advancement of aeronautics and space science. The NASA Scientific and Technical Information (STI) Program Office plays a key part in helping NASA maintain this important role.

The NASA STI Program Office is operated by Langley Research Center, the Lead Center for NASA's scientific and technical information. The NASA STI Program Office provides access to the NASA STI Database, the largest collection of aeronautical and space science STI in the world. The Program Office is also NASA's institutional mechanism for disseminating the results of its research and development activities. These results are published by NASA in the NASA STI Report Series, which includes the following report types:

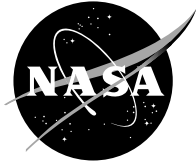
- TECHNICAL PUBLICATION. Reports of completed research or a major significant phase of research that present the results of NASA programs and include extensive data or theoretical analysis. Includes compilations of significant scientific and technical data and information deemed to be of continuing reference value. NASA's counterpart of peer-reviewed formal professional papers but has less stringent limitations on manuscript length and extent of graphic presentations.
- TECHNICAL MEMORANDUM. Scientific and technical findings that are preliminary or of specialized interest, e.g., quick release reports, working papers, and bibliographies that contain minimal annotation. Does not contain extensive analysis.
- CONTRACTOR REPORT. Scientific and technical findings by NASA-sponsored contractors and grantees.

- CONFERENCE PUBLICATION. Collected papers from scientific and technical conferences, symposia, seminars, or other meetings sponsored or cosponsored by NASA.
- SPECIAL PUBLICATION. Scientific, technical, or historical information from NASA programs, projects, and missions, often concerned with subjects having substantial public interest.
- TECHNICAL TRANSLATION. English-language translations of foreign scientific and technical material pertinent to NASA's mission.

Specialized services that complement the STI Program Office's diverse offerings include creating custom thesauri, building customized databases, organizing and publishing research results . . . even providing videos.

For more information about the NASA STI Program Office, see the following:

- Access the NASA STI Program Home Page at <http://www.sti.nasa.gov>
- E-mail your question via the Internet to help@sti.nasa.gov
- Fax your question to the NASA Access Help Desk at 301-621-0134
- Telephone the NASA Access Help Desk at 301-621-0390
- Write to:
NASA Access Help Desk
NASA Center for AeroSpace Information
7121 Standard Drive
Hanover, MD 21076



Fluids and Combustion Facility: Fluids Integrated Rack Modal Model Correlation

Mark E. McNelis and Vicente J. Suarez
Glenn Research Center, Cleveland, Ohio

Timothy L. Sullivan, Kim D. Otten, and James C. Akers
Analex Corporation, Brook Park, Ohio

National Aeronautics and
Space Administration

Glenn Research Center

Trade names or manufacturers' names are used in this report for identification only. This usage does not constitute an official endorsement, either expressed or implied, by the National Aeronautics and Space Administration.

Available from

NASA Center for Aerospace Information
7121 Standard Drive
Hanover, MD 21076

National Technical Information Service
5285 Port Royal Road
Springfield, VA 22100

Available electronically at <http://gltrs.grc.nasa.gov>

TABLE OF CONTENTS

1. Introduction	1
1.1 Background	1
1.2 Purpose of CIR Model Correlation	3
1.3 Applicable Documents	4
2. Model Correlation.....	4
2.1 Requirements.....	4
2.2 Model Correlation Methodology	5
3. Test Hardware Configuration	6
3.1 Hardware Mass and CG Summary	7
3.2 Rack Hardware Modifications	8
3.3 Mass Simulators	11
3.4 Active Rack Isolation System (ARIS)	11
4. FEM Model Description	12
4.1 Rack Coordinate System	13
4.2 Rack Modal Test Fixture	13
4.3 FEM Mass and CG Properties	15
5. Pre-Test Analysis	16
6. Test Results.....	24
7. Model Correlation.....	33
8. Conclusions.....	42
9. References.....	42
10. Acronym List	43
11. Appendices.....	44
Appendix A FIR Optics Bench with FSAP	45
Appendix B Air Thermal Control Unit (ATCU)	53
Appendix C Rack Door	61
Appendix D Lower Structure Assembly	69
Appendix E FIR Rack Modal Instrumentation Plan	77
Appendix F FIR Rack Correlated Model Comparison of Frequency and Cross-Orthogonality	91

1. Introduction

1.1 Background

The Fluids and Combustion Facility (FCF – Figure 1) is a modular, multi-user, two-rack facility dedicated to combustion and fluids science in the US Laboratory Destiny on the International Space Station. FCF is a permanent facility that is capable of accommodating up to ten combustion and fluid science investigations per year. FCF research in combustion and fluid science supports NASA's Exploration of Space Initiative for on-orbit fire suppression, fire safety, and space system fluids management.

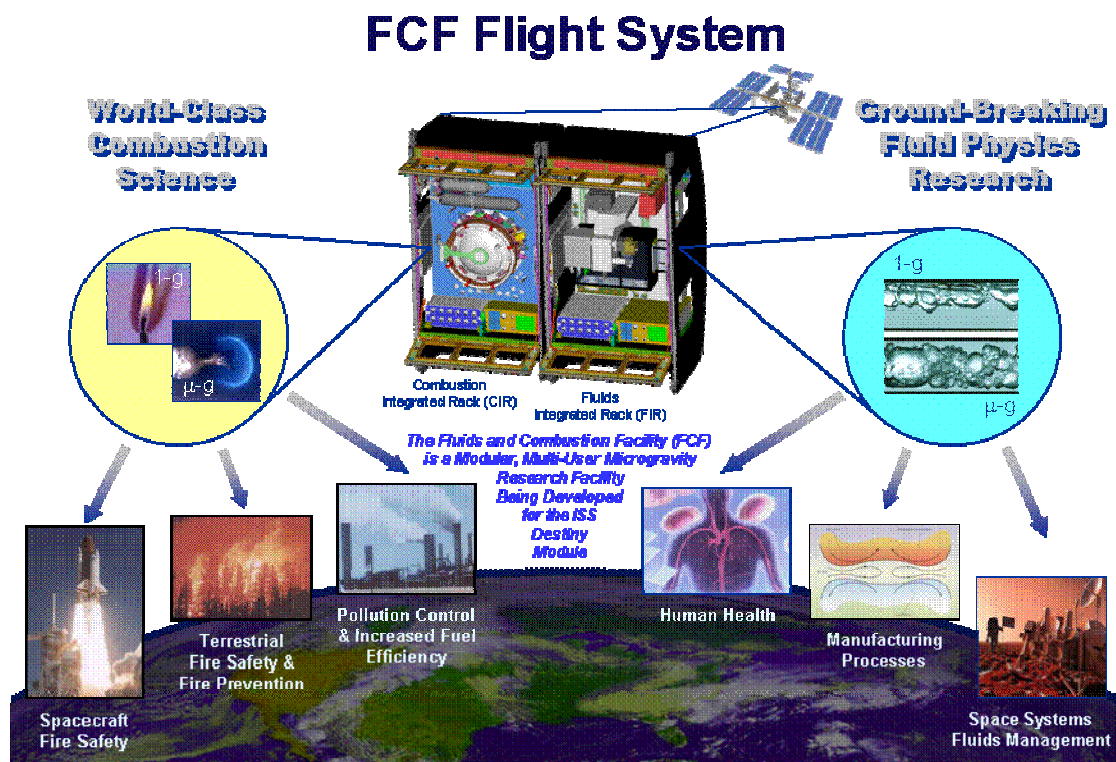


FIGURE 1 – FLUIDS AND COMBUSTION FACILITY

The Fluids Integrated Rack (FIR) is one of two racks in the FCF. The FIR major structural elements (Figure 2) include the International Standard Payload Rack (ISPR), Experiment Assembly (optics bench and combustion chamber), Air Thermal Control Unit (ATCU), Rack Door, Lower Structure Assembly (Input/Output Processor and Electrical Power Control Unit) and Active Rack Isolation System (ARIS). The load path through the rack structure is outlined in Figure 3.

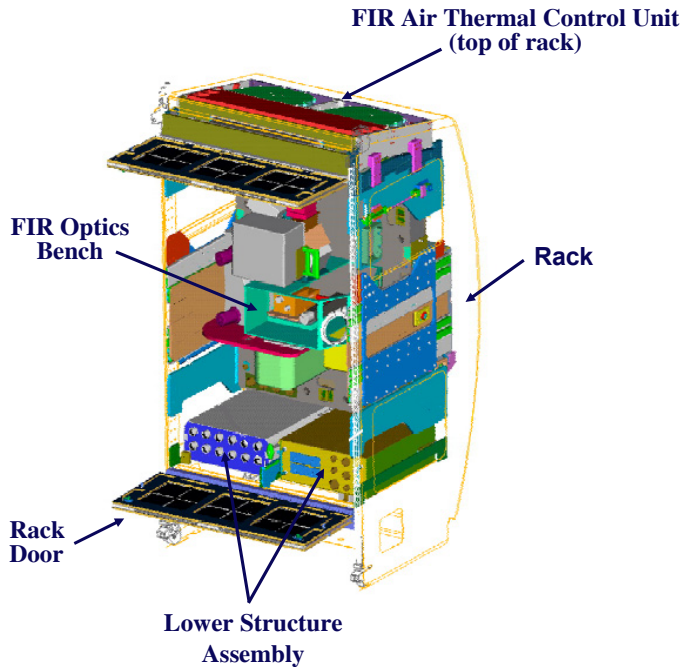


FIGURE 2 – FLUIDS INTEGRATED RACK (FIR)

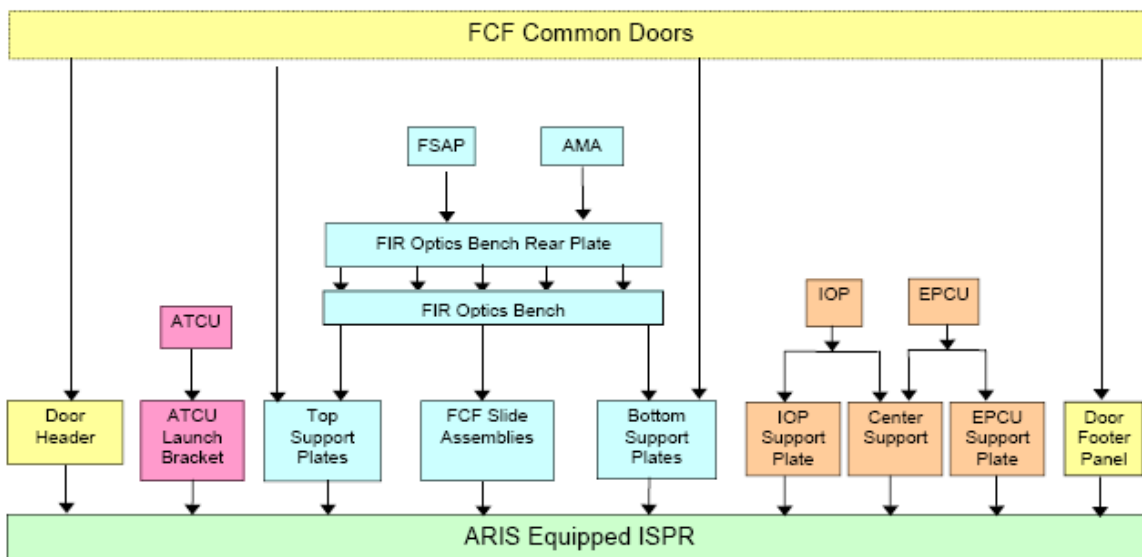


FIGURE 3 – LOAD PATH DIAGRAM

1.2 Purpose of FIR Model Correlation

The FIR modal survey was conducted to validate the load path predicted by the FIR finite element model (FEM). The rack FEM was provided by Boeing - Houston; the FIR package FEMs and analytical integration into the rack was performed by ZIN Technologies. The modal survey is done by experimentally measuring the FIR frequencies and mode shapes. The FIR model was test correlated by updating the model to represent the test mode shapes. The correlated FIR model delivery is required by NASA JSC at Launch-10.5 months.

The test correlated FIR flight FEM is analytically integrated into the Shuttle for a coupled loads analysis of the launch configuration. The analysis frequency range of interest is 0-50 Hz.

A coupled loads analysis is the analytical integration of the Shuttle with its cargo element, the Multi-Purpose Logistics Module (MPLM), in the Shuttle cargo bay (Figure 4). For each Shuttle launch configuration, a verification coupled loads analysis is performed to determine the loads in the cargo bay as part of the structural certification process (Figure 5).

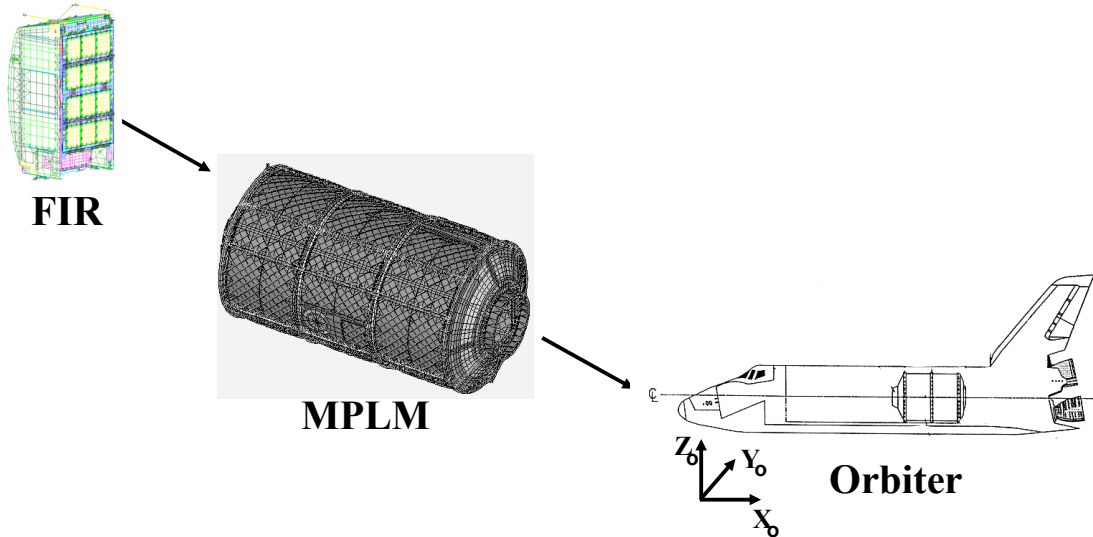


FIGURE 4 – ANALYTICAL INTEGRATION PROCESS FOR COUPLED LOADS ANALYSIS

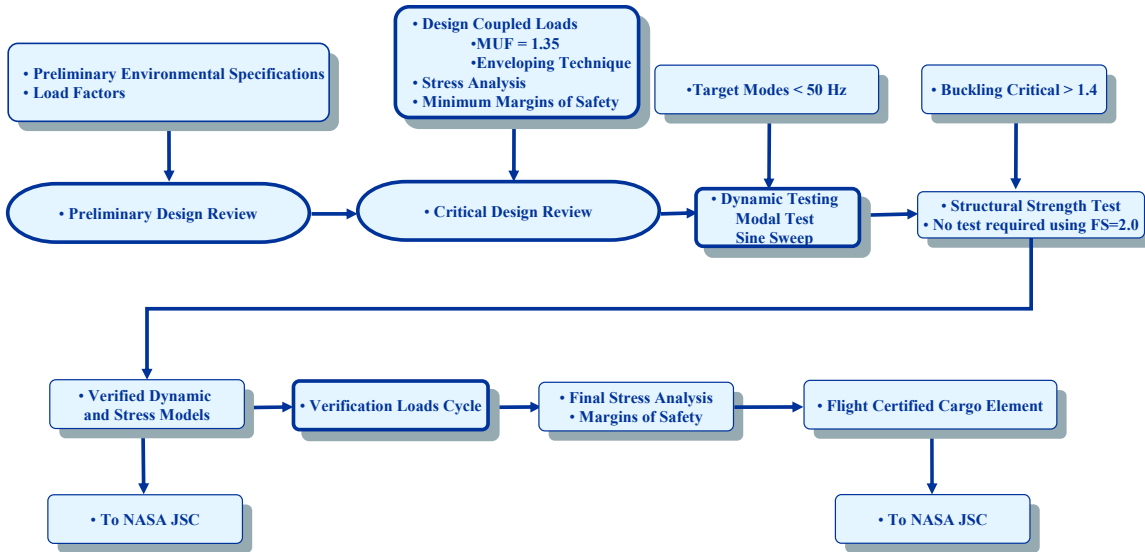


FIGURE 5 – STRUCTURAL CERTIFICATION PROCESS

1.3 Applicable Documents

1. "Payload Verification Requirements," NSTS 14046, Revision E, May 2000.
2. "Rack to Mini Pressurized Logistics Module Interface Control Document," SSP 41017, Part 1, Revision F, May 18, 2001.
3. "Rack to Mini Pressurized Logistics Module Interface Control Document," SSP 41017, Part 2, Revision H, May 18, 2001.
4. "Payload Flight Equipment Requirements and Guidelines for Safety-Critical Structures," SSP 52005, Revision C, Section 7.1 Verification Requirements for Dynamic Structural Models, December 18, 2002.
5. "International Standard Payload Rack (ISPR) Structural Integrator's Handbook," SSP 57007, Revision A, October 31, 2001.

2. Model Correlation

2.1 Requirements

The math model verification requirements for FCF racks are defined in NSTS 14046 and SSP 52005 (see 1.3 Applicable Documents). SSP 52005, Section 7.1 defines that evidence for model correlation is provided through test based frequency and mode shape characterization. The correlation goal for each fundamental frequency is a frequency difference between model and test of less than +/- 5%. For higher order frequencies, the correlation goal is a frequency difference of less than +/- 10%.

Cross-orthogonality between the analytical and test mode shapes is evaluated based on the following calculation:

$$[\emptyset]_A^T [M]_A [\emptyset]_T = [C_{ij}]$$

Where:

$[\emptyset]_A^T$ is the transpose of the analytical mode shape matrix

$[M]_A$ is the analytical consistent mass matrix (as defined in NASTRAN manuals)

$[\emptyset]_T$ is the test mode shape matrix

$[C_{ij}]$ is the correlation matrix.

The correlation goal for the diagonal values of the correlation matrix, $[C_{ij}]$, is a value greater than 0.9 for significant modes. For the off-diagonal terms, the correlation goal is a value of less than 0.1.

2.2 Model Correlation Methodology

The FIR model correlation methodology was based on modal testing and correlating each major structural assembly individually (Reference 1). This building block approach facilitates the model correlation process for the FIR. Previous testing by Boeing correlated the rack model in a configuration with various mass weighted horizontal shelves in the rack (Reference 2). The FCF rack structural configuration was different than the Boeing correlated rack configurations as the FCF racks have a vertical plate (optics bench) instead of horizontal shelves, creating a different load path in the rack. The final step in the correlation process was to modal test and model correlate the FIR.

Model correlation for the major structural assemblies is summarized in the following appendices:

Appendix A – FIR Optics Bench

Appendix B – FIR ATCU

Appendix C – Rack Door

Appendix D – Lower Structure Assembly

The Lower Structure Assembly model was not correlated as the test measured fundamental frequencies were greater than 100 Hz, outside the model correlation frequency range of interest (0-50 Hz).

3. Test Hardware Configuration

FIR Ground Integration Unit (GIU) hardware was used for the FIR test configuration (Figure 6). The overall dimensions of the rack are given in Figure 7. The test rack was a modified 6-post International Standard Payload Rack (ISPR) made of carbon fiber composite material similar to the flight rack. The rack was supplied by Boeing. The FIR GIU hardware is a structural flight duplicate which will be used as an astronaut trainer and for troubleshooting on-orbit facility problems. The FIR test configuration did not include any wiring or harnessing, however, it did include the environmental control system plumbing. The Active Rack Isolation System (ARIS) was represented by a coldplate, hardback, and mass simulators for the major ARIS masses.



FIGURE 6 – FLUIDS INTEGRATED RACK TEST CONFIGURATION

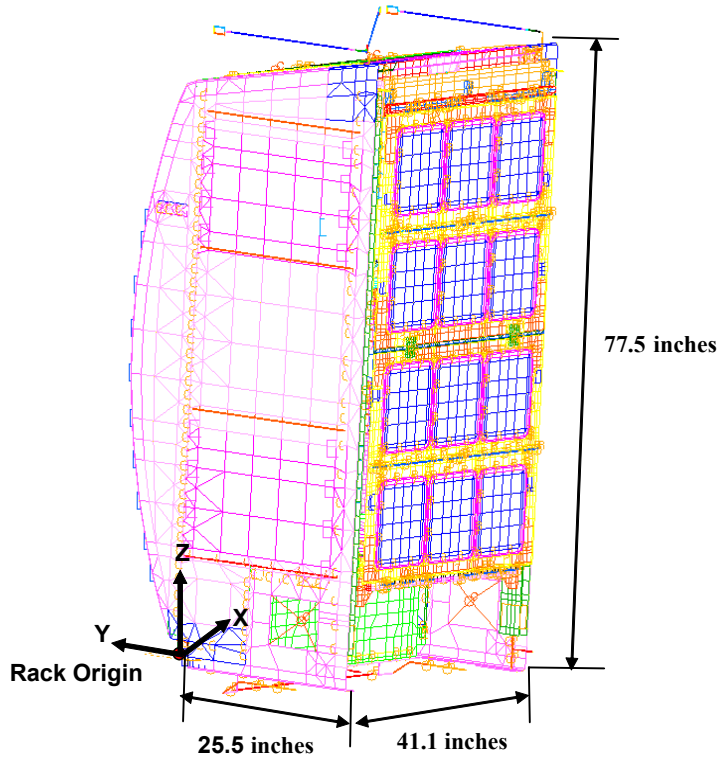


FIGURE 7 – RACK COORDINATE SYSTEM AND OVERALL DIMENSIONS

3.1 Hardware Mass and CG Summary

The FIR test hardware weighs 1390.92 lbs and the FIR flight hardware configuration weighs 1471.03 lbs (Reference 3). The mass difference is 80.11 lbs, representing a difference of 5.4%. A mass and CG summary of the test and flight rack hardware configurations are given in Table 1. The main difference between the test and flight hardware configurations is the test rack does not have wiring or harnessing. The CG properties between the FIR test and flight hardware are very comparable, as seen in Table 1.

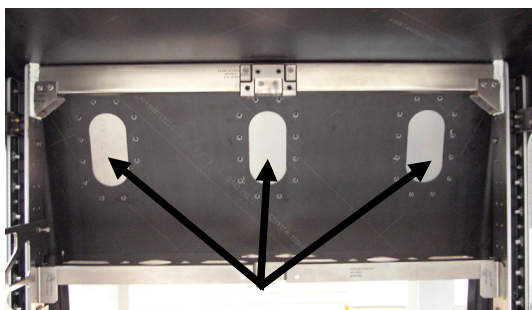
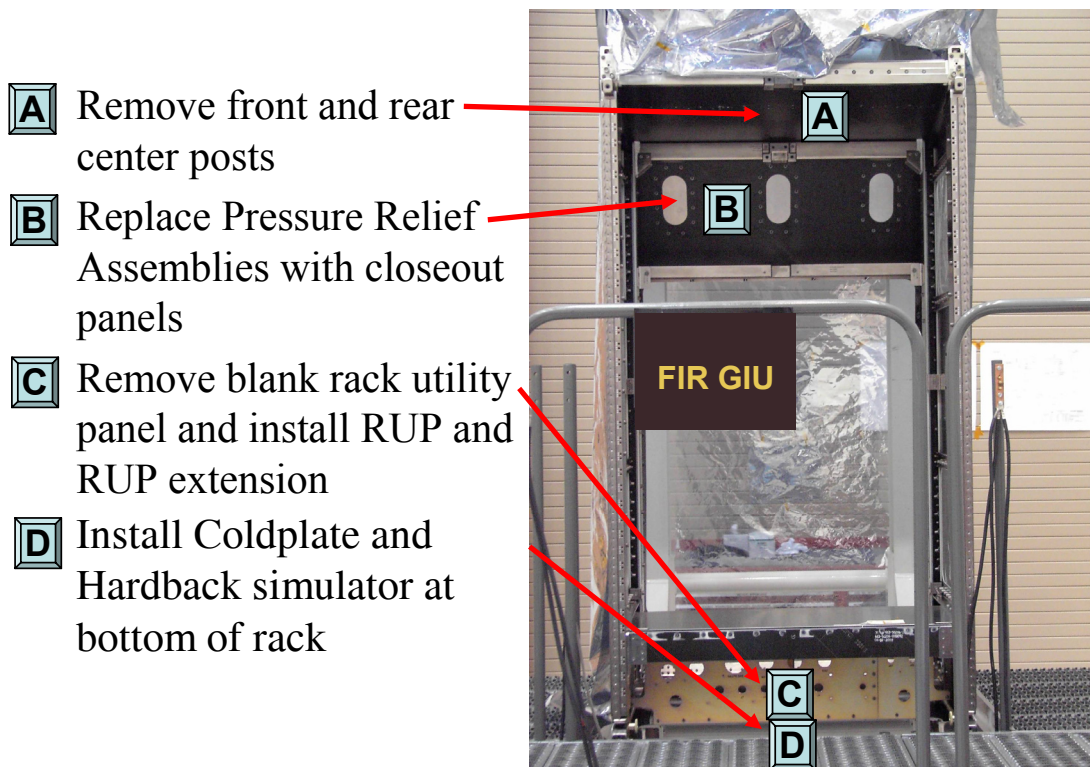
Table 1 – FIR Hardware Mass and CG Summary

Subsystems	Weight (lbf)	CG _x (in)	CG _y (in)	CG _z (in)
ATCU	124.68	19.9	-12.9	69.2
Experiment Assembly	563.15	18.9	-8.3	41.2
Door	92.22	19.8	-27.9	43.7
Rack	305.76	19.3	-8.7	25.5
Lower Structure Assembly (Mass Simulator)	206.49	17.5	-12.6	15.1
Tested FIR GIU	1390.92	18.9	-10.9	36.2
FIR Flight	1471.03	18.6	-10.4	35.2

3.2 Rack Hardware Modifications

Test rack hardware modifications were made to reflect the flight rack structural changes. The modifications include removal of the rack center posts, replacement of pressure relief valve assemblies with closeout panels, installation of coldplate and hardback simulator at bottom of the rack, and removal of a blank Rack Utility Panel (RUP) and installation of a flight-like RUP and RUP extension. The rack modifications are shown in Figure 8.

Structural attachment modifications were made to incorporate FCF hardware in the rack. The Lower Structure Assembly is attached to the rack using modified center-post attachment hardware at the bottom of the rack (Figure 9).



B Pressure Relief closeout panels



C RUP and RUP extension



D Hardback mass simulator
(looking down at bottom of rack)

FIGURE 8 – RACK HARDWARE MODIFICATIONS

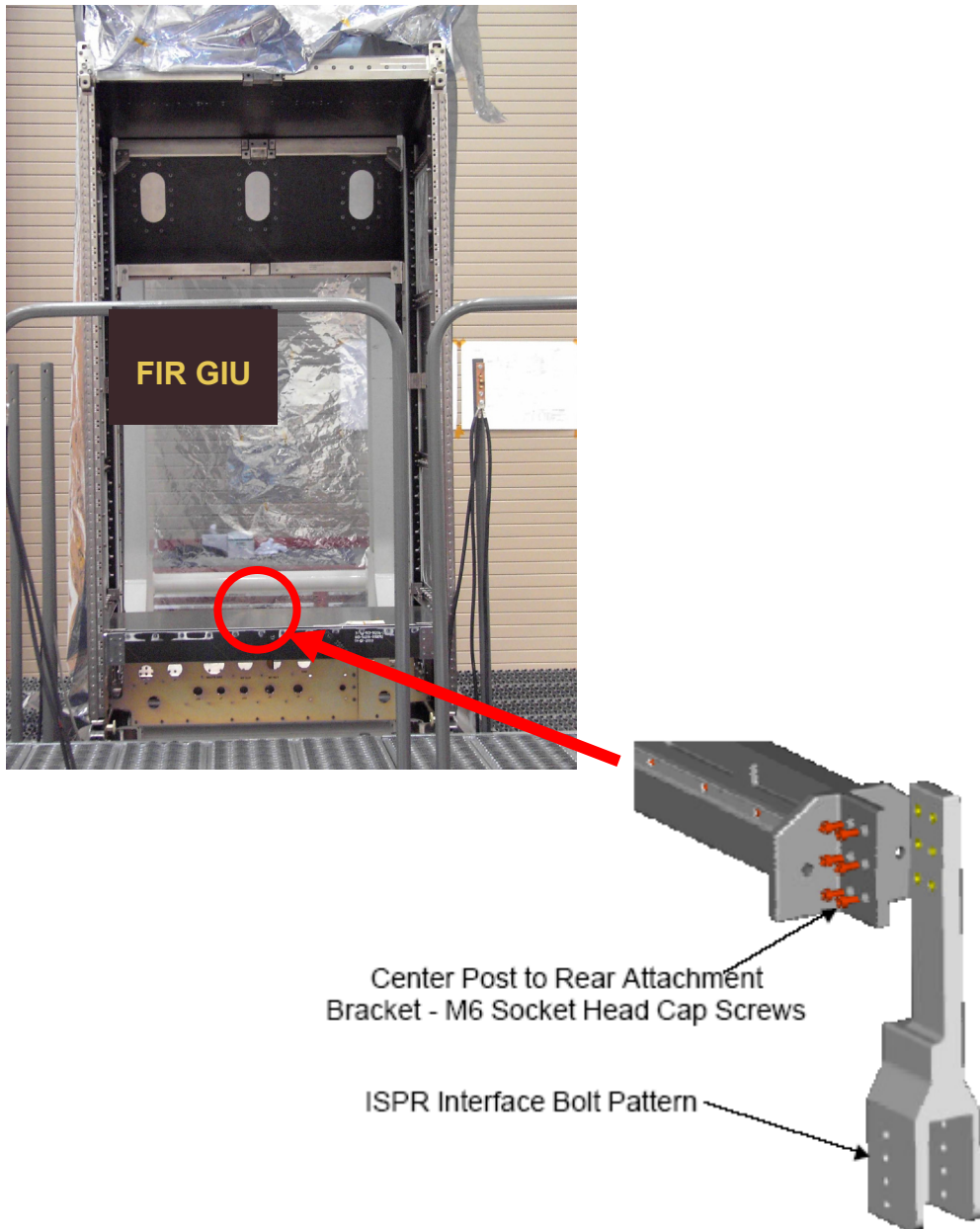


FIGURE 9 – RACK CENTER-POST STRUCTURAL ATTACHMENT MODIFICATION

3.3 Mass Simulators

The general criteria for using mass simulators in the FIR test configuration is based on providing mass representation for any components weighing greater than 5 lbs. For the FIR modal test the only mass simulators used were those associated with the Active Rack Isolation System.

3.4 Active Rack Isolation System (ARIS)

The FIR flight rack will be outfitted with the Active Rack Isolation System (ARIS). The ARIS components are shown in Figure 10. The purpose of ARIS is to isolate the FIR from ISS vibratory acceleration. For the FIR modal survey, mass simulators were used to represent the major ARIS masses. The components simulated and their masses are:

- Three Remote Electronics Units (REU) 9.7 lb. ea
- ARIS Controller 20.0 lb.
- ARIS Actuator Driver 23.4 lb.

The REUs are mounted on the ISPR intercostals with one on the upper intercostal and two on the lower intercostal. The ARIS structure in the lower part of the rack consists of a hardback on which is mounted a coldplate. The ARIS controller and actuator driver are mounted on the coldplate.

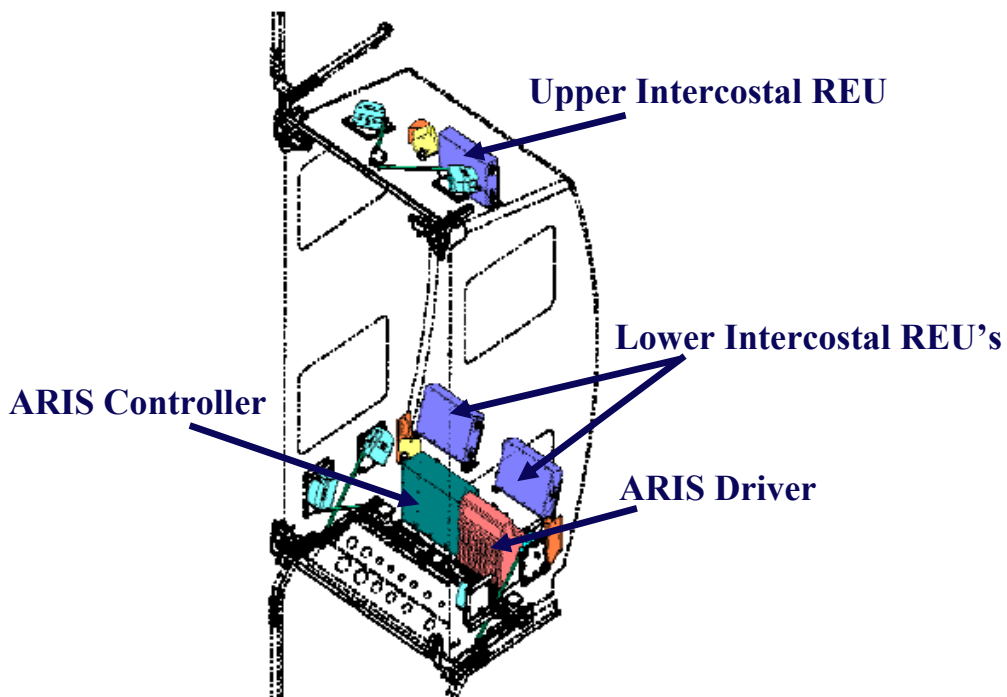


FIGURE 10 – ARIS COMPONENTS

4. FEM Model Description

The FIR modal test configuration finite element model (FEM) is shown in Figure 11. The finite element model was created using MSC/NASTRAN and has the following properties:

M O D E L S U M M A R Y

NUMBER OF GRID	POINTS =	80313
NUMBER OF CBAR	ELEMENTS =	1023
NUMBER OF CBUSH	ELEMENTS =	4
NUMBER OF CELAS1	ELEMENTS =	522
NUMBER OF CHEXA	ELEMENTS =	7613
NUMBER OF CONM2	ELEMENTS =	123
NUMBER OF CPENTA	ELEMENTS =	12
NUMBER OF CQUAD4	ELEMENTS =	53085
NUMBER OF CQUADR	ELEMENTS =	154
NUMBER OF CTETRA	ELEMENTS =	2932
NUMBER OF CTRIA3	ELEMENTS =	7032
NUMBER OF RBAR	ELEMENTS =	81
NUMBER OF RBE2	ELEMENTS =	1973
NUMBER OF RBE3	ELEMENTS =	60

4.1 Rack Coordinate System

The rack coordinate system for the finite element model and modal test is defined in Figure 7. The rack coordinate system is a local coordinate system invariant to the integration position of the rack into the MPLM.

4.2 Rack Modal Test Fixture

The rack modal test fixture is the structural hardware between the rack and the modal floor. The design intent for the rack fixture is to have the fundamental frequency ten times higher than the FIR fundamental frequency to prevent dynamic coupling between the FIR modes and the fixture. The fixture is a frame construction using welded tubular steel with 3/8" wall thickness.

A modal test was conducted on the rack fixture to characterize the fundamental frequencies (Figure 12). The rack fixture finite element model was not correlated. Based on the fixture test results, the fixture stiffness was increased using bookend stiffeners to prevent deflection of the ends of the fixture. Figure 11 illustrates the FEM with rack attachment to the fixture including bookend stiffeners.

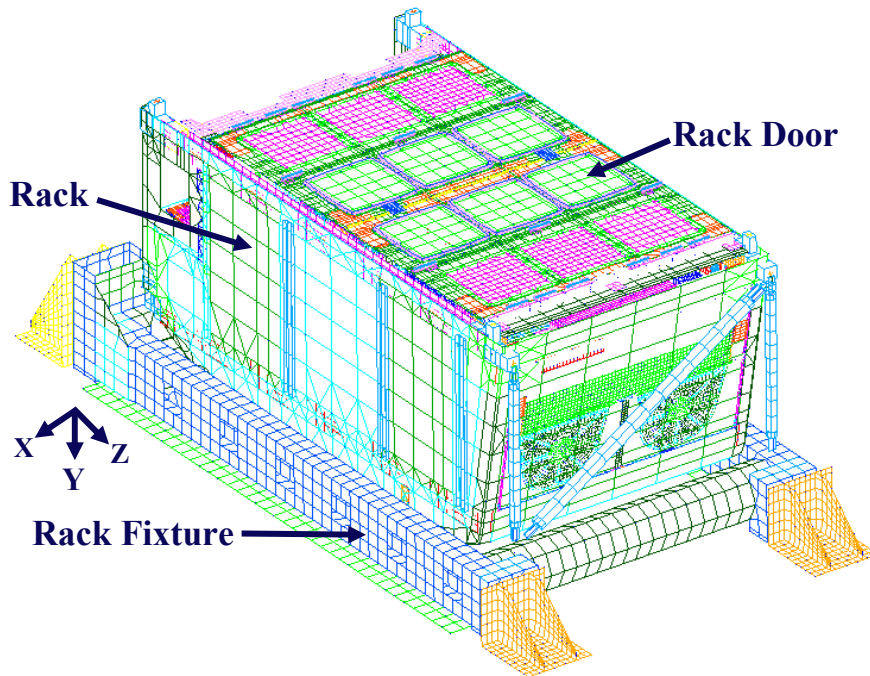
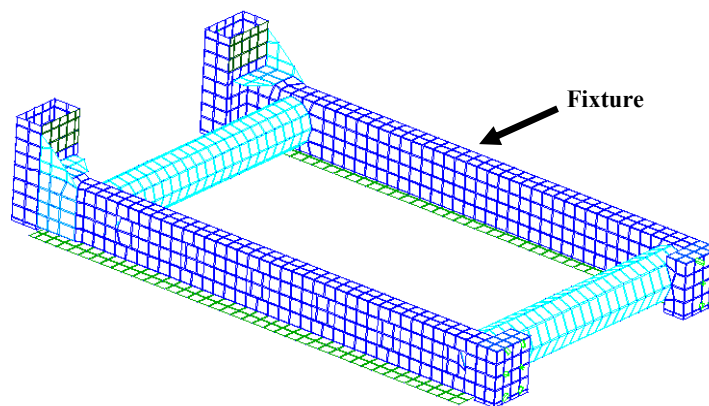


FIGURE 11 – TEST CONFIGURATION FINITE ELEMENT MODEL (FEM)



Fixture Modal Test Results without Bookends		
Mode	Axis	Freq (Hz)
1	X	196.6
2	X	201.1
3	Y	243.3
4	X	289.2
5	X	292.4

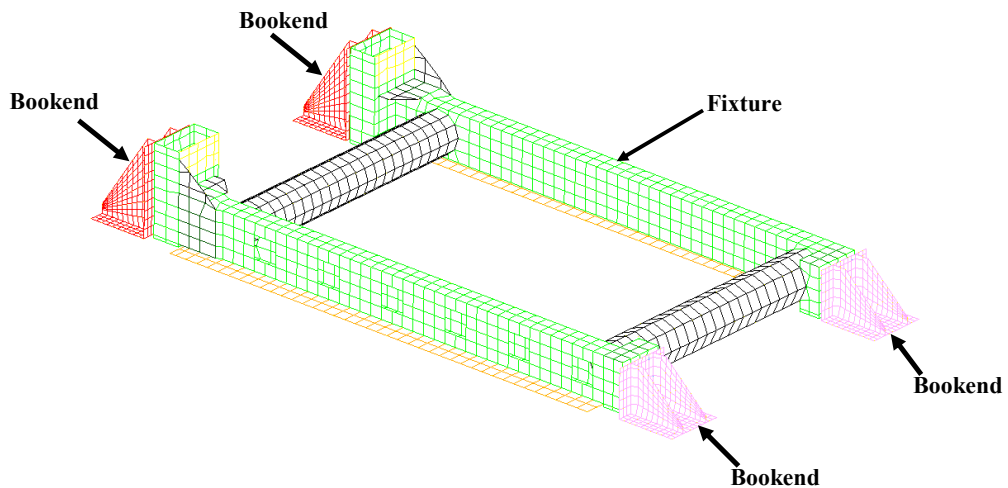
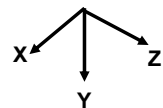


FIGURE 12 – RACK MODAL TEST FIXTURE

4.3 FEM Mass and CG Properties

A mass and CG summary is provided for the FIR test and flight finite element models (FEM) in Tables 2 and 3. The FIR test FEM weighs 1398.36 lbs and the FIR flight FEM weighs 1462.10 lbs. The mass difference between the two finite element models is 63.74 lbs, representing a difference of 4.4%. The CG properties between the test and flight rack are very comparable.

Table 2 – FIR Test Finite Element Model Mass and CG Summary

Subsystems	Weight (lbf)	CG _x (in)	CG _y (in)	CG _z (in)	I _{xx} (lbm-in ²)	I _{yy} (lbm-in ²)	I _{zz} (lbm-in ²)
ATCU	120.52	20.0	-12.6	71.2	20.3	49.0	65.7
Experiment Assembly	553.32	18.5	-7.4	41.3	316.4	545.0	383.8
Door	108.08	19.7	-26.8	44.5	114.5	161.2	47.3
Rack	369.71	19.7	-7.8	24.4	767.9	859.5	323.1
Lower Structure Assembly (Mass Simulator)	139.64	20.2	-10.8	15.8	18.8	43.3	58.0
FIR Test FEM	1398.36	19.1	-9.6	36.1	2186.2	2539.3	1027.0

Table 3 – FIR Flight Finite Element Model Mass and CG Summary

Subsystems	Weight (lbf)	CG _x (in)	CG _y (in)	CG _z (in)	I _{xx} (lbm-in ²)	I _{yy} (lbm-in ²)	I _{zz} (lbm-in ²)
ATCU	120.52	20.0	-12.6	71.2	20.3	49.0	65.8
Experiment Assembly	557.58	18.5	-7.5	41.4	322.0	551.3	388.8
Door	97.18	19.7	-26.9	45.1	107.4	145.6	38.5
Rack	435.47	19.4	-9.0	25.2	875.0	1028.0	411.3
Lower Structure Assembly (Mass Simulator)	139.64	20.2	-10.8	15.8	18.8	43.3	58.0
FIR Flight FEM	1462.10	19.1	-9.8	35.7	2296.3	2712.5	1101.9

The mass difference between the FIR test hardware and the test FEM is 7.44 lbs, representing a 0.5% mass difference. The CG properties between the measured FIR test hardware and FEM are very comparable.

The mass difference between the FIR flight hardware and the flight FEM is 8.93 lbs, representing a 0.6% mass difference. The CG properties between the measured FIR flight hardware and FEM are very comparable.

5. Pre-Test Analysis

Pre-test modal analysis was performed to identify target modes between 0-50 Hz and determine the accelerometer instrumentation layout. The methodology used to verify the finite element model is outlined in Figure 13. The general criterion used to define the primary target modes are modes with greater than 10% effective mass and a frequency less than 50 Hz. Secondary target modes are defined based on modes with less than 10% effective mass and frequencies greater than 50 Hz. Engineering judgment was also used to select target modes by visualizing animated mode shapes.

Three modes were defined as target modes for the Fluids Integrated Rack (FIR) modal test. Two rack translational modes in the X, and Y axes were identified as primary target modes. A secondary target mode was identified as the FIR Z axis mode.

The predicted X-axis FIR translational mode was 26.6 Hz, with an effective weight of 1229.2 lb. The predicted Y-axis FIR translational mode was 41.8 Hz, with an effective weight of 772.9 lbs. The predicted Z-axis FIR translational mode was 49.2 Hz, with an effective weight of 702.1 lb. Figures 14-16 illustrate the primary and secondary target modes for the FIR modal test.

The target modes were compared between the FIR test FEM and TAM, with and without the test fixture, and flight FEM and flight ASET configurations to assure that the test configuration was representative of flight. These comparisons are summarized in Tables 4 and 5, and Figures 14–16 indicating that the test configuration modes are comparable to the flight modes.

Selection of the accelerometer locations (NASTRAN A-SET) for the FIR modal test was based on a two-tiered approach using kinetic energy (choosing grid points from the finite element mode with high kinetic energy) and engineering judgment (visualizing the mode shape and placing instrumentation at high deformation locations).

The criterion for selecting the final instrumentation was based on computing the cross-orthogonality between the test finite element model (FEM) and the Test Analysis Model (TAM - test finite element model including only the instrumentation locations). The cross-orthogonality between the test configuration FEM and the TAM are summarized in Table 6 and Figures 17-19. One hundred twenty six (126) degrees of freedom were used in the TAM. Cross-orthogonality was greater than 90% for the primary target modes satisfying the criteria for instrumentation selection. The secondary target mode for the FIR Z axis had 93.8% cross-orthogonality. The final instrumentation plan is documented in Appendix E.

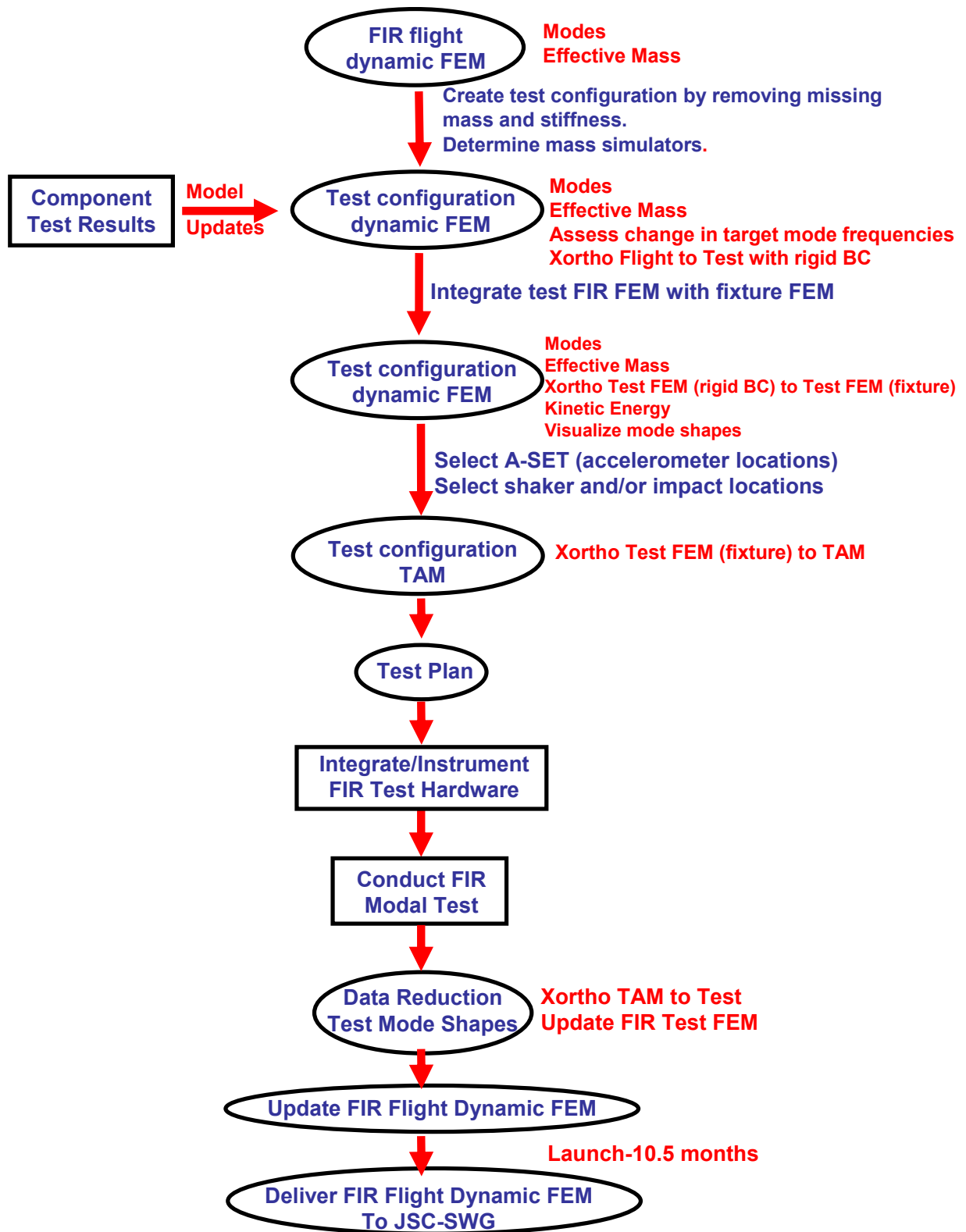


FIGURE 13 – FIR MODEL VERIFICATION METHODOLOGY

TABLE 4 – COMPARISON OF FLIGHT FEM (IN RIGID BOUNDARY CONDITIONS) AND TAM (IN RIGID BOUNDARY CONDITIONS) TARGET MODE FREQUENCY DIFFERENCE AND CROSS-ORTHOGONALITY

		FLIGHT ASET Rigid BC				Delta Freq	Mode Shape Description
Mode		3	8	9	9		
TAM Rigid BC	Mode	Freq (Hz)					
	3	30.3	47.5	57.1	57.1		
	8	100.26	0	0	0	3.0%	Rack X-axis Translation
	9	46.3	0.931	0	0	-2.5%	Rack Y-axis Translation
	9	53.1	0	0	-0.713	-7.0%	Rack Z-axis Translation

TABLE 5 – COMPARISON OF TEST FEM (IN RIGID BOUNDARY CONDITIONS) AND TEST FEM (IN FIXTURE) TARGET MODE FREQUENCY DIFFERENCE AND CROSS-ORTHOGONALITY

		Test FEM Rigid BC			Delta Freq	Mode Shape Description
Mode		3	8	9		
Test FEM w/Fixture	Mode	Freq (Hz)				
	1	30.6	45.6	52.4		
	8	26.6	0.878	0.100	0	-13.1%
	9	41.8	0	0.833	0.110	-8.3%
	9	49.2	0	0	0.770	-6.1%

TABLE 6 – COMPARISON OF TEST AND TAM TARGET MODE FREQUENCY DIFFERENCE AND CROSS-ORTHOGONALITY

		TAM			Delta Freq	Mode Shape Description
Mode		2	8	9		
Test FEM w/Fixture	Mode	Freq (Hz)				
	1	27.1	42.4	50.2		
	8	26.6	0.931	0	0	-1.9%
	9	41.8	0	0.902	0	-1.4%
	9	49.2	0	0	-0.938	-2.0%

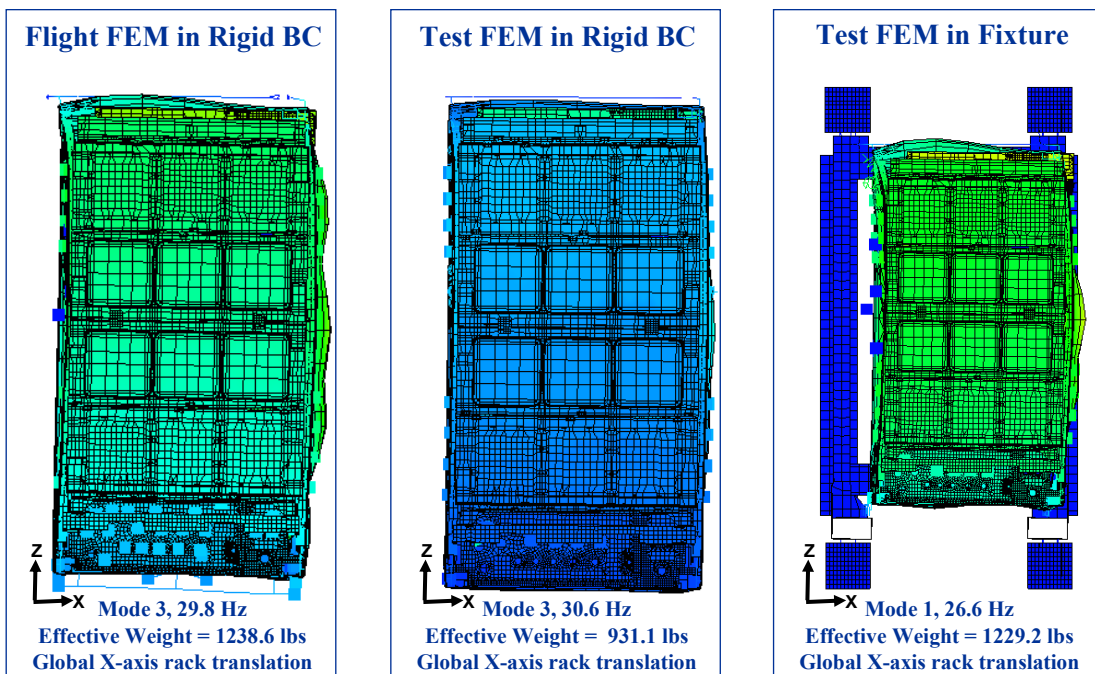


FIGURE 14 – X-AXIS PRIMARY TARGET MODE

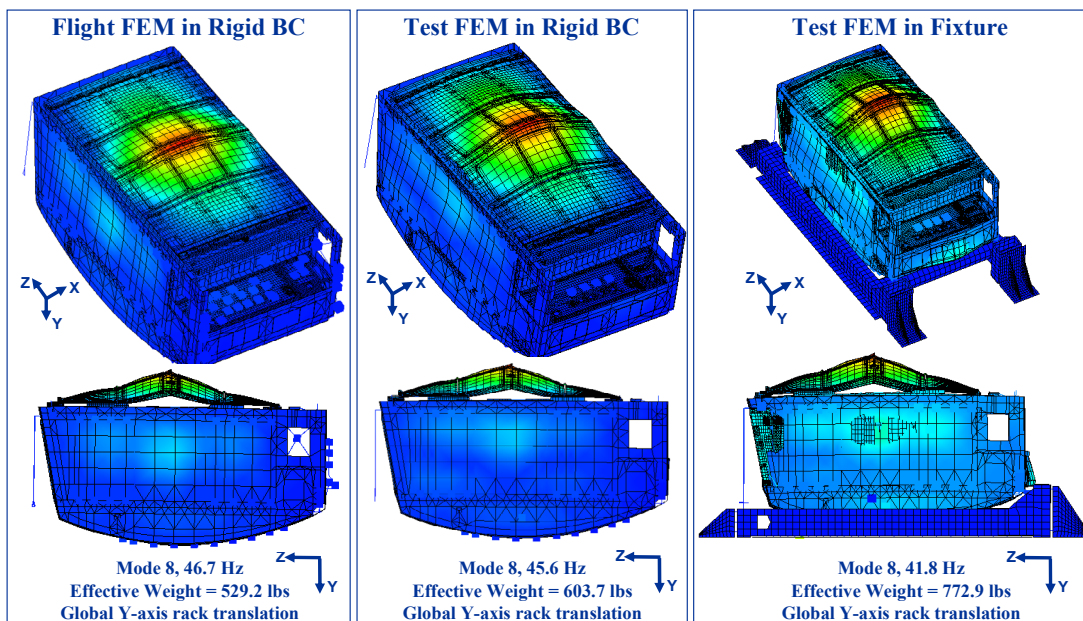


FIGURE 15 – Y-AXIS PRIMARY TARGET MODE

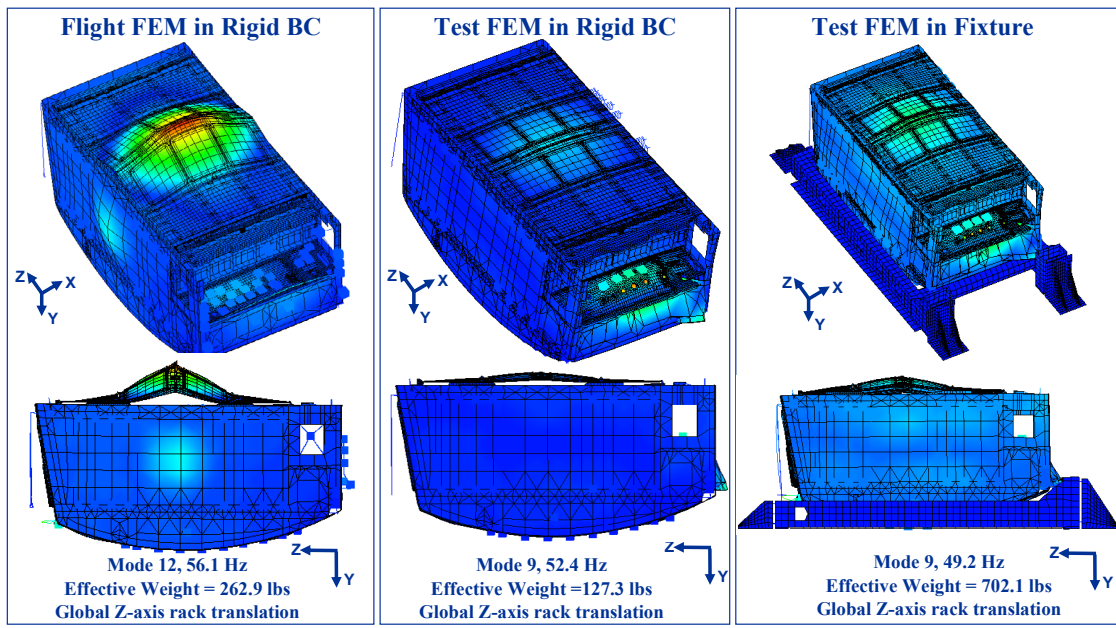


FIGURE 16 – Z-AXIS SECONDARY TARGET MODE

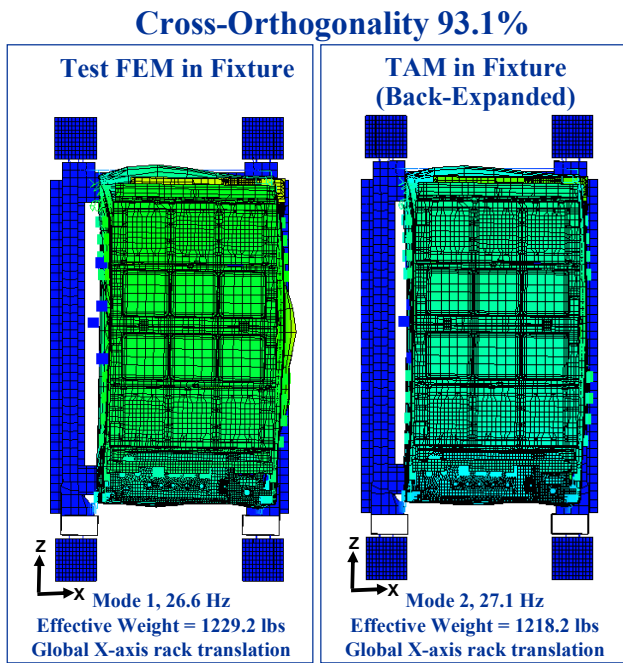


FIGURE 17 – COMPARISON OF TEST FEM TO TAM FOR THE X-AXIS TARGET MODE

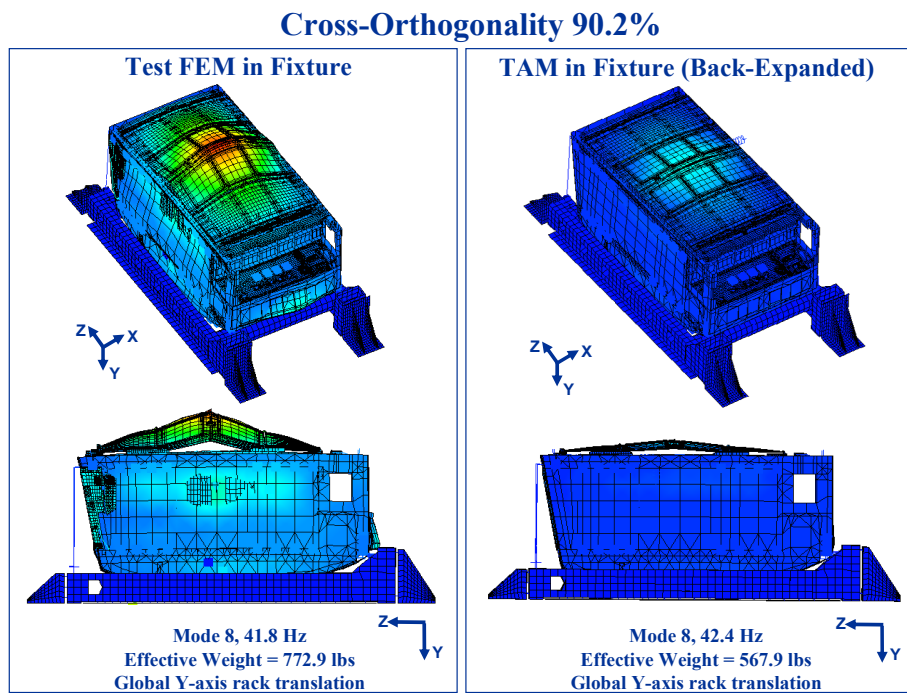


FIGURE 18 – COMPARISON OF TEST FEM TO TAM FOR THE Y-AXIS TARGET MODE

Cross-Orthogonality 93.8%

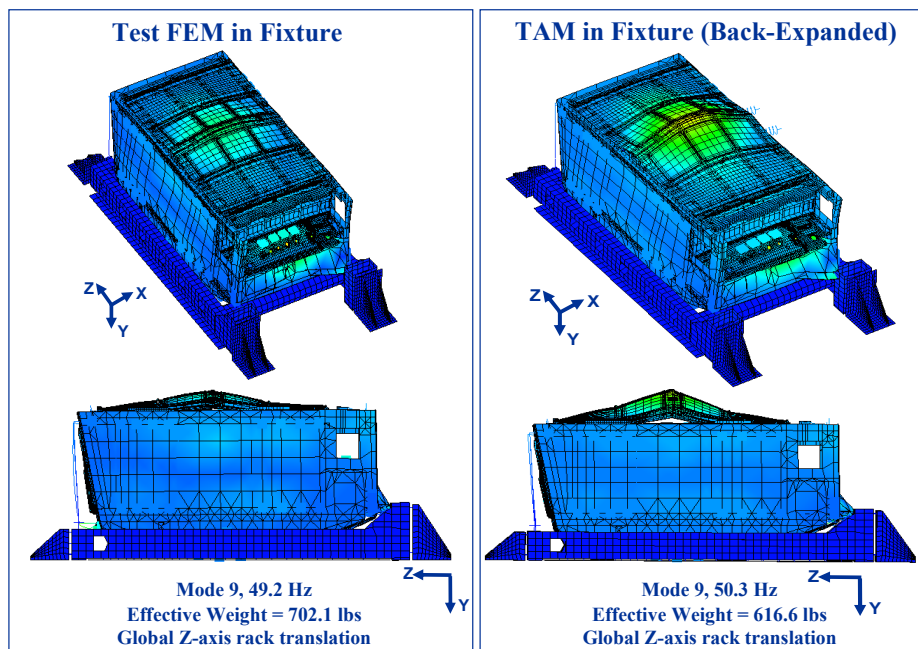


FIGURE 19 – COMPARISON OF TEST FEM TO TAM FOR THE Z-AXIS TARGET MODE

Past experience in developing A-SETs for modal analysis has shown that it is important to include major masses. Therefore, the GRID points representing the 3 REUs were included in the FIR A-set.

When the model correlation effort was begun (see Sec. 7), there was difficulty in getting the cross orthogonality for the Y target mode above 75%. Based on viewing a comparison of the test mode shapes and the analytical mode shapes using the test display model, it was clear that there were significant differences in the lower part of the rack. Most obvious was the behavior of the lower intercostal with 2 REUs mounted to it.

Because the poor cross orthogonality appeared to be associated with the ARIS hardware, a study was conducted to determine its influence on the results (Figure 20). When all the ARIS components were eliminated from the problem, the cross orthogonality of the Y mode increased from 70% to 92%. This change also had a beneficial effect on the X and Z modes. Then the effect of adding ARIS components back into the problem was determined. Optimum results were obtained when all ARIS components except the two REUs on the lower intercostal were included in the problem.

The validity of removing the two lower REUs from the A-SET was determined by reviewing the frequency and effective mass with and without ARIS. Since there was no change in either of these two parameters when ARIS was removed from the A-SET, it was concluded the ARIS response was a local response and its removal did not affect the global modes of the rack.

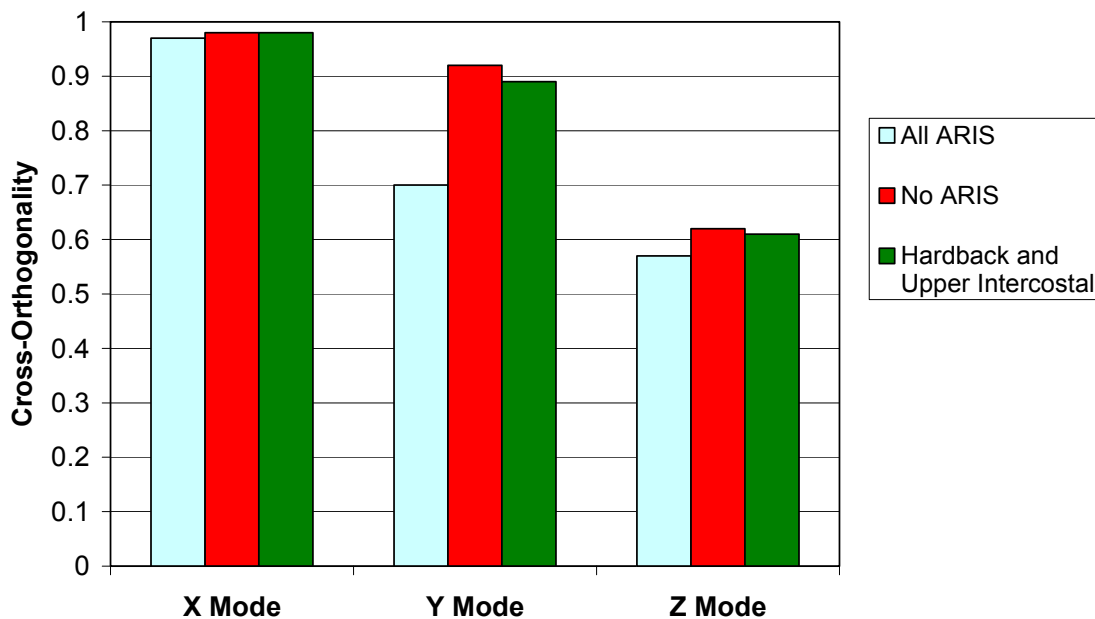


FIGURE 20 – EFFECT OF INCLUDING ARIS COMPONENTS ON FIR CROSS-ORTHOGONALITY (BEFORE OPTIMIZATION)

6. Test Results

The Fluids Integrated Rack (FIR) modal test was conducted at the NASA Glenn Research Center Structural Dynamics Laboratory from May 16 – June 10, 2005. The test was performed using a fixed base interface between the test article and the modal floor. One-hundred twenty six (126) response accelerometers were used during the test. Four (4) load cells were mounted between the rack and fixture attachment locations to measure interface forces (Figure 21). Interface accelerometers were also used to monitor any relative motion between the fixture and rack. Minimal relative interface motion was observed, indicating that the fixture was not participating in the FIR target modes response.

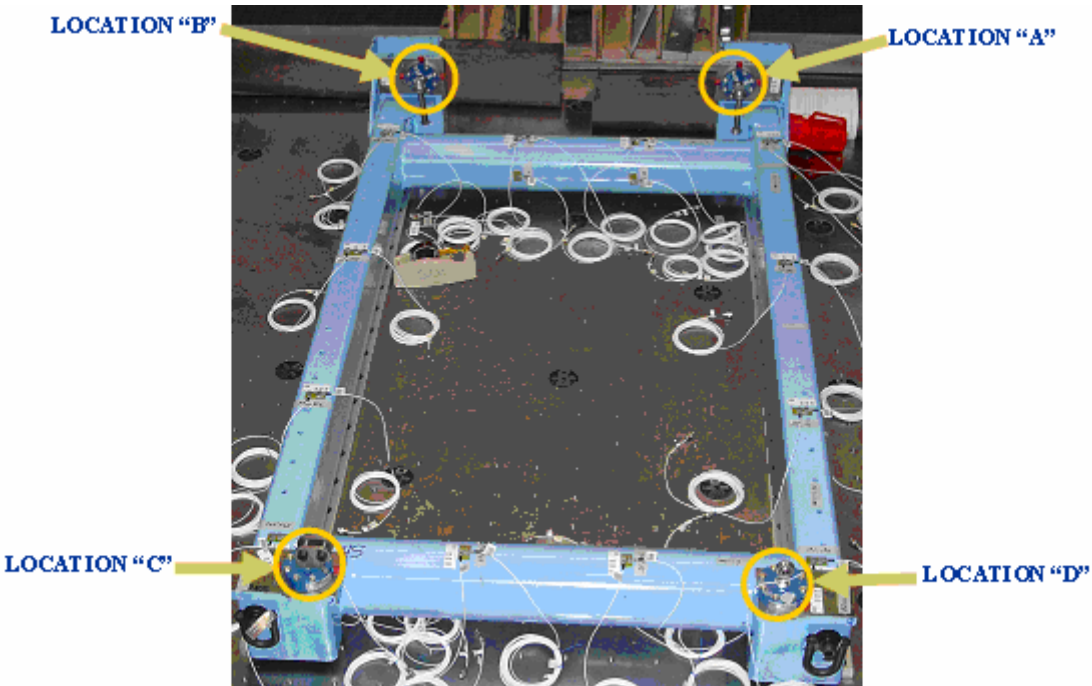


FIGURE 21 – LOAD CELLS

MB Dynamics (Modal 50) 50 lb_{rms} shakers were used to excite the FIR. One shaker was used for X and Z-axis excitation. Two shakers were used in the Y and Z-axis to excite symmetric and anti-symmetric modes. Initially, impact tests were conducted to evaluate data quality, identify potential shaker locations, and to obtain preliminary modal data. Shaker locations were selected at hard points on the rack to optimally excite the target modes (Figures 23– 26). Multiple shaker excitation levels were used to address linearity of the FIR test configuration. Sine excitation levels included 1, 2, 5, 10, 15, and 20 lb_{peak} from 10-80 Hz. Burst random excitation levels included ½, 1, 2, 5, 10 and 15 lb_{rms}. For the X-axis target mode a slight nonlinearity was observed, otherwise linearity was excellent for the primary target modes (Figures 26 and 27). The frequency shift observed was less than 1.5 Hertz (less than 5%). Linearity studies were not conducted for the Z-axis secondary target mode.

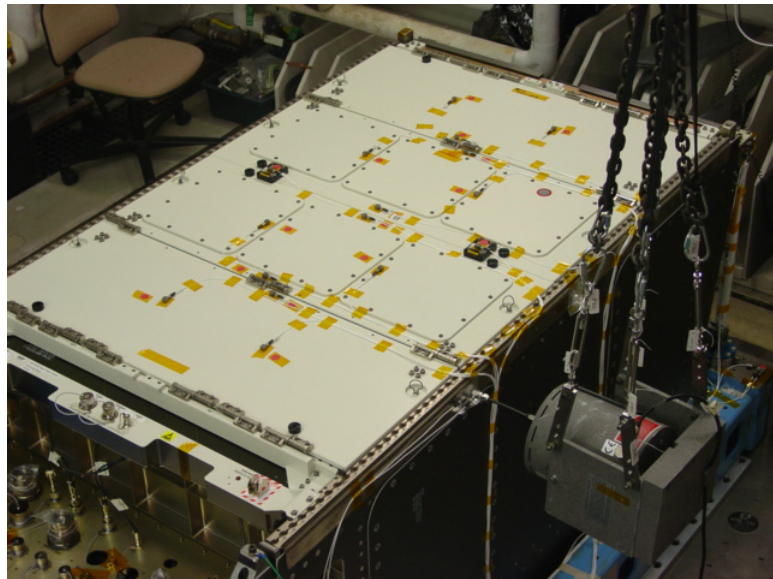


FIGURE 22 – X-AXIS SHAKER EXCITATION

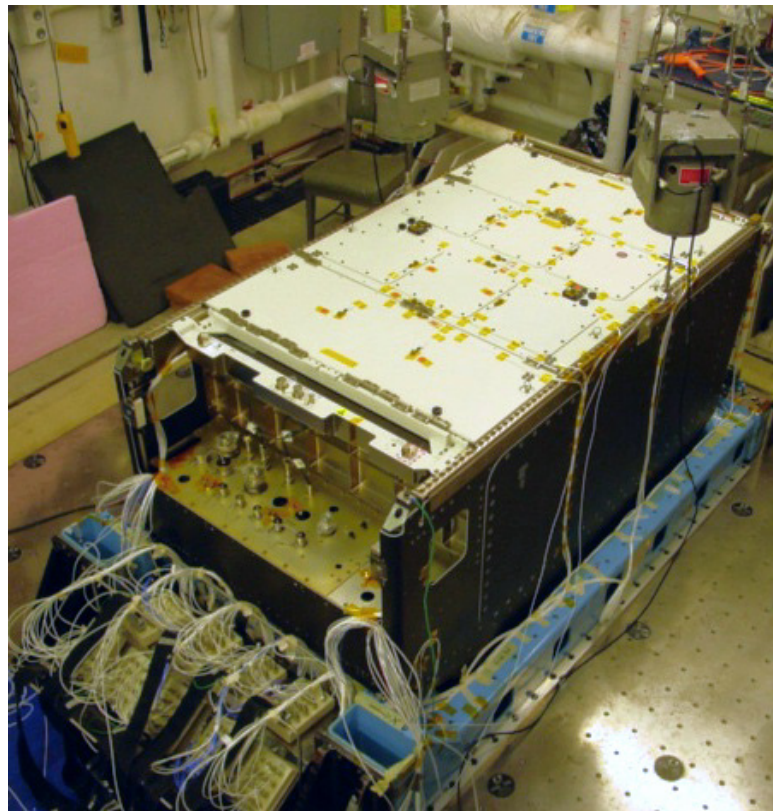


FIGURE 23 – Y-AXIS SHAKER EXCITATION

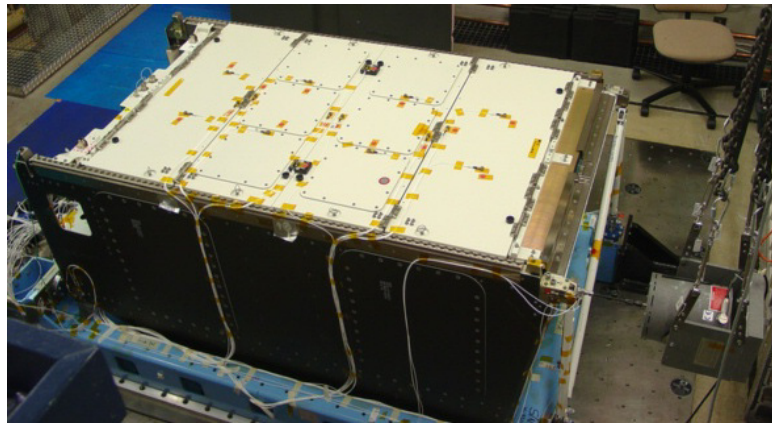


FIGURE 24 – Z-AXIS SHAKER EXCITATION

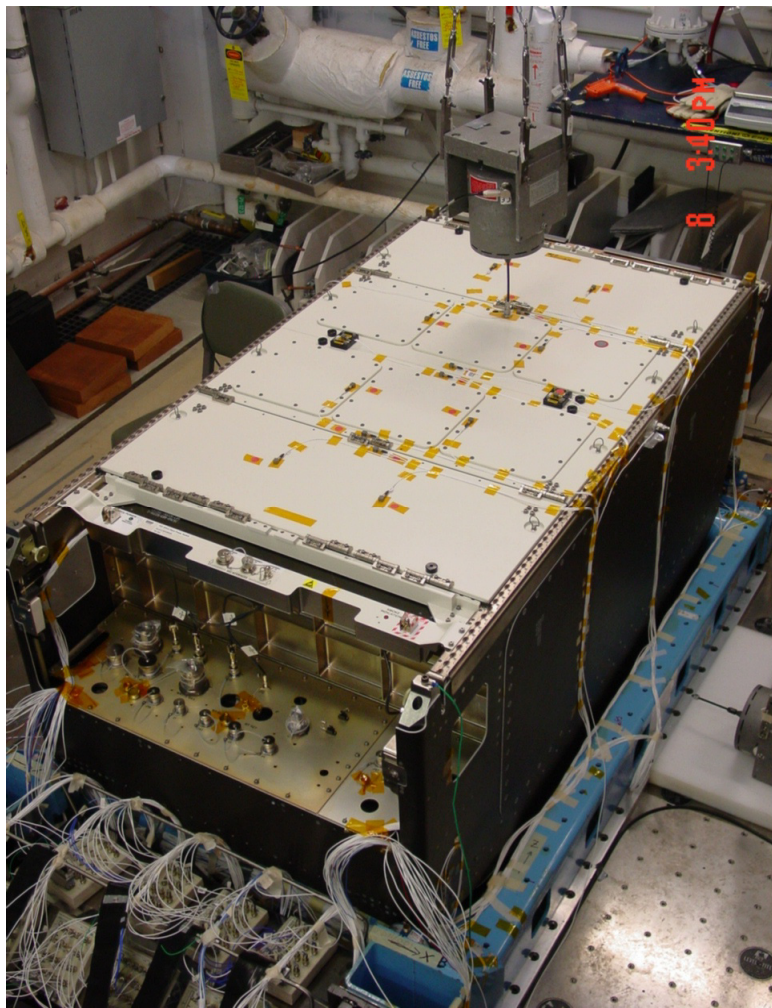


FIGURE 25 – DOOR SHAKER EXCITATION

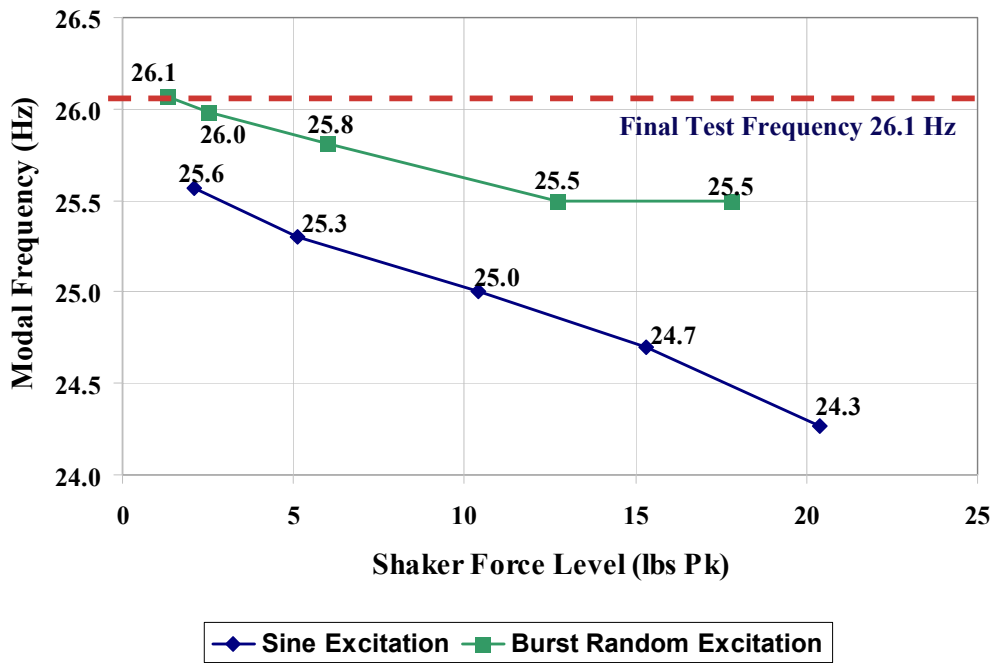


FIGURE 26 – LINEARITY OF X-AXIS RACK TRANSLATION MODE USING SINE SWEEP AND BURST RANDOM EXCITATION

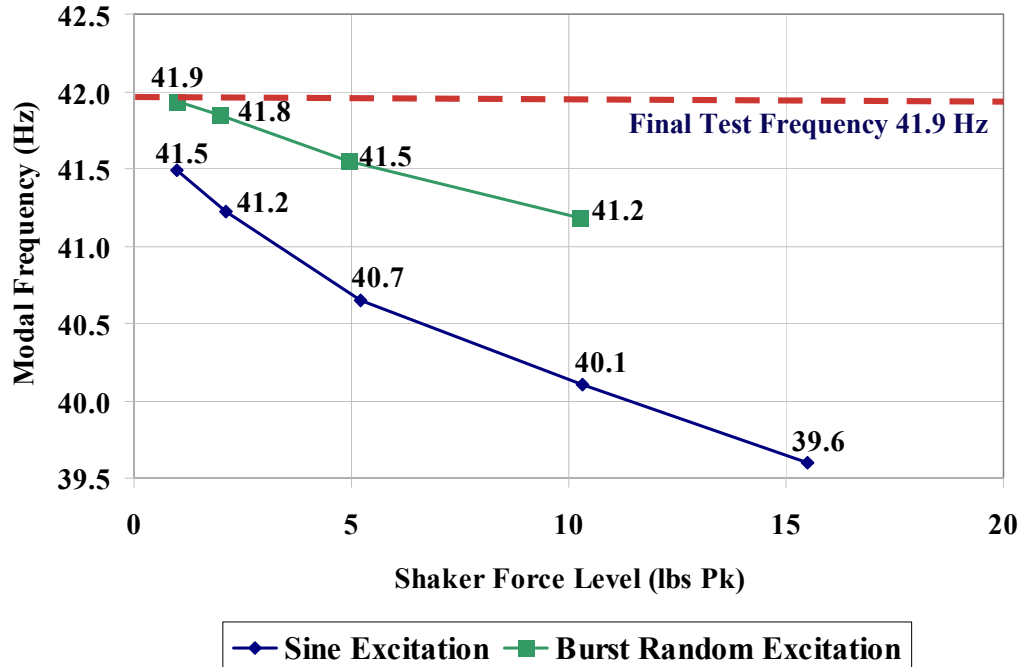


FIGURE 27 – LINEARITY OF Y-AXIS RACK TRANSLATION MODE USING SINE SWEEP AND BURST RANDOM EXCITATION

The FIR modal test had high data quality and low extraneous noise. Typical sine sweep excitation Frequency Response Functions (FRFs) and coherence graphs from the test are shown in Figures 28 – 31. Typical burst random excitation Frequency Response Functions (FRFs) and coherence graphs from the test are shown in Figures 32 – 35. Test data results can be found in the Structural Dynamics Laboratory test report number SDL-TR-05-12 (Reference 4).

Three global rack translational modes were identified during FIR modal testing using burst random excitation. The X-axis mode occurred at 26.1 Hz, the Y-axis mode occurred at 41.9 Hz, and the Z-axis mode occurred at 51.9 Hz.

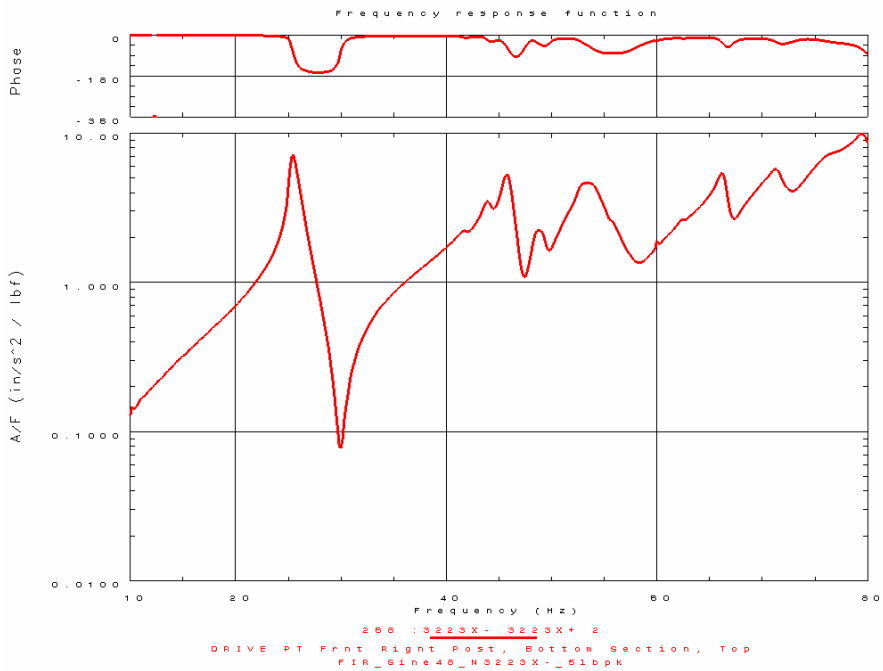


FIGURE 28 – TYPICAL DRIVE POINT FRF FROM X-AXIS SINE SWEEP EXCITATION

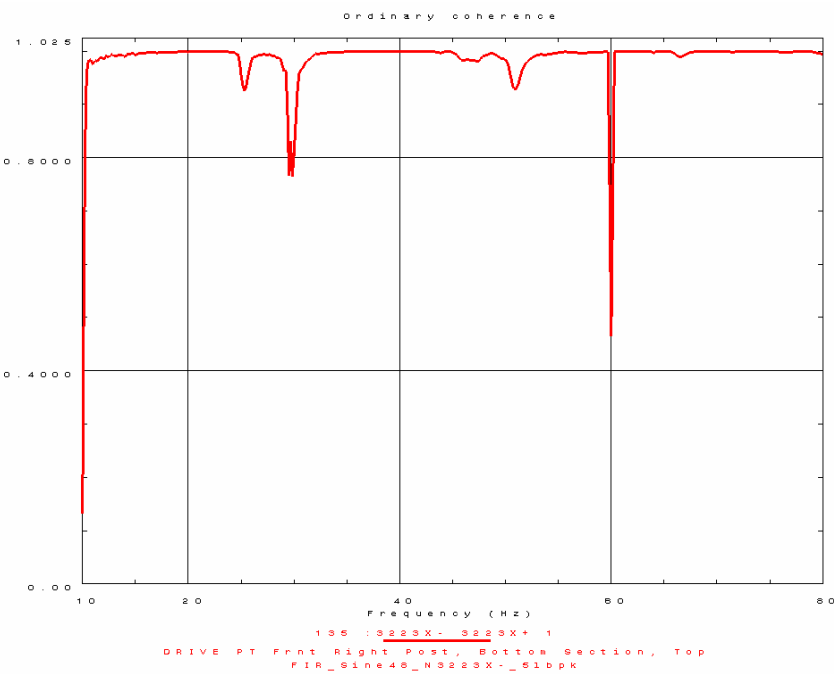


FIGURE 29 – TYPICAL DRIVE POINT COHERENCE FROM X-AXIS SINE SWEEP EXCITATION

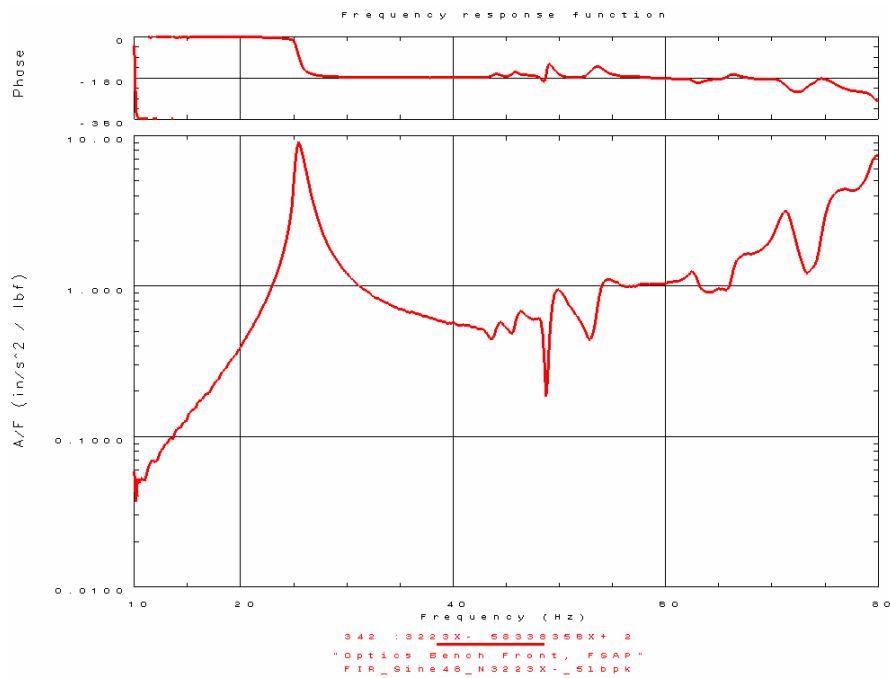


FIGURE 30 – TYPICAL FRF FROM X-AXIS SINE SWEEP EXCITATION

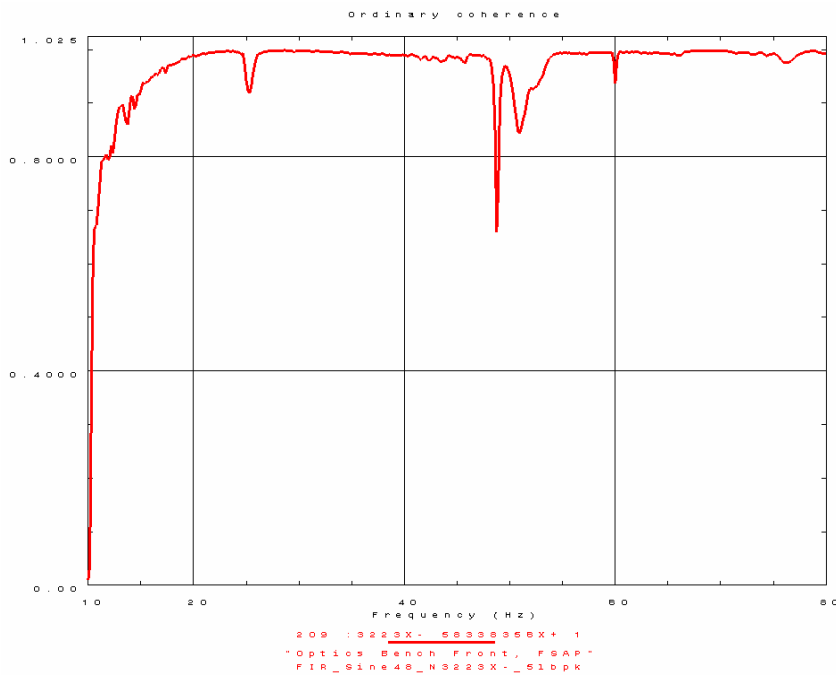


FIGURE 31 – TYPICAL COHERENCE FROM X-AXIS SINE SWEEP EXCITATION

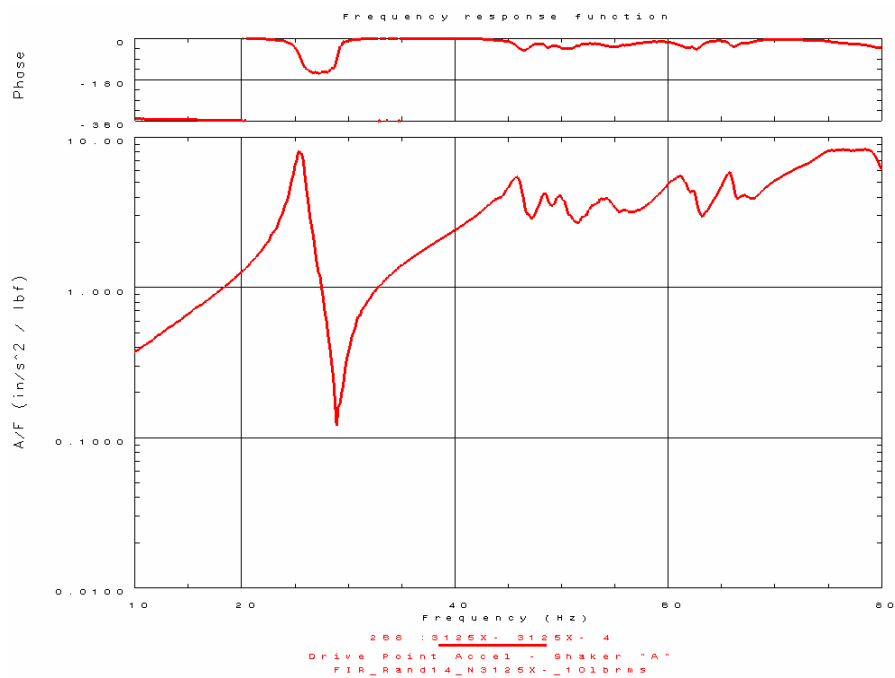


FIGURE 32 – TYPICAL DRIVE POINT FRF FROM X-AXIS BURST RANDOM EXCITATION

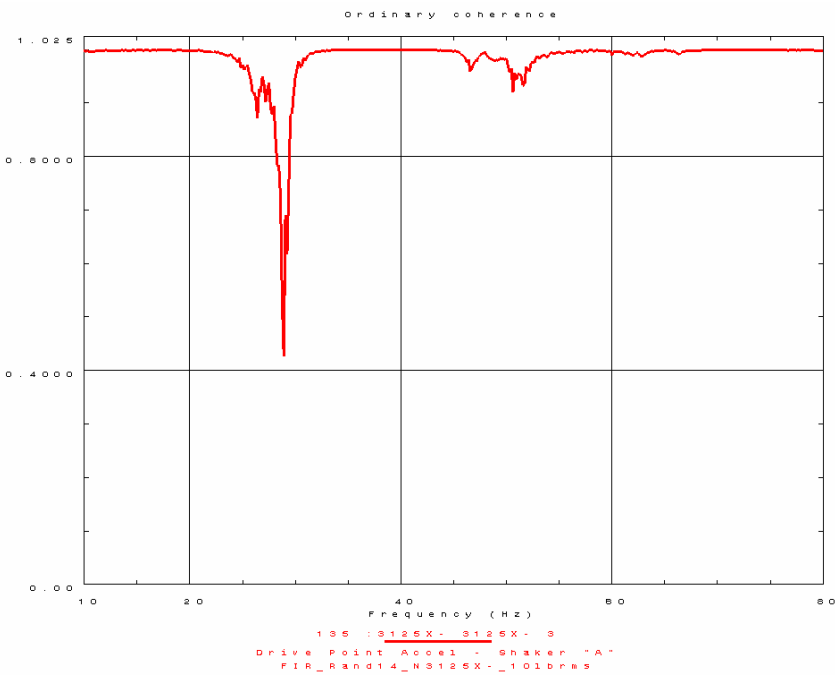


FIGURE 33 – TYPICAL DRIVE POINT COHERENCE FROM X-AXIS BURST RANDOM EXCITATION

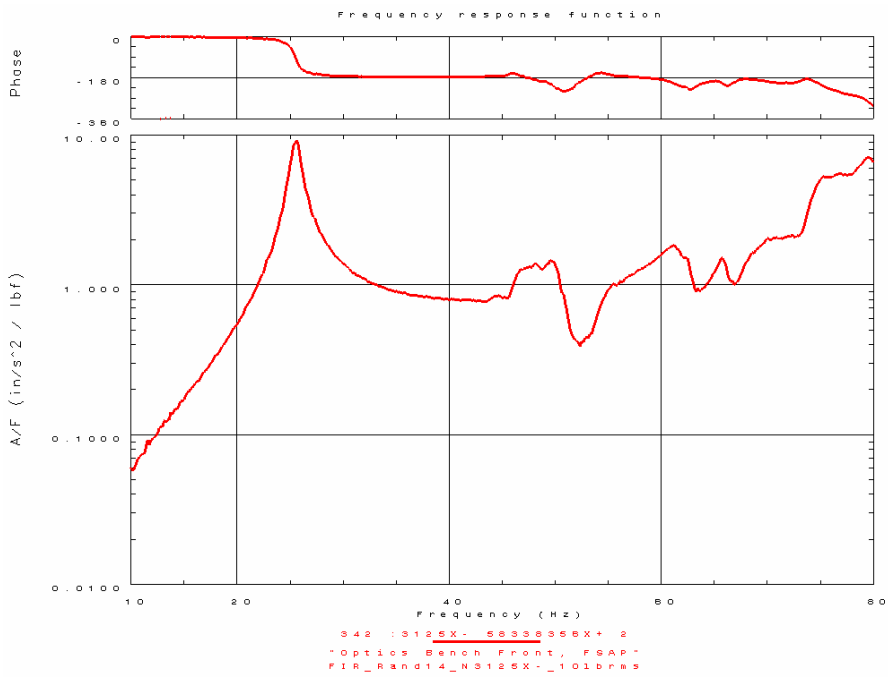


FIGURE 34 – TYPICAL FRF FROM X-AXIS BURST RANDOM EXCITATION

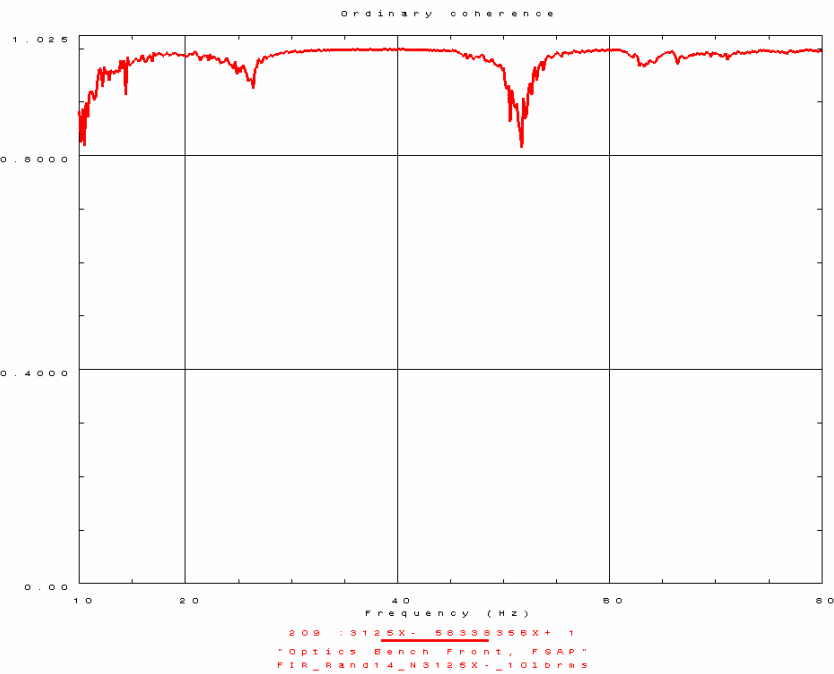


FIGURE 35 – TYPICAL COHERENCE FROM X-AXIS BURST RANDOM EXCITATION

7. Model Correlation

The FIR finite element model was updated based on initial low cross-orthogonality of the primary target modes (rack X and Y translation) and the secondary mode (Z translation).

FIR model correlation was accomplished using Attune (Reference 5) test/analysis correlation and model updating software. Attune uses design sensitivity and optimization methods to identify FEM model changes that minimize the difference between test and analysis results (objective function). Design sensitivity coefficients are used that identify important properties in the finite element model (FEM) for optimization. Upper and lower bounds are assigned to the design variables to account for parameter uncertainty. Weights can be assigned to the design variables to emphasize their importance on the objective function. State variables (design constraints) used in the optimization include frequency and cross-orthogonality. The Attune optimization flowchart is shown in Figure 36. After each iteration, the eigensolution is recalculated in NASTRAN using the updated design variables.

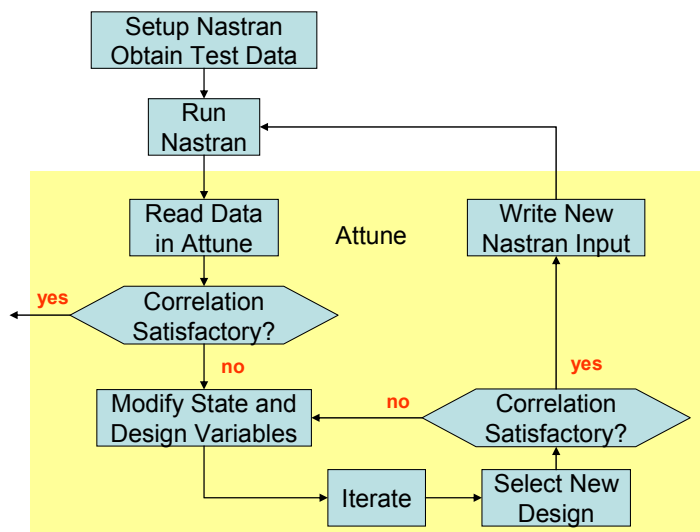


FIGURE 36 – ATTUNE OPTIMIZATION FLOWCHART

The FIR FEM was correlated using three different optimization algorithms: Genetic, Monte Carlo, and Gradient methods.

The Genetic and Monte Carlo algorithms both utilize randomly generated candidate designs, and update the stiffness matrix based on modal matrix sensitivities. The Genetic algorithm evaluates a set of randomly chosen designs against the objective function, and then tries to systematically improve the designs through iteration. The advantage of the Genetic and Monte Carlo methods is that these methods are not trapped by local minima. The Genetic and

Monte Carlo algorithms are generally used to tune the FEM when the design properties are not well known, and there is a large design space.

The Gradient method is best used when the design variables are well known, and only small changes are required to correlate the model. Problems associated with the Gradient method are encountered when the algorithm is trapped in local minima, causing inaccuracies in the linear approximation of the derivatives.

The FIR model correlation methodology was based on modal testing and correlating each major structural assembly FEM individually (FIR Optics Bench, FIR Air Thermal Control Unit, Rack Door, and Lower Structure Assembly). This developed confidence that the major assemblies were correlated before the start of the FIR modal test. The final step in the correlation process was to modal test and model correlate the FIR. This building block approach facilitated the model correlation process. Once the major structure assemblies FEMs were individually correlated, the only areas of uncertainty in the fully populated FIR model were the structural connections between the assemblies, the rack, and the fixture.

The FIR FEM was updated using the following design variables:

- Load cell and attachment clevis (Figure 37) X, Y, Z-axes translational spring stiffness (PBUSH)
- Door (Figure 38) Young's Modulus
- Coldplate (Figure 39) Young's Modulus
- Hardback (Figure 39) Young's Modulus
- Upper Intercostal (Figure 40) Bending Moment of Inertia

In the Boeing rack with ARIS finite element model, the coldplate and hardback assembly representation is low fidelity. Based on hardware drawings, the coldplate and hardback assembly was replaced with a detailed finite element model (Figure 39) improving the characterization of the bending stiffness.

Using the detailed FEM of the coldplate and hardback assembly, a final assessment was made comparing the target modes between the FIR test FEM and TAM, with and without the test fixture, and flight FEM and flight ASET configurations to assure that the test configuration was representative of flight. The cross-orthogonality between the test configuration FEM and the TAM were also re-evaluated. These comparisons are documented in Appendix F.

In order to correlate the FIR FEM, two iterations were performed in Attune to update the design parameters. Table 7 summarizes the design parameter changes made between the pre-test and correlated FIR models.

Table 7 – Comparison of FIR FEM Design Variable Sensitivities Between the Pre-Test and Correlated Models

Description	Type	PID	Property	Design Variable	Design Sensitivity	Pre-Test Model	Correlated Model	Percent Change
Load Cell Translational Spring Stiffness at "A" fixture location	PBUSH	42122192	Stiffness (lb/in)	Kx Ky Kz	KABTX KABTY KABTZ	-9.358E-02 6.077E-02 8.941E-02	64382.5 1.500E+05 5.850E+05	0.0% 0.0% 0.0%
Load Cell Translational Spring Stiffness at "C" fixture location	PBUSH	42122189	Stiffness (lb/in)	Kx Ky Kz	KCTX KCTY KCTZ	2.397E-05 1.840E-02 5.603E-09	8.529E+07 1.084E+06 8.529E+07	0.0% 0.0% 0.0%
Load Cell Translational Spring Stiffness at "D" fixture location	PBUSH	42122190	Stiffness (lb/in)	Kx Ky Kz	KDTX KDTY KDTZ	1.296E-09 1.955E-05 2.154E-10	1.050E+08 1.230E+06 8.529E+07	0.0% 0.0% 0.0%
Coldplate Young's Modulus	MAT1	41459866	Modulus (lb/in ²)	E	COLDE	-1.529E-01	9.900E+06	1.014E+07
Door Young's Modulus	MAT1	13129298	Modulus (lb/in ²)	E	DOORE	1.967E-01	1.140E+07	1.178E+07
Hardback Young's Modulus	MAT1	41459865	Modulus (lb/in ²)	E	HARDE	-7.833E-02	9.900E+06	9.989E+06
Upper Intercostal Bending Moment of Inertia	PSHELL	32	Bending Moment of Inertia	UPPERBMI	7.542E-03	1.0	0.91529	-9.3%

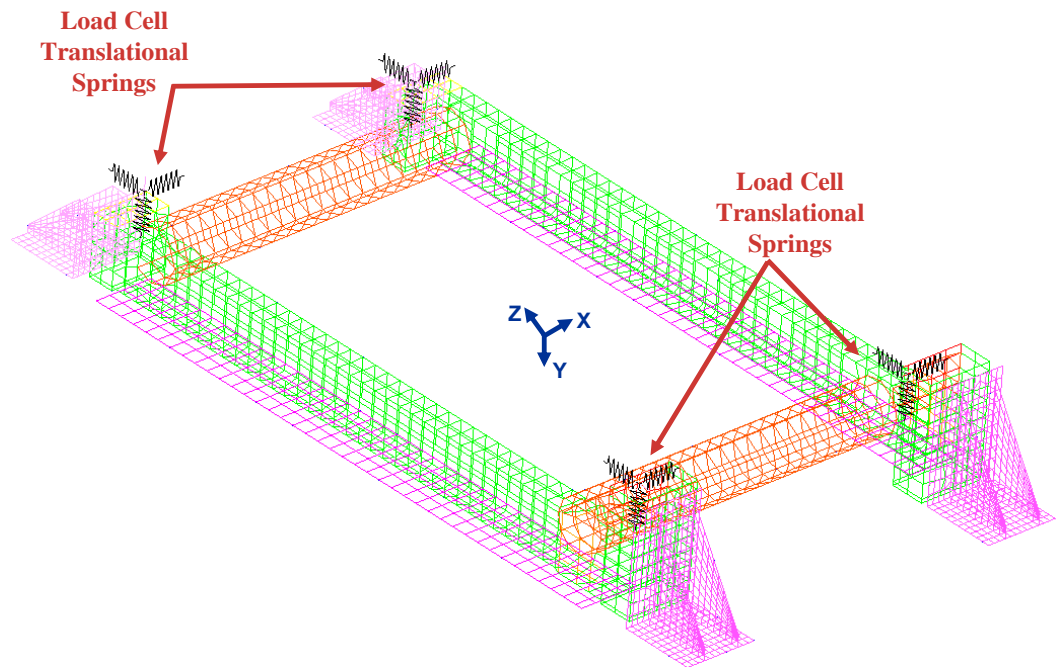


FIGURE 37– LOAD CELL TRANSLATIONAL SPRINGS

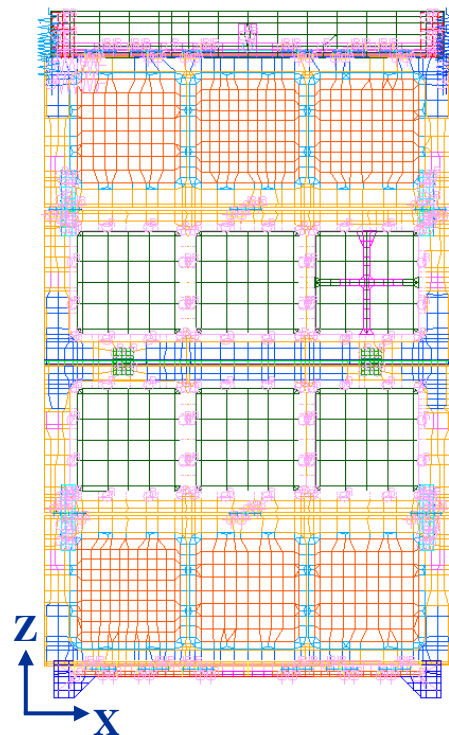


FIGURE 38– DOOR

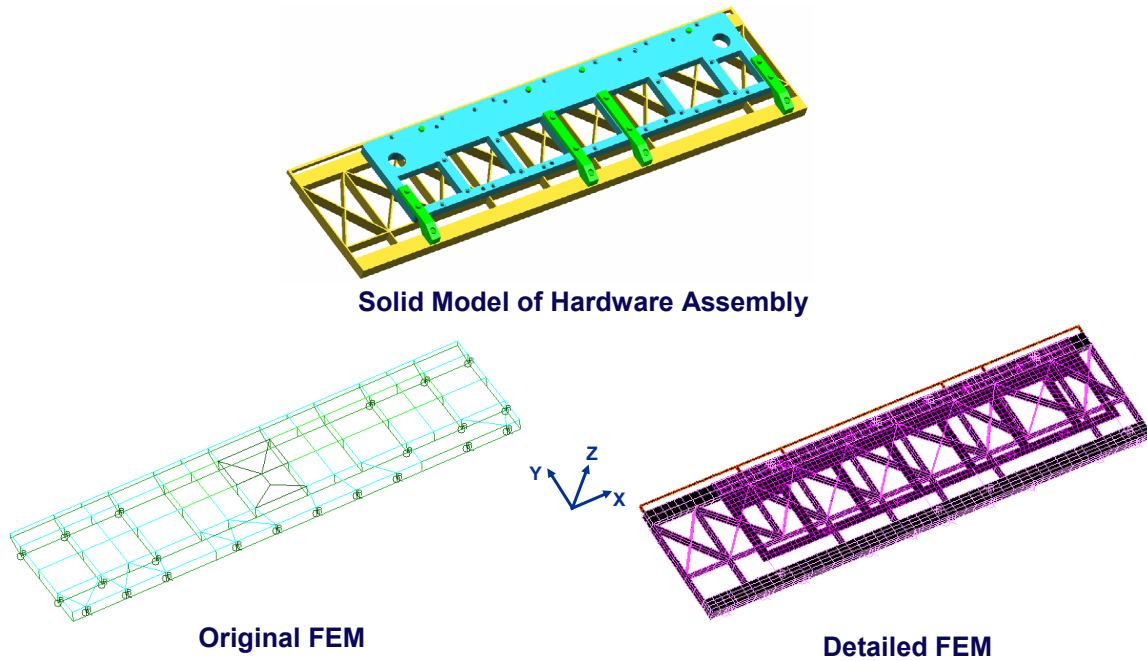


FIGURE 39 – COMPARISON OF COLDPLATE AND HARDBACK HARDWARE ASSEMBLY TO THE ORIGINAL AND DETAILED FEM

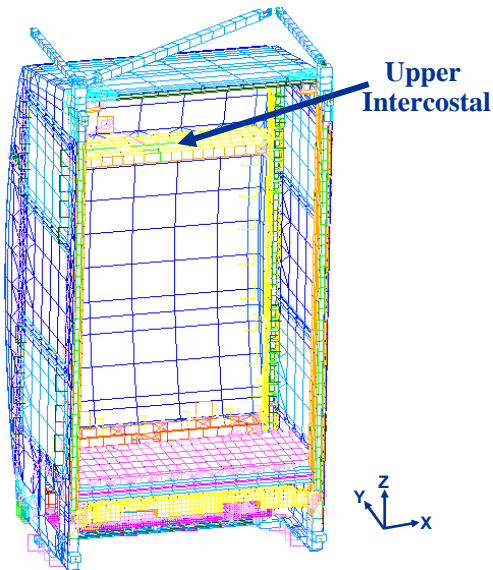


FIGURE 40 – UPPER INTERCOSTAL

Design variables having the greatest change from the pre-test model to the correlated model were the Upper Intercostal bending moment of inertia (-9.3% change), Door Young's Modulus (3.2% change), Coldplate Young's Modulus (2.3% change), and Hardback Young's Modulus (0.9% change). The load cell interface spring stiffness properties were previously correlated during the CIR modal test.

The Genetic algorithm was primarily used to correlate the model, with an overall RMS state variable error of 5.76% for the objective function (comparing the test and TAM target mode frequencies and cross-orthogonalities). The X-axis target mode frequency difference was -4.2%, the Y-axis target mode frequency difference was 2.1%, the Z-axis target mode frequency difference was 6.4%. All primary target mode cross-orthogonality values were greater than 90% (Figure 41). The Z-axis target mode was outside the frequency range of interest (0-50 Hz) for model correlation. These results are summarized in Table 8.

Figures 42 – 44 illustrate a comparison between the test and TAM modes, effective weight, and cross-orthogonality. The test and TAM modes shapes are dynamically back-expanded to improve visualization. The correlated model has high cross-orthogonality (>90%) for the primary target modes, satisfying the ISS model correlation criteria.

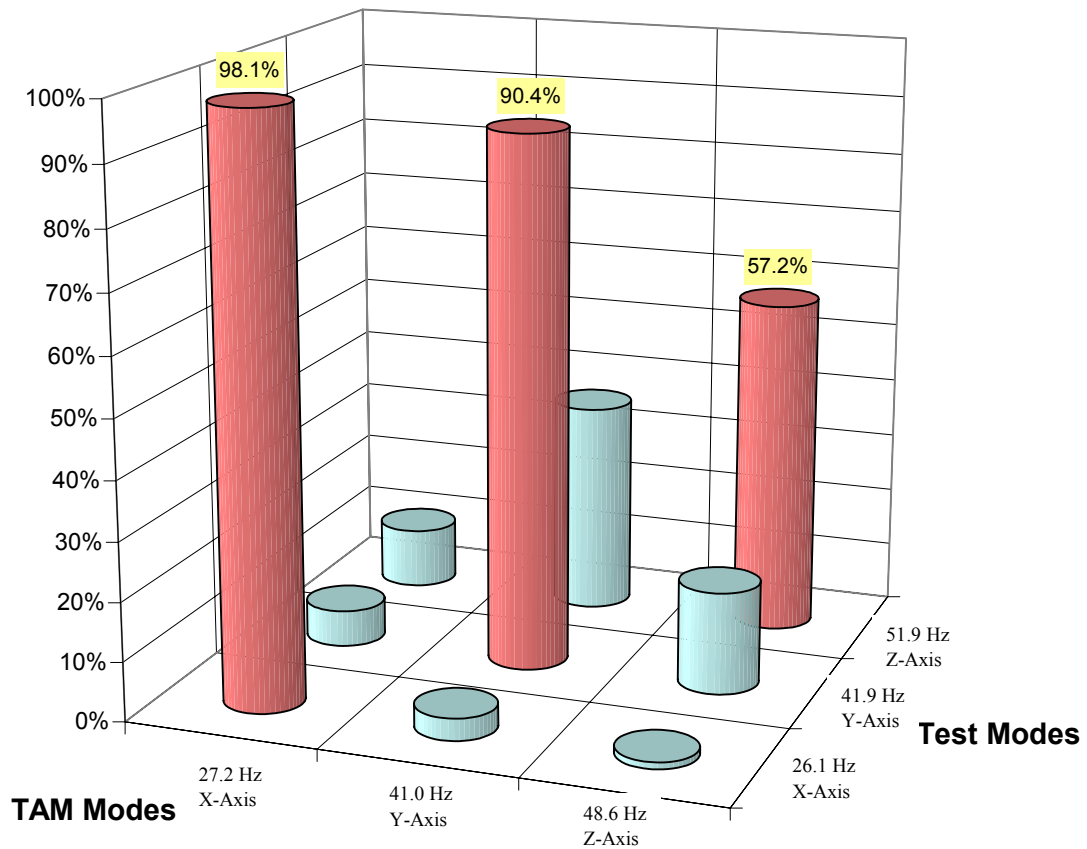


FIGURE 41 – FINAL CROSS-ORTHOGONALITY FOR TARGET MODES

Table 8 – Comparison of Test and TAM Target Mode Frequency Difference and Cross-Orthogonality

Mode	Freq (Hz)	TAM			Delta Freq	Mode Shape Description
		1	2	6		
Test	1	26.1	0.981	-0.037	-0.015	Rack X-axis Translation
	2	41.9	0.062	0.904	0.174	Rack Y-axis Translation
	3	51.9	-0.102	0.36	-0.572	Rack Z-axis Translation

Cross-Orthogonality 98.1%

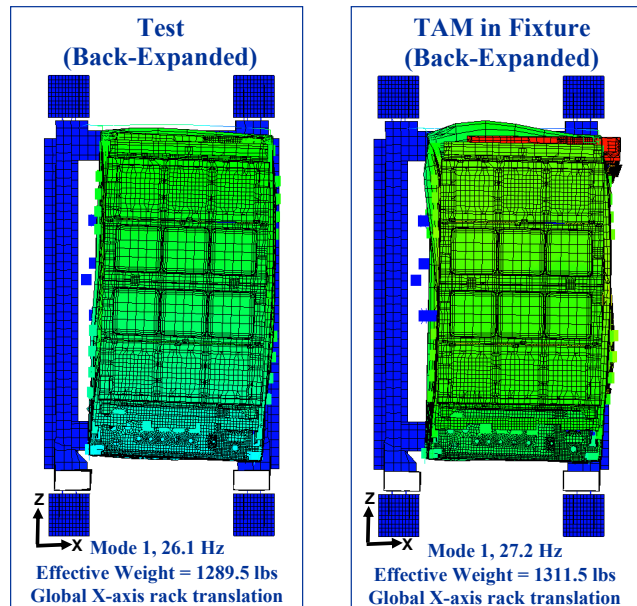


FIGURE 42 – X-AXIS TARGET MODE SHAPES, EFFECTIVE WEIGHT, AND CROSS-ORTHOGONALITY

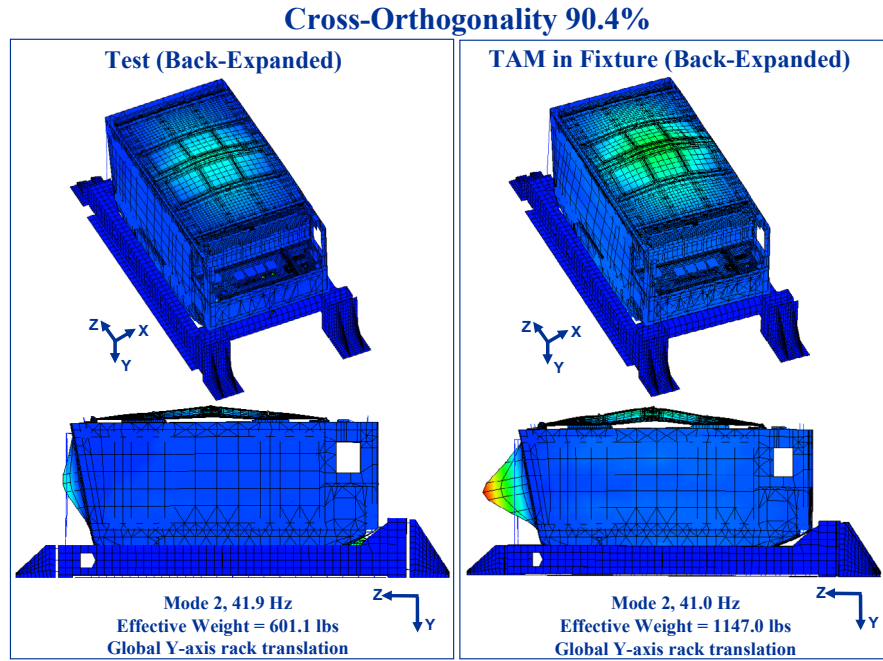


FIGURE 43 – Y-AXIS TARGET MODE SHAPES, EFFECTIVE WEIGHT, AND CROSS-ORTHOGONALITY

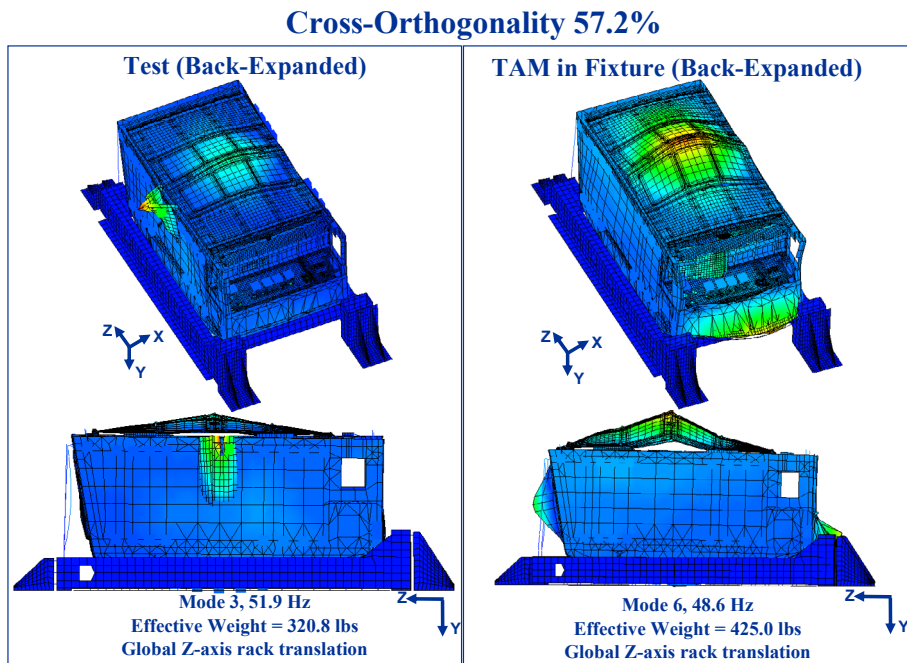


FIGURE 44 – Z-AXIS TARGET MODE SHAPES, EFFECTIVE WEIGHT, AND CROSS-ORTHOGONALITY

8. Conclusions

The FIR rack finite element model was successfully correlated based on the International Space Station model correlation criteria.

Three target modes were identified in test including two primary rack translation modes (X and Y axes) and a secondary Z axis mode. All model primary target modes had frequency differences less than 5% compared to test. The model secondary target mode has a frequency difference less than 6.4% compared to test (Table 8). The final cross-orthogonality between the correlated TAM and test mode shapes (Figure 41) was greater than 90% for all primary target modes.

9. References

1. "ISS Fluids and Combustion Facility Loads Model Verification Plan," NASA GRC presentation to the NASA JSC Structures Working Group, September 24, 2003.
2. "ISPR Qualification Modal Test Correlation," prepared by J. A. Knoll and H.A. Britt, Boeing rack model correlation report, 2-8F1A-HAB-049/95, Revision A, January 12, 1996.
3. "FIR Mass Properties Report," FIR-RPT-1734, Final, April 20, 2005.
4. "FCF FIR GIU Rack Modal Survey Test Report," SDL TR-05-12.
5. "Attune User's Guide," test/analysis correlation and modal updating software, Version 1.1, ATA Engineering, January 2005.

10. Acronym List

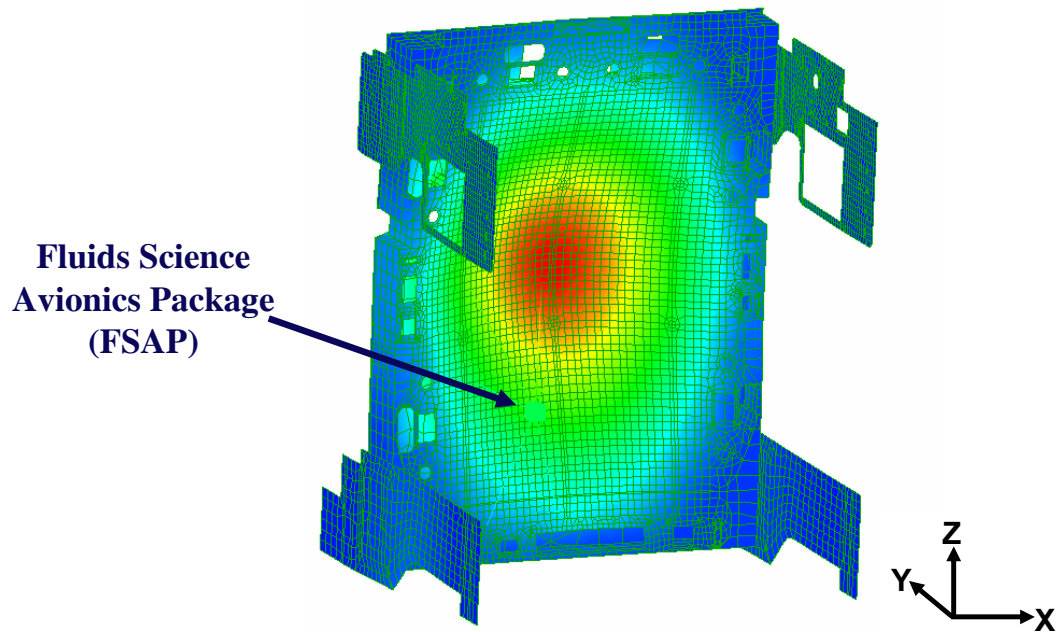
ARIS	Active Rack Isolation Subsystem	FSAP	Fluids Science Avionics Package
ATCS	Air Thermal Control System	FSR	Flight Safety Review
ATCU	Air Thermal Control Unit	GCIP	Gas Chromatograph Instrumentation Package
CDR	Critical Design Review	GN2	Gaseous Nitrogen
CIR	Combustion Integrated Rack	GIS	Gas Interface System
CSCI	Computer Software Configuration Item	GIU	Ground Integration Unit
DCM	Diagnostics Control Module	GSE	Ground Support Equipment
ECS	Environmental Control Subsystem	HFR	High Frame Rate
EDA	Engineering Development Article	HbMs	High Bit depth Multi Spectral Camera Package
EDU	Experiment Development Unit	HR	High Resolution
EM	Engineering Model	H/W	Hardware
EMI	Electro- Magnetic Interference	I&T	Integration and Test
EA	Experiment Assembly	IAM	Image Acquisition Module
EPCU	Electrical Power Control Unit	ICD	Interface Control Document
EVP	Exhaust Vent Package	I/F	Interface
Fab	Fabrication	IOP	Input/ Output Processor
FCF	Fluids and Combustion Facility	IPP	Image Processing Package
FCU	FOMA Control Unit	IPSU	Image Processing and Storage Unit
FDSS	Fire Detection and Suppression System	IPSU-A	Image Processing and Storage Unit, Version A
FEA	Fluids Experiment Assembly	IR	Infrared
FHA	Flight Hardware Availability	ISPR	International Standard Payload Rack
FIR	Fluids Integrated Rack	ISS	International Space Station
FMEA	Failure Modes and Effects Analysis		
FOMA	Fuel/Oxidizer Management Assembly		
LED	Light Emitting Diode	RMSA	Rack Maintenance Switch Assembly
LLL	Low Light Level	RPC	Remote Power Controller
LMM	Light Microscopy Module	RPCM	Remote Power Controller Module
MDCA	Multi-user Droplet Combustion Assembly	RUP	Rack Utility Panel
MEL	Microgravity Emissions Laboratory	SAMS	Space Acceleration Measurement System
MFC	Mass Flow Controller	SDL	Serial Data Link
MRDOC	Microgravity Research, Development and Ops Contract	SEI	Software Engineering Institute
MCF	Modal Confidence Factor	SMD	Silicon Mountain
NGIT	Northrop Grumman Information Technology	SPEL	Station Power Electronics Laboratory
OB	Optics Bench	SSC	Station Support Computer
OM	Optics Module	Temp	Temporary
OPI	Optics Plate Interface	TSC	Telescience Support Center
PaRIS	Passive Rack Isolation System	TSH	Tri-axial Sensor Head
PCS	Portable Computer System	T/O	Turnover
PFE	Portable Fire Extinguisher	UIP	Utility Interface Panel
PI	Principal Investigator	UF	Utilization Flight
PIA	Payload Integration Agreement	ULF	Utilization and Logistics Flight
PPH	Program-Provided Hardware	UV	Ultraviolet
PSH	Payload Support Hardware	VES	Vacuum Exhaust System
PSR	Pre-Ship Review	VP	Verification Plan
PTCU	Payload Training Center Unit	VRS	Vacuum Resource System
Qual	Qualification	VTR	Verification and Test Readiness
REU	Remote Electronic Unit	VVS	Vacuum Vent System
RFCA	Rack Flow Control Assembly	WFCA	Water Flow Control Assembly
RHA	Rack Handling Adapter	WTCS	Water Thermal Control System

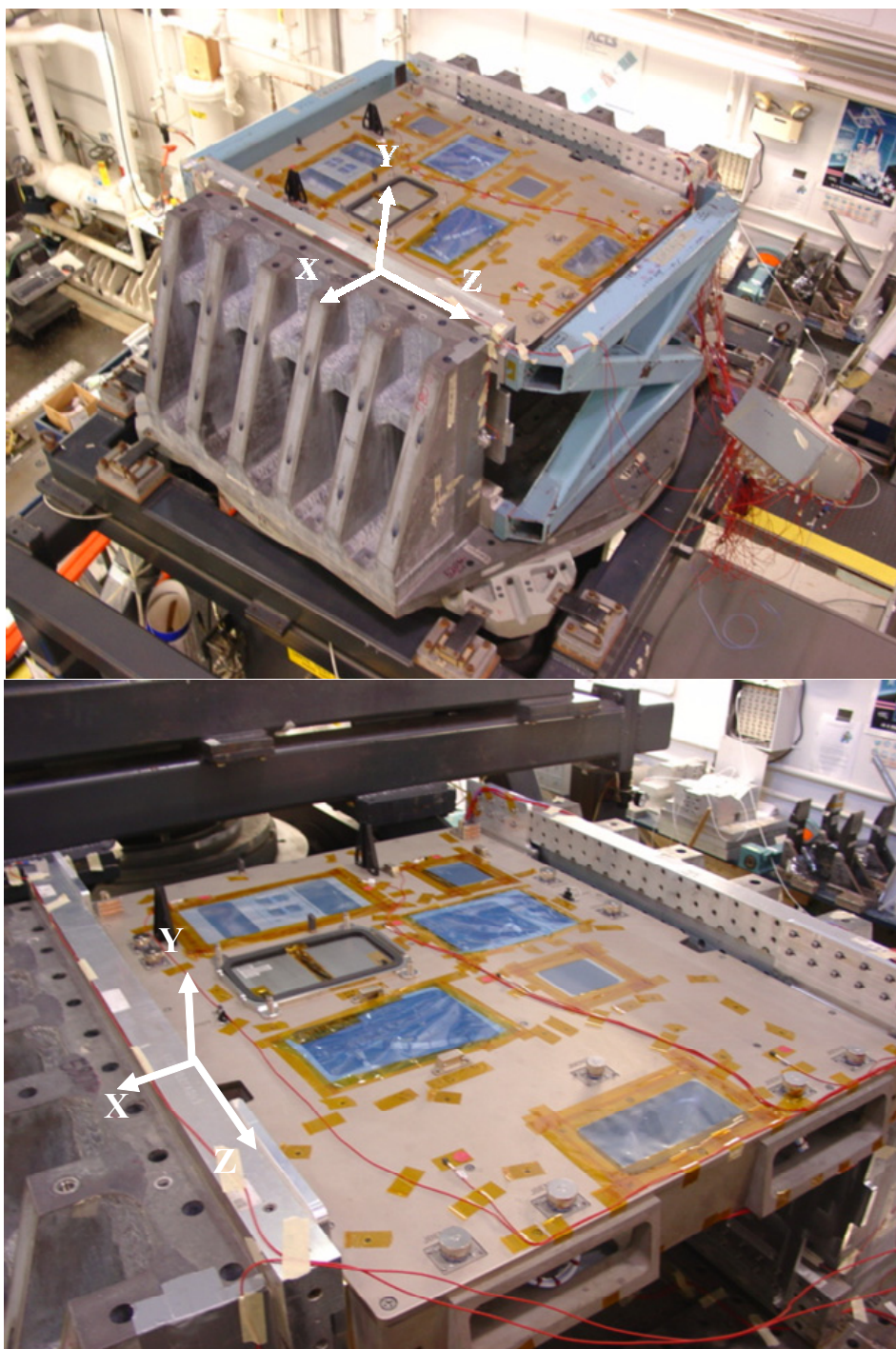
11. Appendices

Appendix A	FIR Optics Bench Model Correlation
Appendix B	Air Thermal Control Unit (ATCU) Model Correlation
Appendix C	Rack Door Model Correlation
Appendix D	Lower Package Structure Model Correlation
Appendix E	FIR Rack Modal Instrumentation Plan
Appendix F	FIR Rack Correlated Model Comparison of Frequency and Cross-Orthogonality

Appendix A

FIR Optics Bench with FSAP Model Correlation





FIR Optics Bench with FSAP Test Configuration

FIR Optics Bench with FSAP Comparison of FEM to TAM

FEM (65,568 DoF)			TAM (29 DoF)		
Mode	Frequency (Hz)	Effective Mass (%)	Mode	Frequency (Hz)	Effective Mass (%)
1	119.57	35.5% - Y	1	122.3	52.2% - Y
2	146.67	71.2% - X	2	148.5	65.9% - X
3	155.42	18.3% - X	3	158.7	28.4% - X
4	198.65		4	215.1	
5	220.76		5	242.4	17.3% - Y
6	261.86		6	300.5	35.6% - Z
7	263.41		7	327.3	37.7% - Z
8	267.77				
9	280.35				
10	281.44				
11	283.59	23.8% - Z			

BOLD INDICATES TARGET MODES

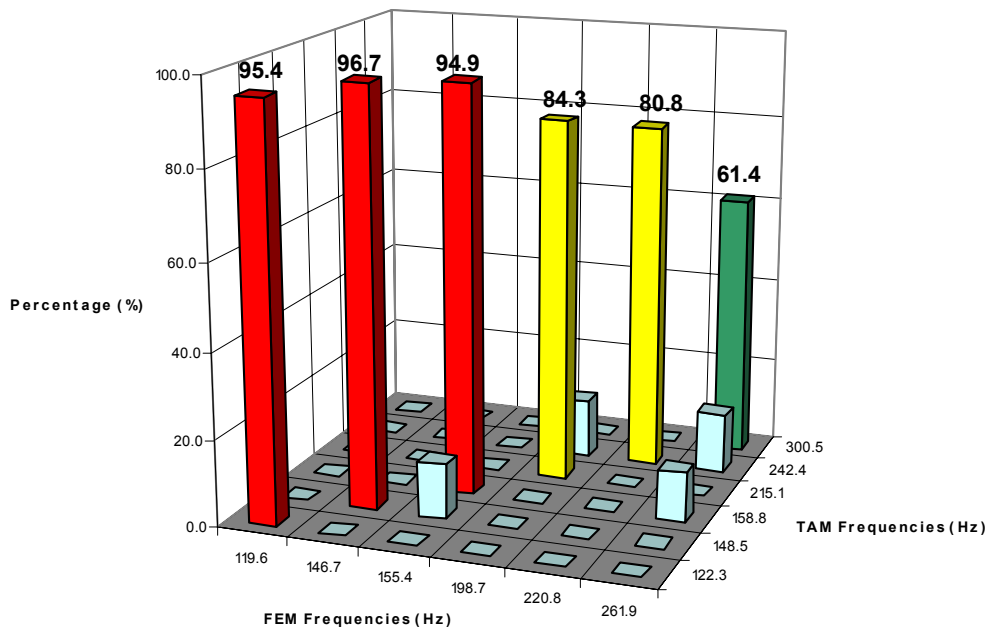
FIR Optics Bench with FSAP Comparison of FEM to TAM

MODE SHAPE DESCRIPTION	FEM FREQ (Hz)	TAM FREQ (Hz)	XORTHO %	% FREQ DIFF
Translation of FIR Optics Bench in Y-Axis	119.6	122.3	95.4	-2.30
Translation of FIR Optics Bench in X-Axis	146.7	148.5	96.7	-1.27

FIR Optics Bench with FSAP
Cross Orthogonality
FEM vs TAM

		TAM MODE FREQUENCIES						
		Mode Number	1	2	3	4	5	6
		Hz	122.3	148.5	158.8	215.1	242.4	300.5
FEM MODES FREQUENCIES	1	119.6	95.4	0.0	0.0	0.0	0.0	0.0
	2	146.7	0.0	96.7	0.0	0.0	0.0	0.0
	3	155.4	0.0	12.8	94.9	0.0	0.0	0.0
	4	198.7	0.0	0.0	0.0	84.3	13.6	0.0
	5	220.8	0.0	0.0	0.0	0.0	80.8	0.0
	6	261.9	0.0	0.0	11.4	0.0	14.1	61.4

FIR Optics Bench with FSAP
Cross Orthogonality Graph
FEM vs TAM



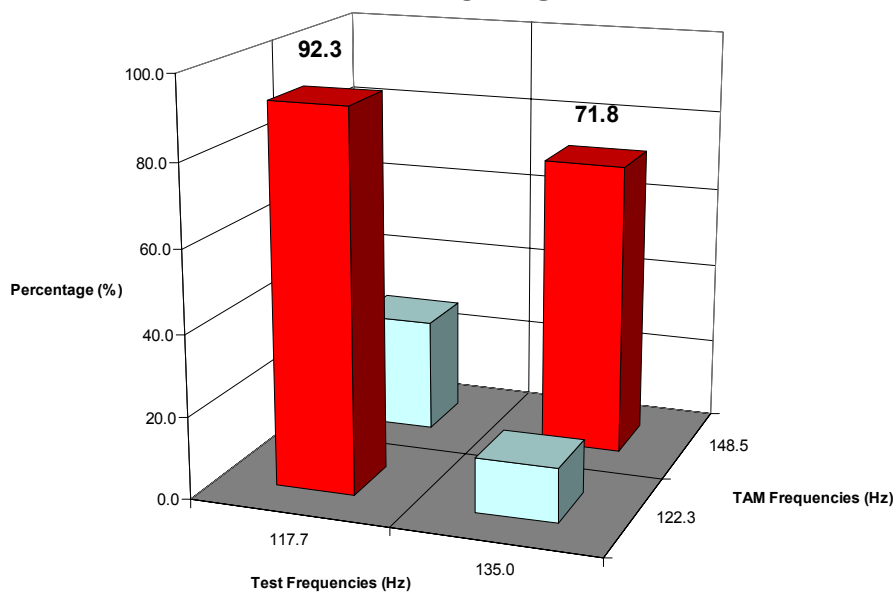
FIR Optics Bench with FSAP Comparison of TAM to TEST

MODE SHAPE	TAM	TEST	XORTHO	% FREQ
DESCRIPTION	FREQ (Hz)	FREQ (Hz)	%	DIFF
Translation of FIR Optics Bench in Y-Axis	122.3	117.7	92.3	-3.91
Translation of FIR Optics Bench in X-Axis	148.5	135.0	71.8	-10.00

FIR Optics Bench with FSAP Cross Orthogonality TAM vs TEST

		TEST MODE FREQUENCIES		
		Mode Number	1	2
TAM		Hz	117.7	135.0
MODE	1	122.3	92.3	27.7
FREQUENCIES	2	148.5	13.2	71.8

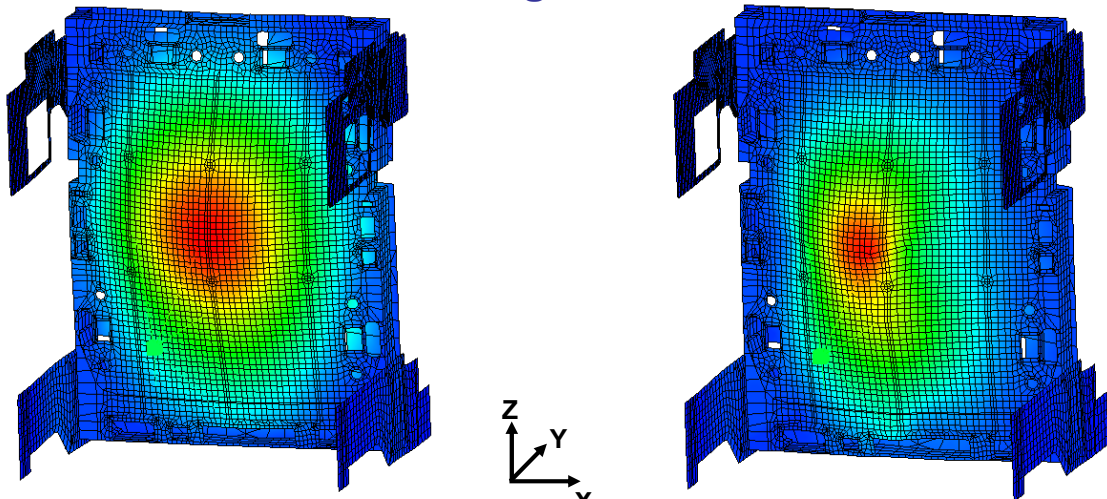
FIR Optics Bench with FSAP Cross Orthogonality Graph TAM vs TEST



FIR Optics Bench with FSAP Comparison of FEM to TEST

MODE SHAPE	FEM	TEST	% FREQ
DESCRIPTION	FREQ (Hz)	FREQ (Hz)	DIFF
Translation of FIR Optics Bench in Y-Axis	119.6	117.7	-1.59
Translation of FIR Optics Bench in X-Axis	146.7	135.0	-8.64

FIR Optics Bench with FSAP Comparison of FEM to Test Mode Shapes - Y Axis Cross-Orthogonality 92.3%

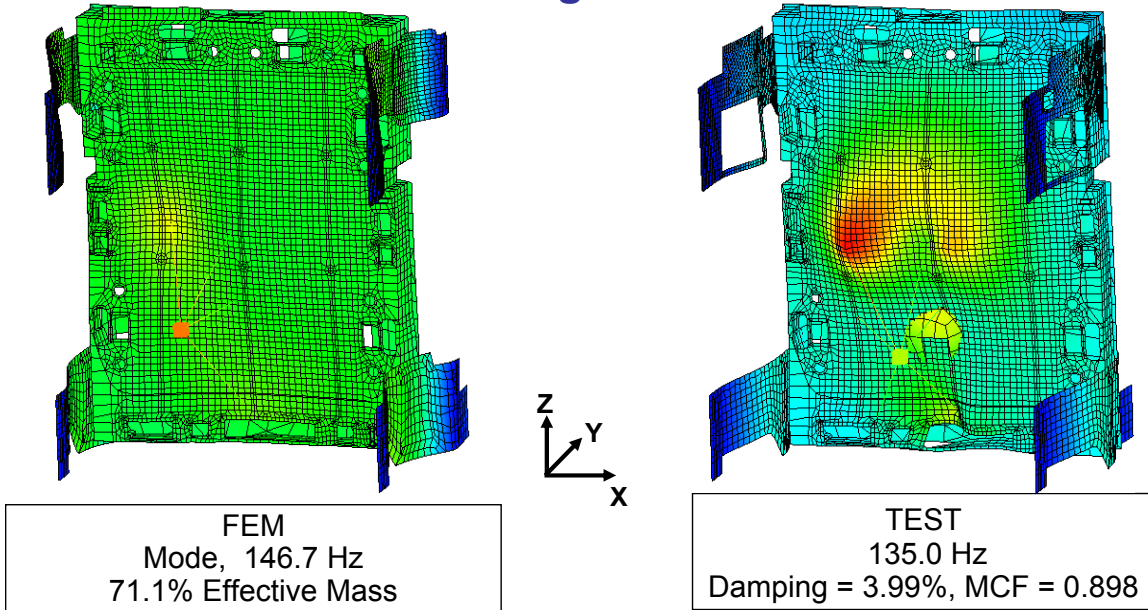


FEM
Mode 1, 119.6 Hz
35.5 % Effective Mass

TEST
117.7 Hz
Damping = 4.22%, MCF = 0.487

1st Bending Mode of the Optics Bench in the Y-Axis

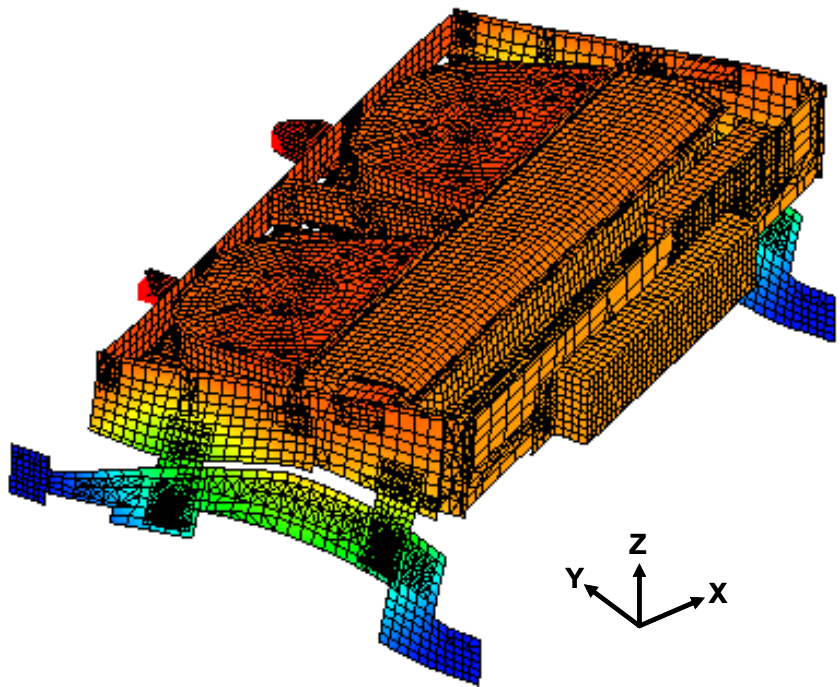
FIR Optics Bench with FSAP
Comparison of FEM to Test
Mode Shapes - X Axis
Cross-Orthogonality 71.8%

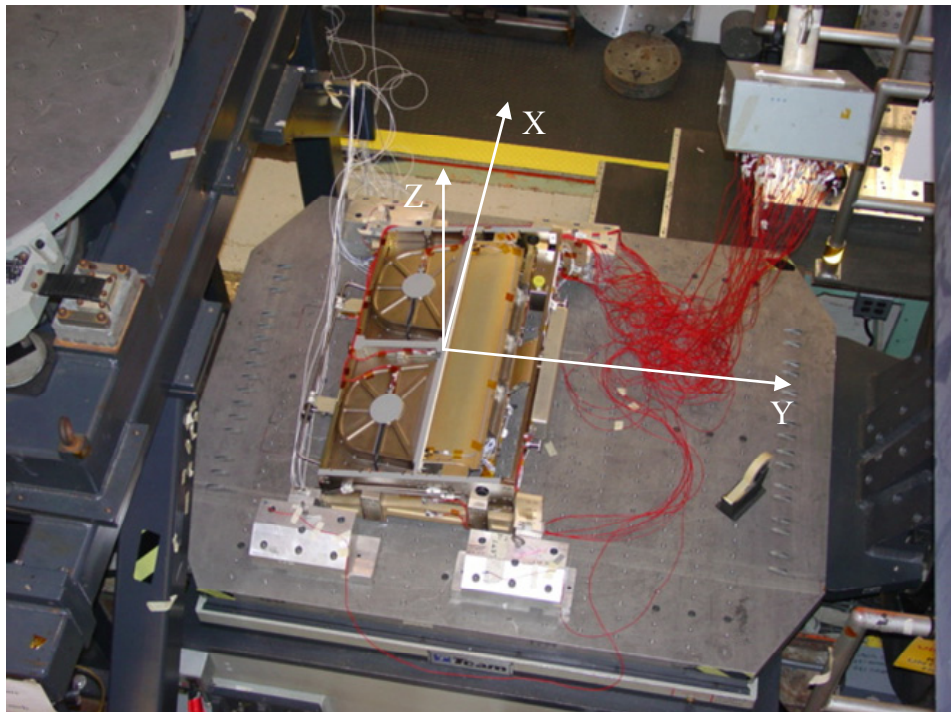
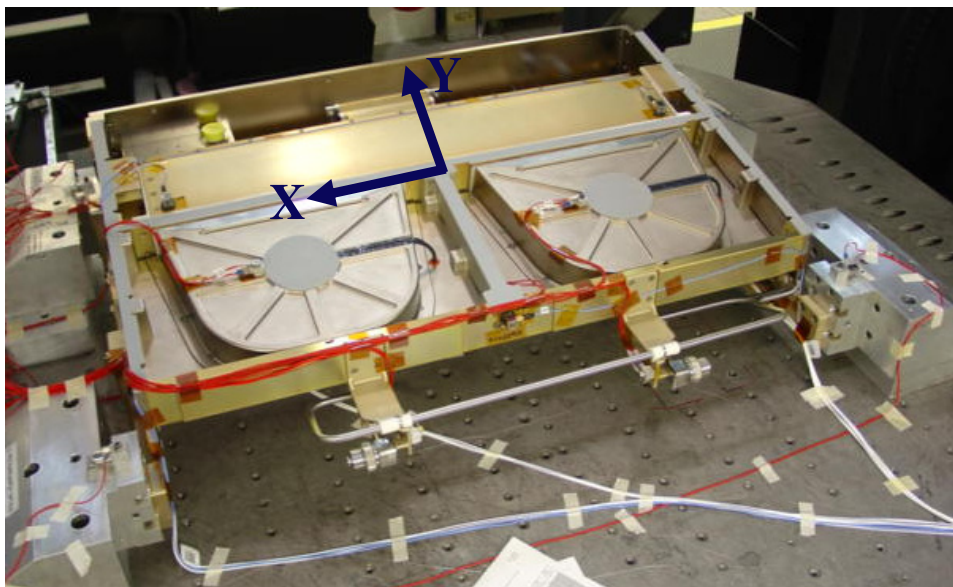


Translation of the Optics Bench in the X-Axis

Appendix B

FIR ATCU Model Correlation





ATCU Test Configuration

FIR ATCU Comparison of FEM to TAM

FEM (20,392 DoF)			TAM (55 DoF)		
Mode	Frequency (Hz)	Effect Mass (%)	Mode	Frequency (Hz)	Effect Mass (%)
1	60.9	94.8-X	1	61.4	99.7-X
2	77.0	27.1-X	2	85.5	46.2-Z
3	89.3		3	110.5	59.8-Y
4	93.2	16.1-Z			
5	103.3	49.7-Y			

BOLD INDICATES TARGET MODES

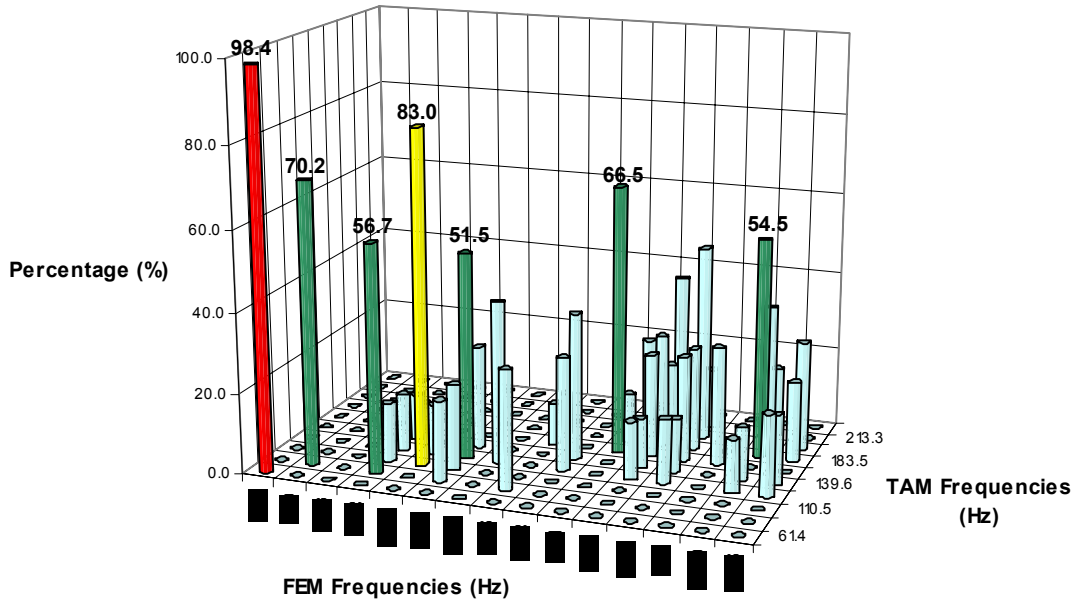
FIR ATCU Comparison of FEM to TAM

MODE SHAPE DESCRIPTION	FEM	TAM	XORTHO	% FREQ
	FREQ (Hz)	FREQ (Hz)	%	DIFF
Translation of the ATCU in the X-Axis	60.9	61.4	98.7	0.8
In Phase Translation of the ATCU Fans in the Z-Axis	77.0	85.5	94.9	9.9
Translation of the ATCU in the Y-Axis	103.3	110.5	80.7	6.5

FIR ATCU Cross Orthogonality FEM vs TAM

FEM MODE FREQUENCIES	Mode Number	TAM MODE FREQUENCIES									
		1	2	3	4	5	6	7	8	9	10
		Hz	61.4	85.5	110.5	135.3	139.6	176.4	183.5	199.4	213.3
	1	60.9	98.4	0.0	0.0	0.0	0.0	0.0	0.0	0.0	0.0
	2	77.0	0.0	70.2	0.0	0.0	0.0	0.0	0.0	0.0	0.0
	3	89.3	0.0	0.0	0.0	0.0	0.0	0.0	0.0	0.0	0.0
	4	93.2	0.0	56.7	14.8	14.3	11.5	0.0	0.0	0.0	0.0
	5	103.3	0.0	0.0	83.0	12.6	0.0	0.0	0.0	0.0	0.0
	6	145.0	0.0	20.1	21.5	51.5	25.7	0.0	0.0	0.0	0.0
	7	124.4	0.0	0.0	0.0	40.3	0.0	0.0	0.0	0.0	0.0
	8	155.5	0.0	29.6	0.0	0.0	0.0	10.5	10.2	0.0	0.0
	9	157.2	0.0	0.0	0.0	28.4	36.7	0.0	0.0	0.0	0.0
	10	161.1	0.0	0.0	0.0	0.0	0.0	66.5	12.2	0.0	21.0
	11	167.2	0.0	0.0	0.0	14.4	12.5	25.8	28.0	18.1	38.2
	12	168.5	0.0	0.0	0.0	16.1	13.4	26.2	25.7	48.8	15.3
	13	175.1	0.0	0.0	0.0	0.0	0.0	29.3	0.0	0.0	0.0
	14	180.9	0.0	0.0	0.0	13.2	13.3	0.0	54.5	35.5	17.3
	15	184.5	0.0	0.0	0.0	20.3	17.4	0.0	20.0	27.6	0.0

FIR ATCU Cross Orthogonality Graph FEM vs TAM



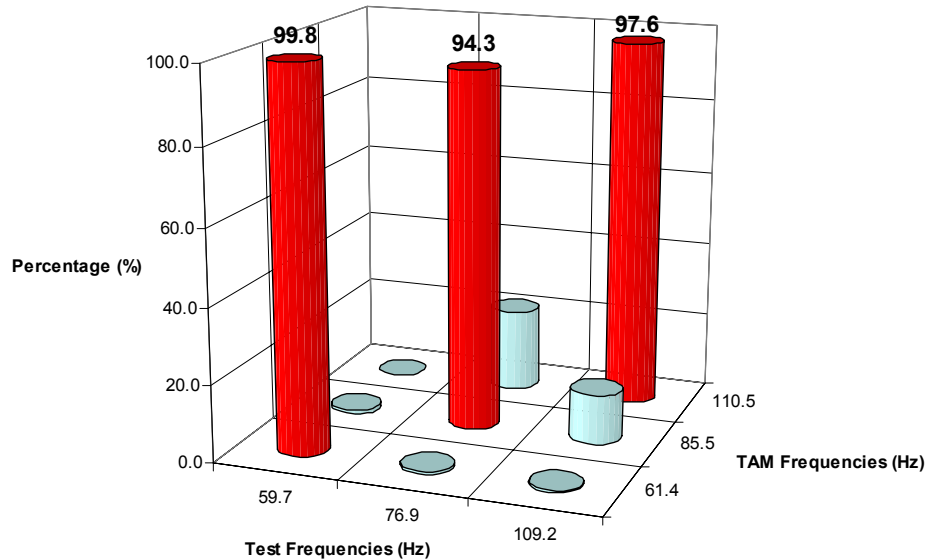
FIR ATCU Comparison of TAM to TEST

MODE SHAPE DESCRIPTION	TAM FREQ (Hz)	TEST FREQ (Hz)	XORTHO %	% FREQ DIFF
Translation of ATCU in the X-axis	61.4	59.7	99.8	-2.8
In Phase Translation of the ATCU Fans in the Z-Axis	85.5	79.6	94.3	-7.4
Translation of ATCU in Y-axis	110.5	109.2	97.6	-1.2

FIR ATCU Cross Orthogonality TAM vs TEST

	Mode Number	TEST MODE FREQUENCIES			
		1	2	4	
TAM		Hz	59.7	76.9	109.2
MODE	1	61.4	99.8	0.7	0.4
FREQUENCIES	2	85.5	0.8	94.3	13.1
	3	110.5	0.0	21.8	97.6

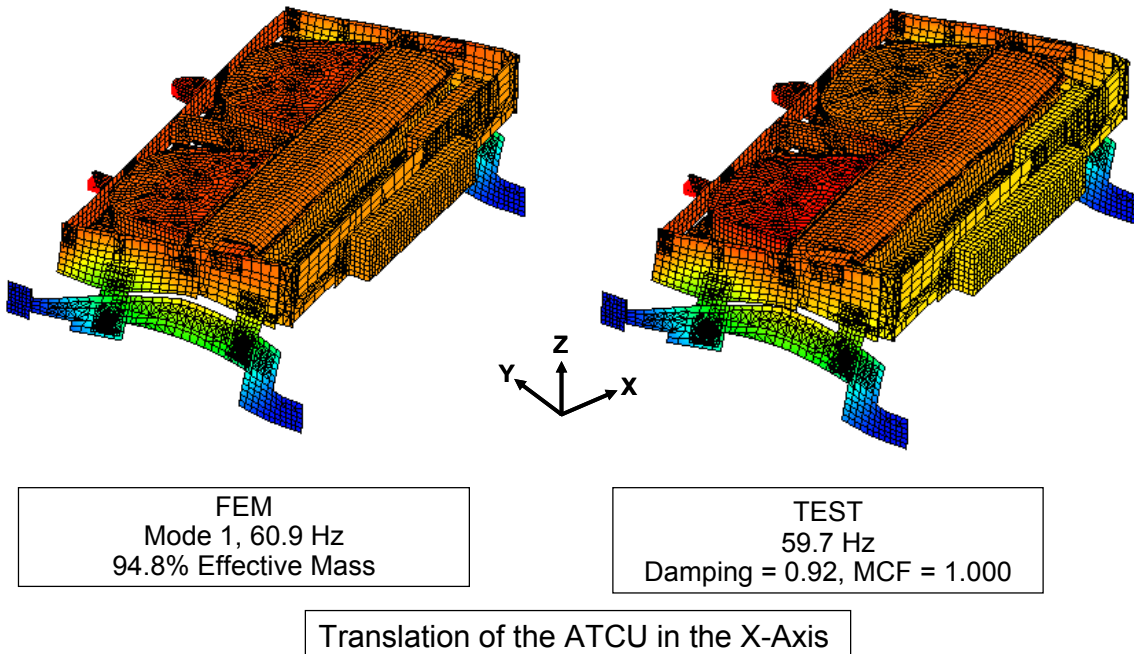
FIR ATCU
Cross Orthogonality Graph
TAM vs TEST



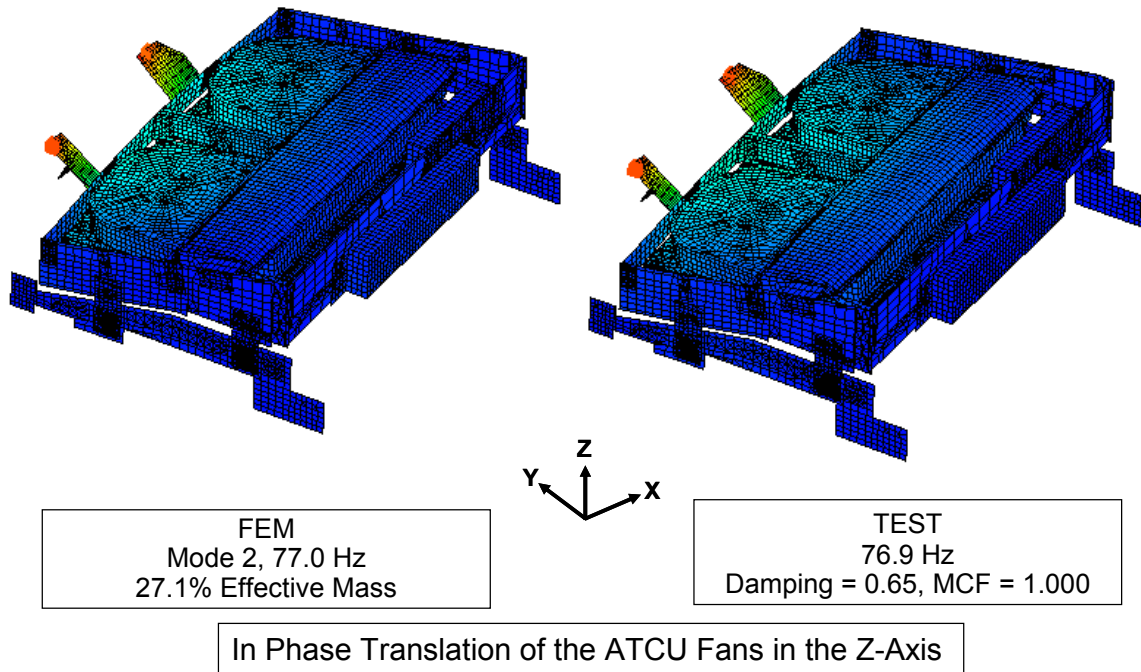
FIR ATCU
Comparison of FEM to TEST

MODE SHAPE DESCRIPTION	FEM FREQ (Hz)	TEST FREQ (Hz)	% FREQ DIFF
Translation of the ATCU in the X-Axis	60.9	59.7	2.0
In Phase Translation of the ATCU Fans in the Z-Axis	77.0	76.9	0.1
Translation of the ATCU in the Y-Axis	103.3	109.2	5.4

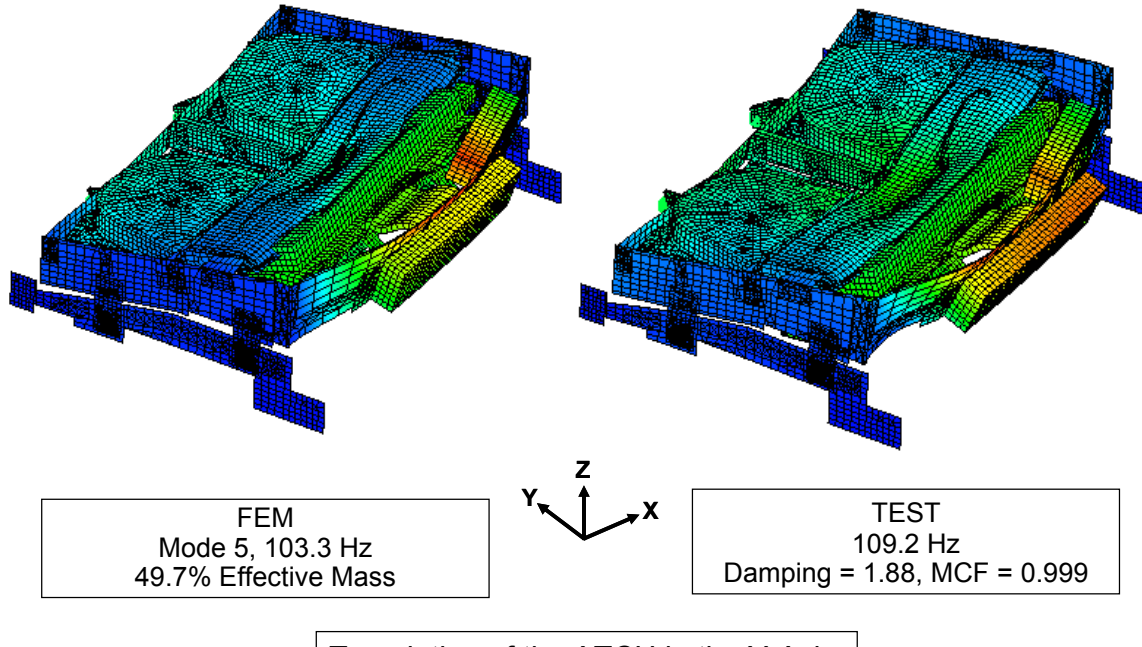
**Comparison of FIR ATCU FEM with Test
Mode Shapes - X Axis
Cross-Orthogonality 99.8%**



**Comparison of FIR ATCU FEM with Test
Mode Shapes - Z Axis
Cross-Orthogonality 94.3%**

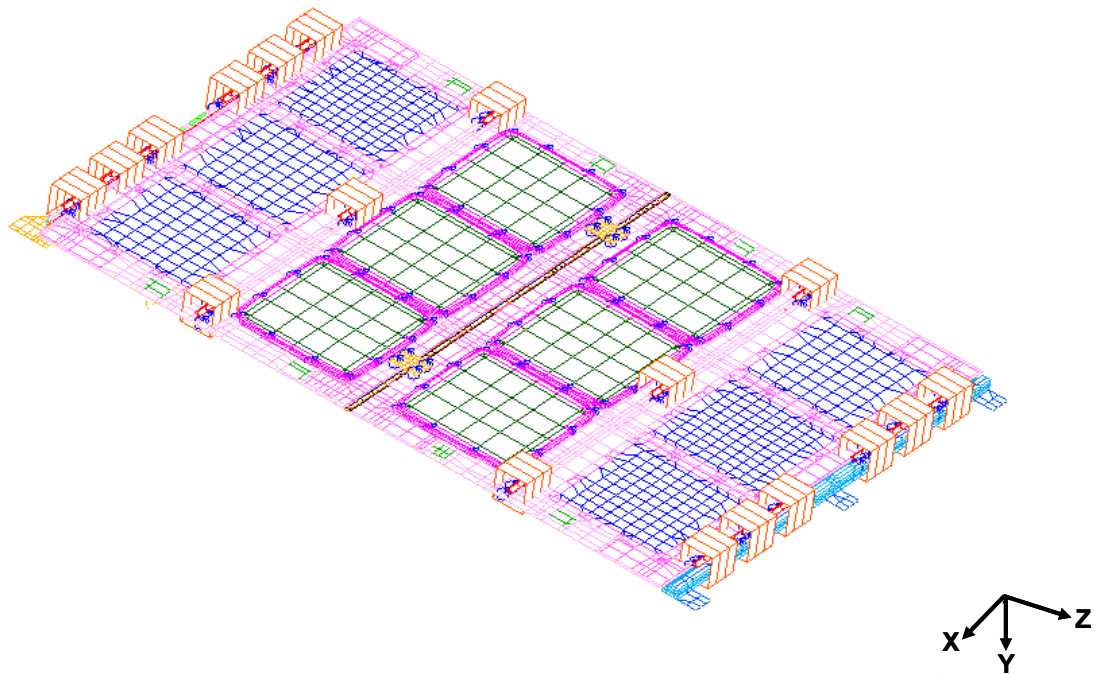


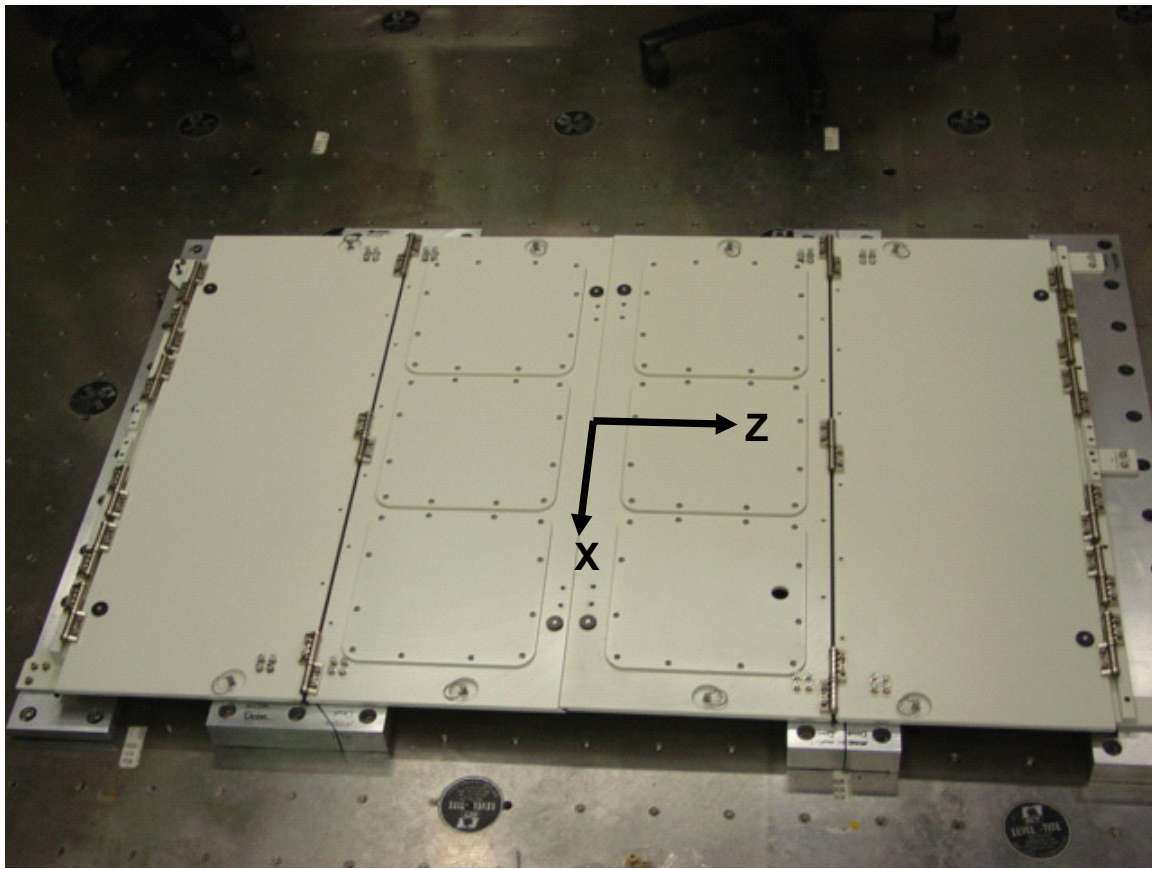
**Comparison of FIR ATCU FEM with Test
Mode Shapes - Y Axis
Cross-Orthogonality 92.3%**



Appendix C

CIR Rack Door Model Correlation





Rack Door Test Configuration

CIR Rack Door Comparison of FEM to TAM

FEM (33,396 Grid Pts)			TAM (39 DoF)		
Mode	Frequency (Hz)	Effect Mass (%)	Mode	Frequency (Hz)	Effect Mass (%)
1	57.9	33.3-Y	1	58.2	57.3-Y
2	90.1	1.6-Y	2	91.5	
3	99.7	12.3-Y	3	101.6	17.1-Y
4	112.1		4	113.9	

BOLD INDICATES TARGET MODES

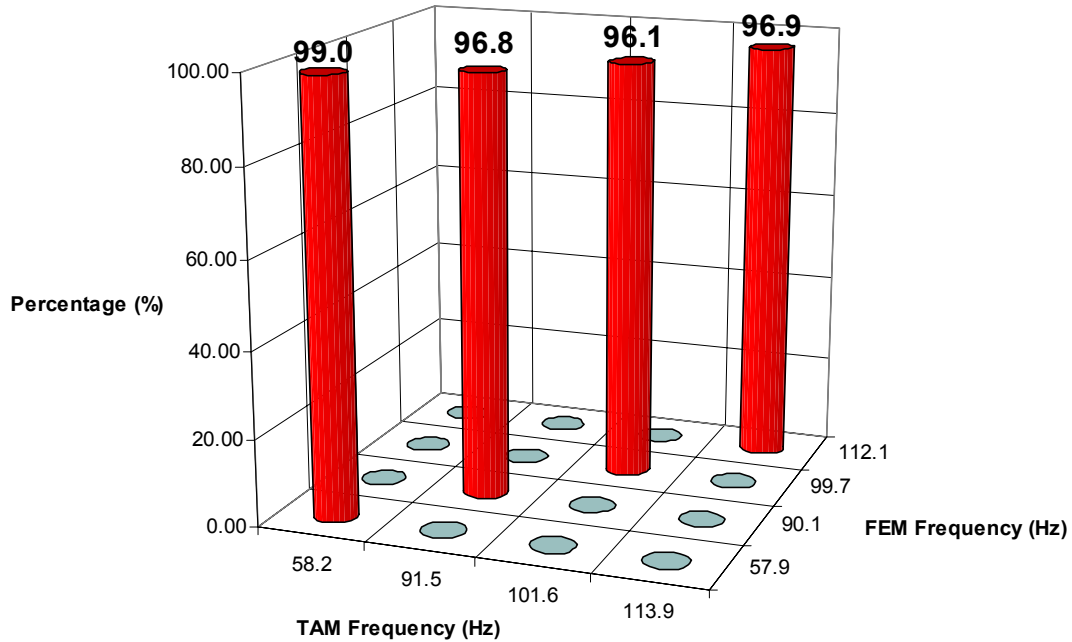
Comparison of CIR Rack Door FEM with TAM

MODE SHAPE	FEM	TAM	XORTHO	% FREQ
DESCRIPTION	FREQ (Hz)	FREQ (Hz)	%	DIFF
Y-axis First Bending Mode of the Doors	57.9	58.2	99.0	0.5
Y-axis Second Bending Mode of the Doors	90.1	91.5	96.8	1.6
Y-axis Third Bending Mode of the Doors	99.7	101.6	96.1	1.9

CIR Rack Door Cross Orthogonality FEM vs TAM

				TAM MODE													
	Mode Number			1	2	3	4	5	6	7	8	9	10				
		Hz	58.2	91.5	101.6	113.9	163.3	176.0	203.3	223.7	230.3	247.3					
	1		57.9	99.0	0.0	0.0	0.0	0.0	0.0	0.0	0.0	0.0	0.0				
FEM	2		90.1	0.0	96.8	0.0	0.0	0.0	0.0	0.0	0.0	0.0	0.0				
MODE	3		99.7	0.0	0.0	96.1	0.0	0.0	0.0	0.0	0.0	0.0	0.0				
	4		112.1	0.0	0.0	0.0	96.9	0.0	0.0	0.0	0.0	0.0	0.0				

CIR Rack Door Cross Orthogonality Graph FEM vs TAM



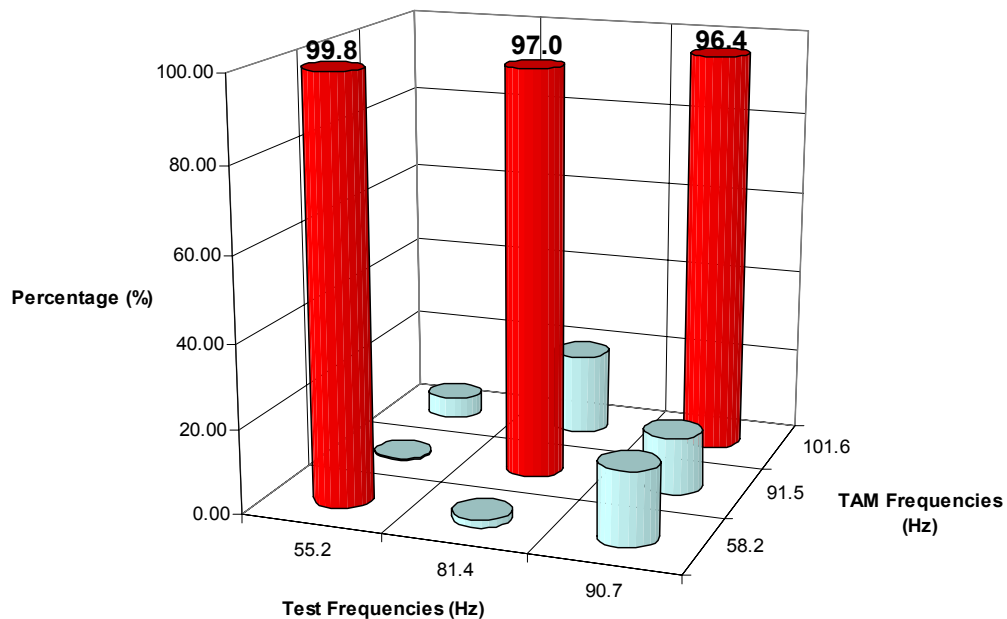
Comparison of CIR Rack Door TAM with Test

MODE SHAPE DESCRIPTION	TAM FREQ (Hz)	TEST FREQ (Hz)	XORTHO %	% FREQ DIFF
Y-axis First Bending Mode of the Doors	58.2	55.2	99.8	5.2
Y-axis Second Bending Mode of the Doors	91.5	81.4	97.0	11.1
Y-axis Third Bending Mode of the Doors	101.6	90.7	96.4	10.8

CIR Rack Door Cross Orthogonality TAM vs TEST

		TEST MODE			
		Mode Number	1	2	3
TAM	Mode Number	Freq (Hz)	55.2	81.4	90.7
	1	58.2	99.8	1.7	17.5
	2	91.5	0.4	97.0	13.7
	3	101.6	4.9	19.7	96.4

CIR Rack Door Cross Orthogonality Graph TAM vs TEST

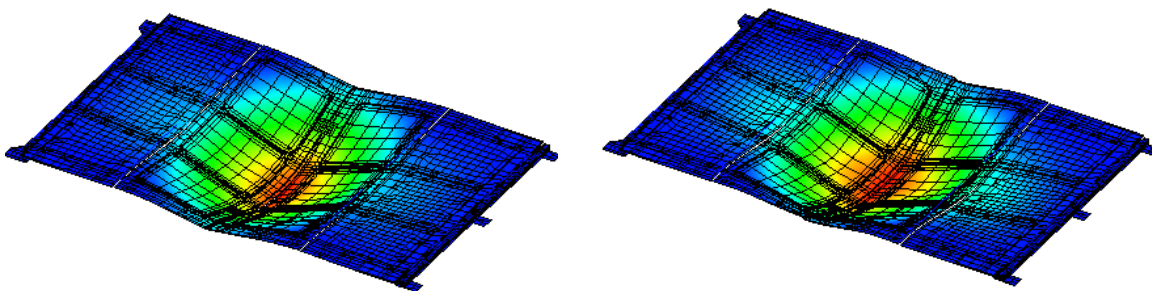


Comparison of CIR Rack Door FEM with Test

MODE SHAPE	FEM	TEST	% FREQ
DESCRIPTION	FREQ (Hz)	FREQ (Hz)	DIFF
Y-axis First Bending Mode of the Doors	57.9	55.2	4.9
Y-axis Second Bending Mode of the Doors	90.1	81.4	10.7
Y-axis Third Bending Mode of the Doors	99.7	90.7	9.9

Comparison of CIR Rack Door FEM with Test

Mode Shapes - Y Axis
Cross-Orthogonality 99.8%

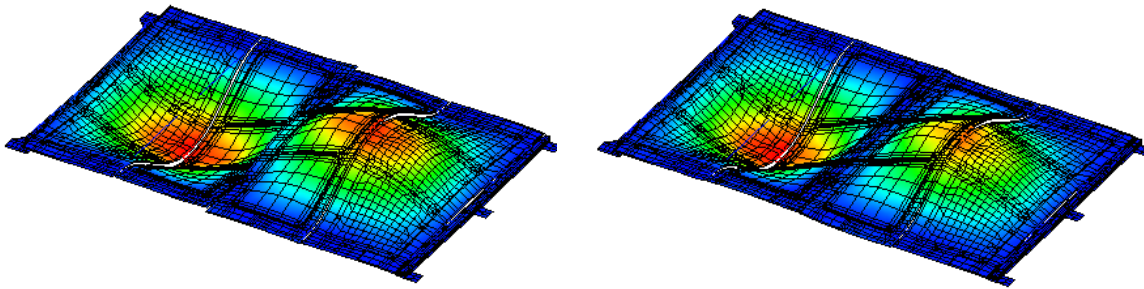


FEM
Mode 1, 57.9 Hz
33.3 % Effective Mass

TEST
55.2 Hz
Damping = 0.636 , MCF = 1.000

Y-axis First Bending Mode of the Doors

**Comparison of CIR Rack Door
FEM with Test
Mode Shapes - Y Axis
Cross-Orthogonality 97.0%**

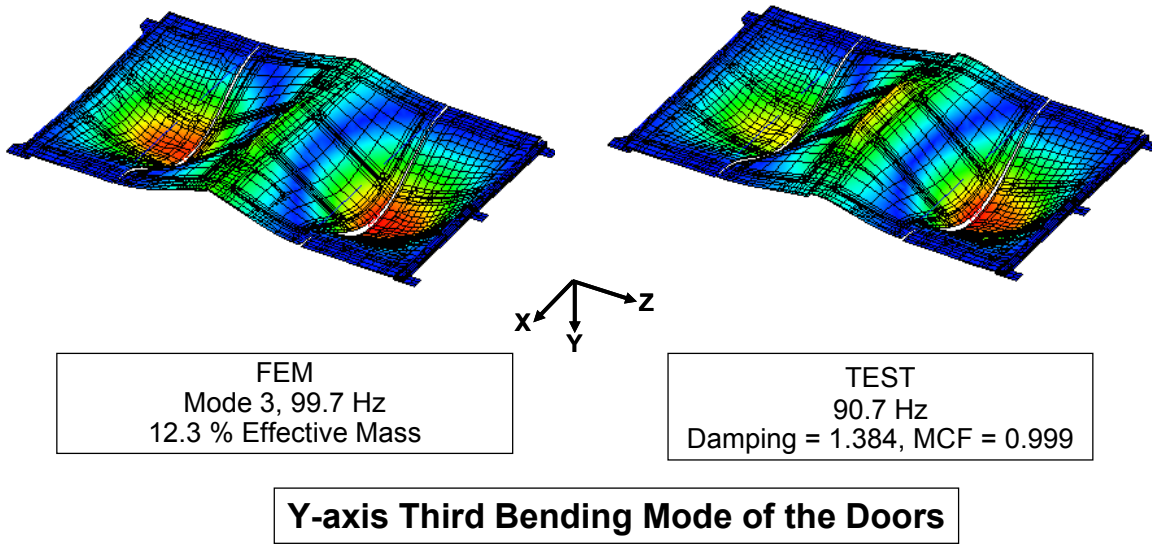


FEM
Mode 2, 90.1 Hz
1.6 % Effective Mass

TEST
81.4 Hz
Damping = 1.666 , MCF = 0.997

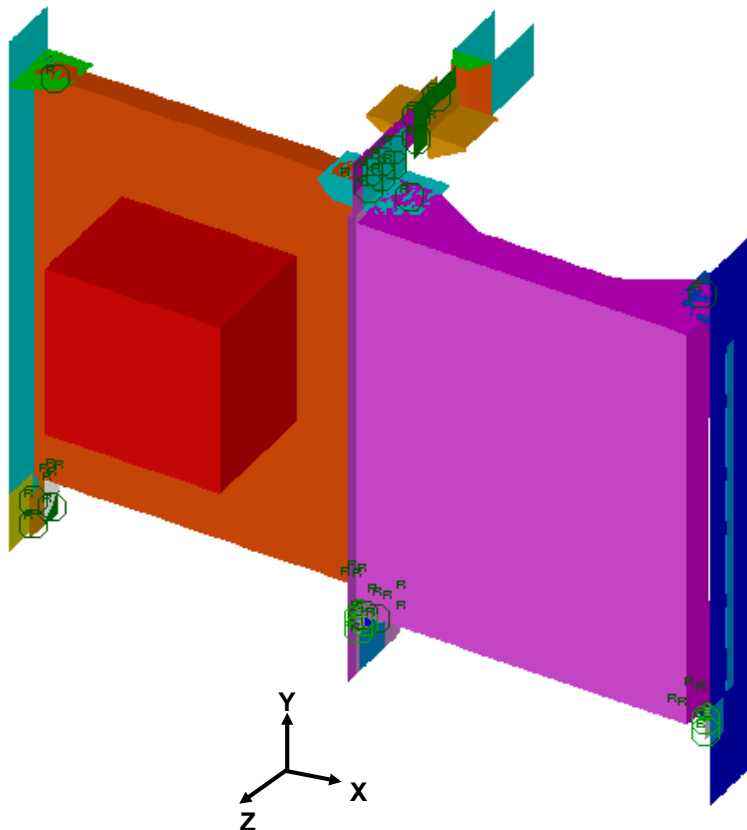
Y-axis Second Bending Mode of the Doors

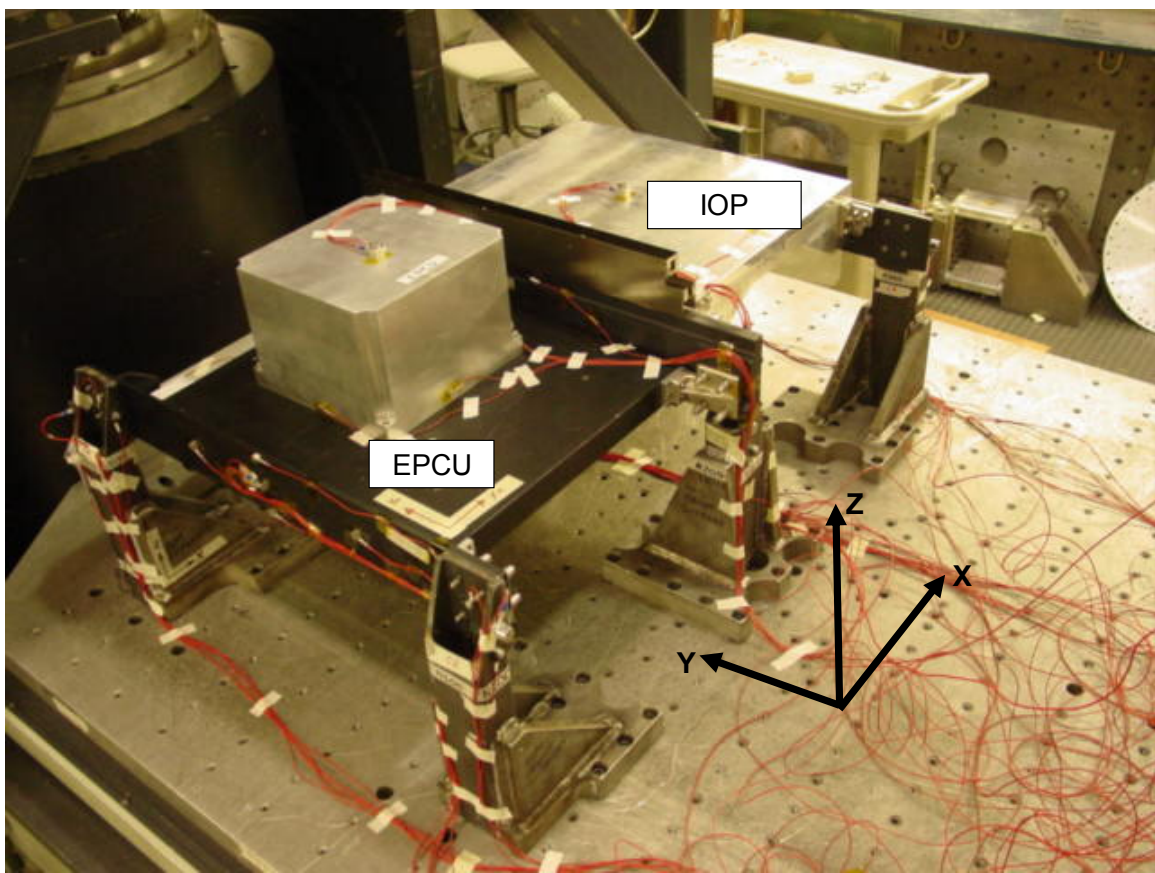
**Comparison of CIR Rack Door
FEM with Test
Mode Shapes - Y Axis
Cross-Orthogonality 96.4%**



Appendix D

CIR Lower Structure Assembly Model Correlation





Lower Structure Assembly Test Configuration

CIR Lower Structure Assembly
Comparison of FEM to TAM

FEM (100,944 DoF)			TAM (38 DoF)		
Mode	Frequency (Hz)	Effect Mass (%)	Mode	Frequency (Hz)	Effect Mass (%)
1	105.7	25.8-X	1	106.4	29.5-X
2	125.2	44.5-Z	2	127.3	55.7-Z
3	143.9	21.4-X	3	145.7	25.5-X
4	173.8		4	176.7	
5	175.2	60.2-Y	5	177.9	56.3-Y

BOLD INDICATES TARGET MODES

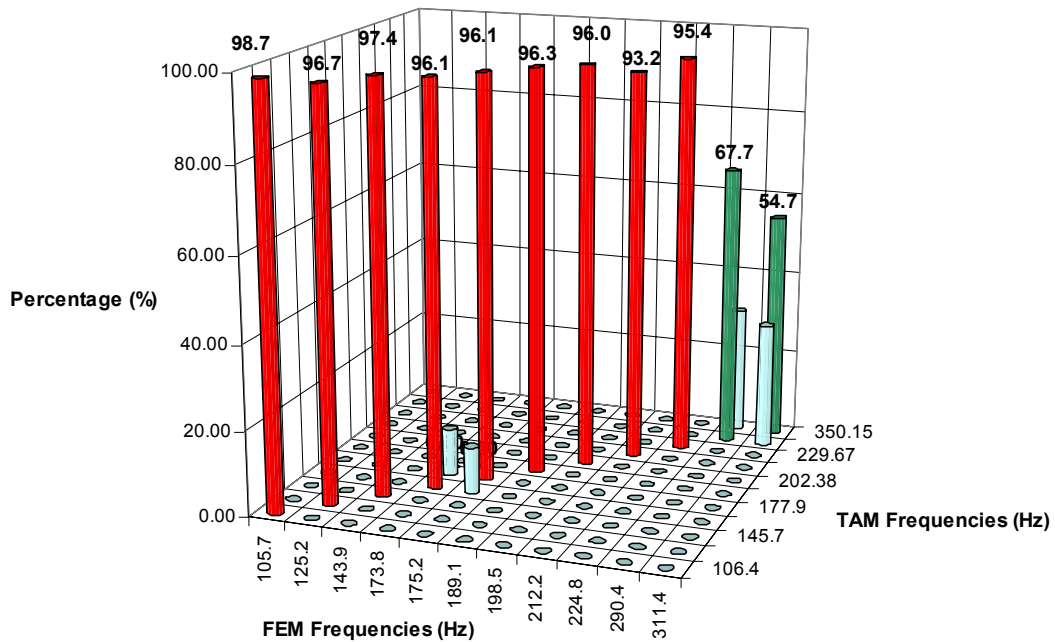
Comparison of CIR Lower Structure
FEM with TAM

MODE SHAPE DESCRIPTION	FEM FREQ (Hz)	TAM FREQ (Hz)	XORTHO %	% FREQ DIFF
Translation of the Lower Structure in the X-Axis	105.7	106.4	98.7	0.6
Translation of the EPCU in the Z-Axis	125.2	127.3	96.7	1.7
Translation of the Lower Structure in the Y-Axis	175.2	177.9	96.1	1.6

CIR Lower Structure Assembly Cross Orthogonality FEM vs TAM

	Mode Number	TAM MODE										
		1	2	3	4	5	6	7	8	9	10	11
	Hz	106.4	127.3	145.7	176.5	177.9	192.4	202.4	219.0	229.7	331.5	350.2
1		105.7	98.7	0.0	0.0	0.0	0.0	0.0	0.0	0.0	0.0	0.0
2		125.2	0.0	96.7	0.0	0.0	0.0	0.0	0.0	0.0	0.0	0.0
3		143.9	0.0	0.0	97.4	0.0	0.0	0.0	0.0	0.0	0.0	0.0
FEM MODE	4	173.8	0.0	0.0	0.0	96.1	11.0	0.0	0.0	0.0	0.0	0.0
	5	175.2	0.0	0.0	0.0	11.3	96.1	0.0	0.0	0.0	0.0	0.0
	6	189.1	0.0	0.0	0.0	0.0	96.3	0.0	0.0	0.0	0.0	0.0
	7	198.5	0.0	0.0	0.0	0.0	0.0	96.0	0.0	0.0	0.0	0.0
	8	212.2	0.0	0.0	0.0	0.0	0.0	0.0	93.2	0.0	0.0	0.0
	9	224.8	0.0	0.0	0.0	0.0	0.0	0.0	0.0	95.4	0.0	0.0
	10	290.4	0.0	0.0	0.0	0.0	0.0	0.0	0.0	0.0	67.7	30.1
	11	311.4	0.0	0.0	0.0	0.0	0.0	0.0	0.0	0.0	30.4	54.7

CIR Lower Structure Assembly Cross Orthogonality Graph FEM vs TAM



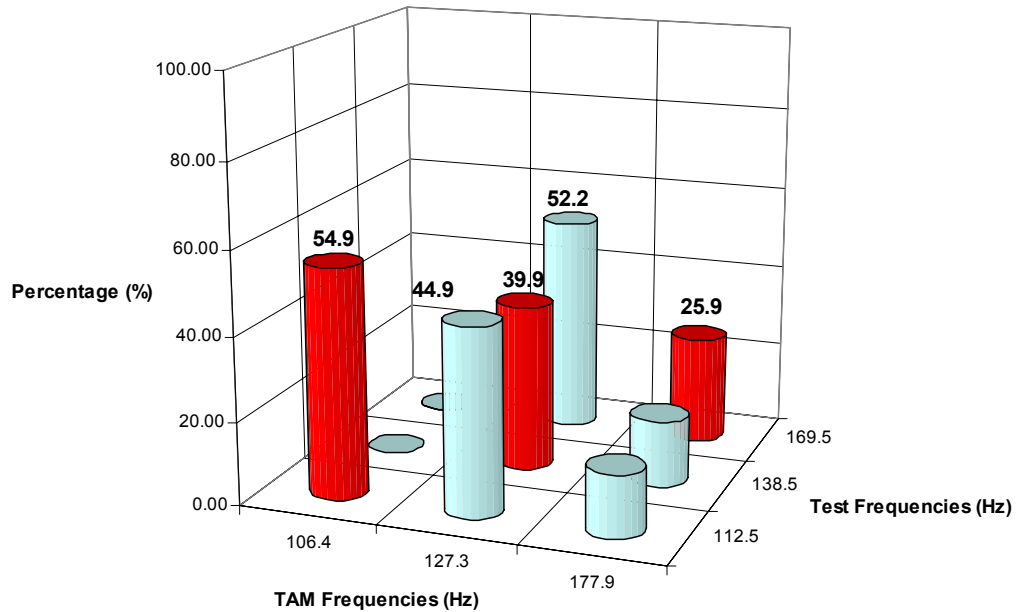
Comparison of CIR Lower Structure TAM with TEST

MODE SHAPE	TAM	TEST	XORTHO	FREQ
DESCRIPTION	FREQ (Hz)	FREQ (Hz)	%	DIFF (%)
Translation of the Lower Structure in the X-Axis	106.4	112.5	54.9	5.4
Translation of the EPCU in the Z-Axis	127.3	138.5	39.9	8.1
Translation of the Lower Structure in the Y-Axis	177.9	169.5	29.9	5.0

CIR Lower Structure Assembly Cross Orthogonality TAM vs TEST

		TEST MODE		
		1	2	4
		Freq (Hz)	112.5	138.5
TAM	1	106.4	54.9	44.9
MODE	2	127.3	0.0	39.9
	5	177.9	0.3	52.2
				25.9

CIR Lower Structure Assembly Cross Orthogonality Graph TAM vs TEST

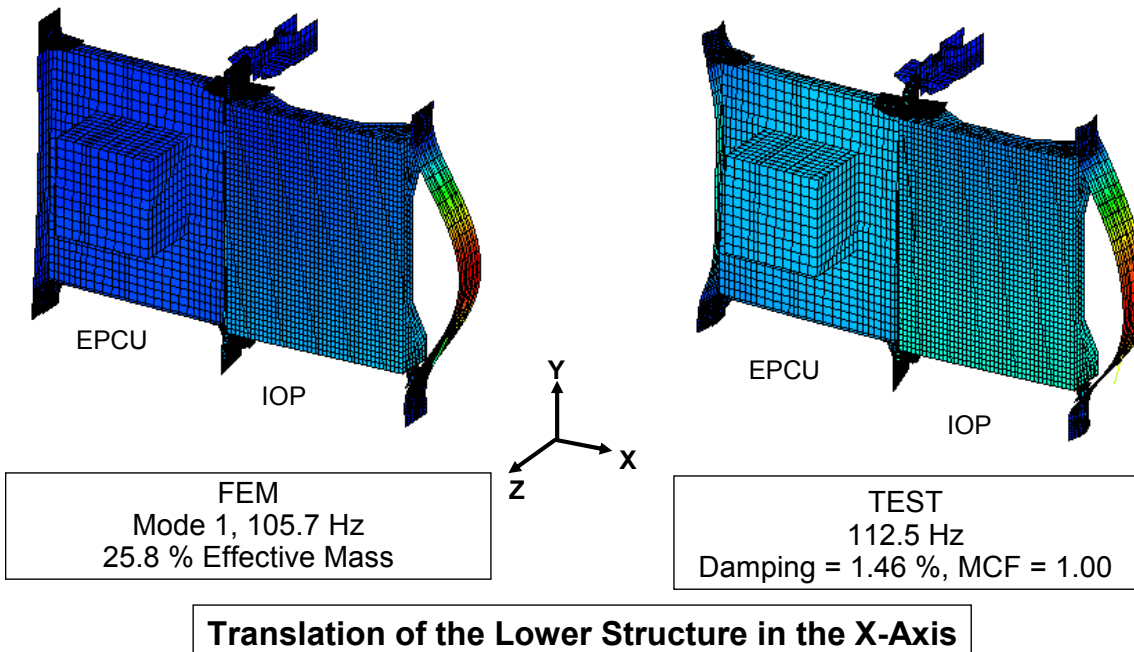


Comparison of CIR Lower Structure FEM with TEST

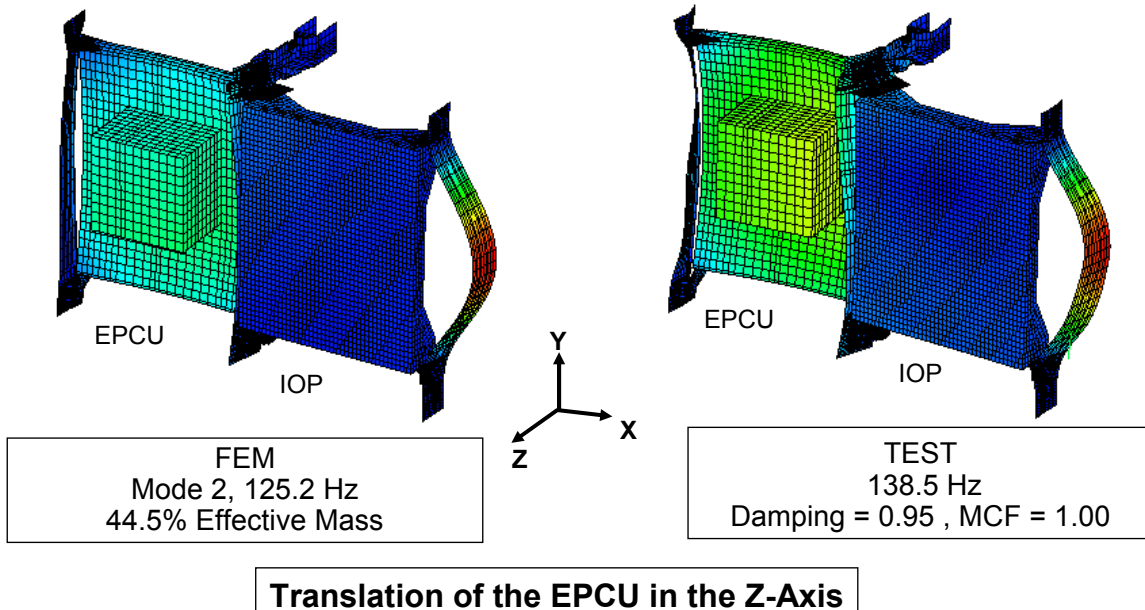
MODE SHAPE	FEM	TEST	FREQ
DESCRIPTION	FREQ (Hz)	FREQ (Hz)	DIFF (%)
Translation of the Lower Structure in the X-Axis	105.7	112.5	6.1
Translation of the EPCU in the Z-Axis	125.2	138.5	9.6
Translation of the Lower Structure in the Y-Axis	175.2	169.5	3.3

Comparison of CIR Lower Structure Assembly FEM with Test

**Mode Shapes - X Axis
Cross-Orthogonality 54.9%**



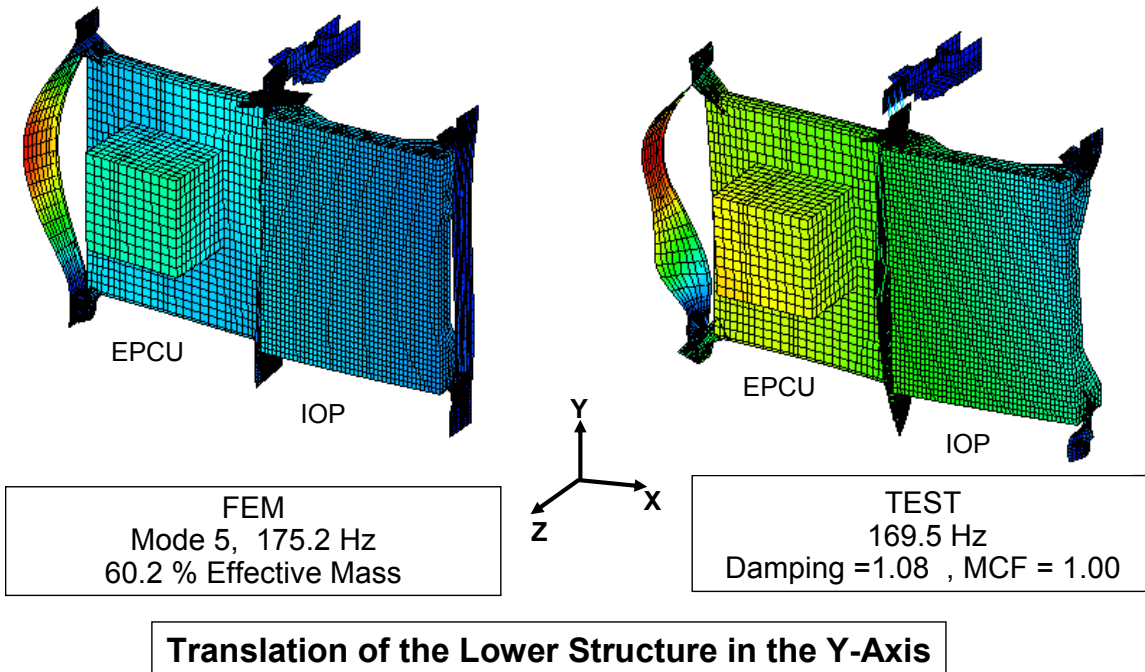
**Comparison of CIR Lower Structure Assembly
FEM with Test
Mode Shapes - Z Axis
Cross-Orthogonality 39.9%**



Comparison of CIR Lower Structure Assembly FEM with Test

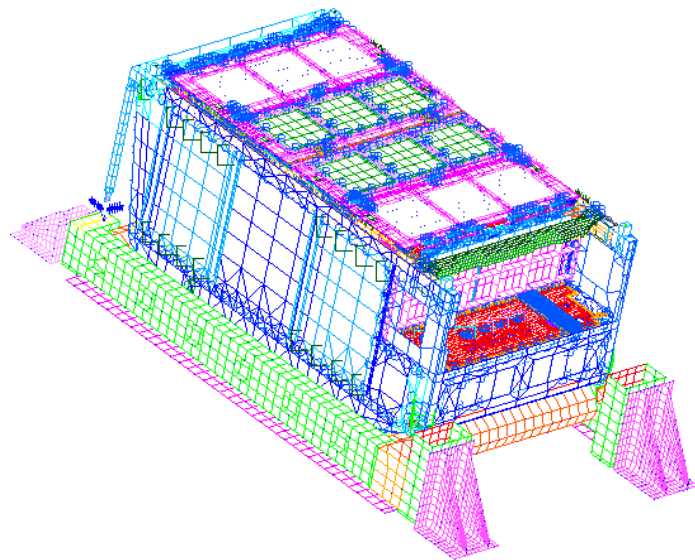
Mode Shapes - Y Axis

Cross-Orthogonality 25.9%



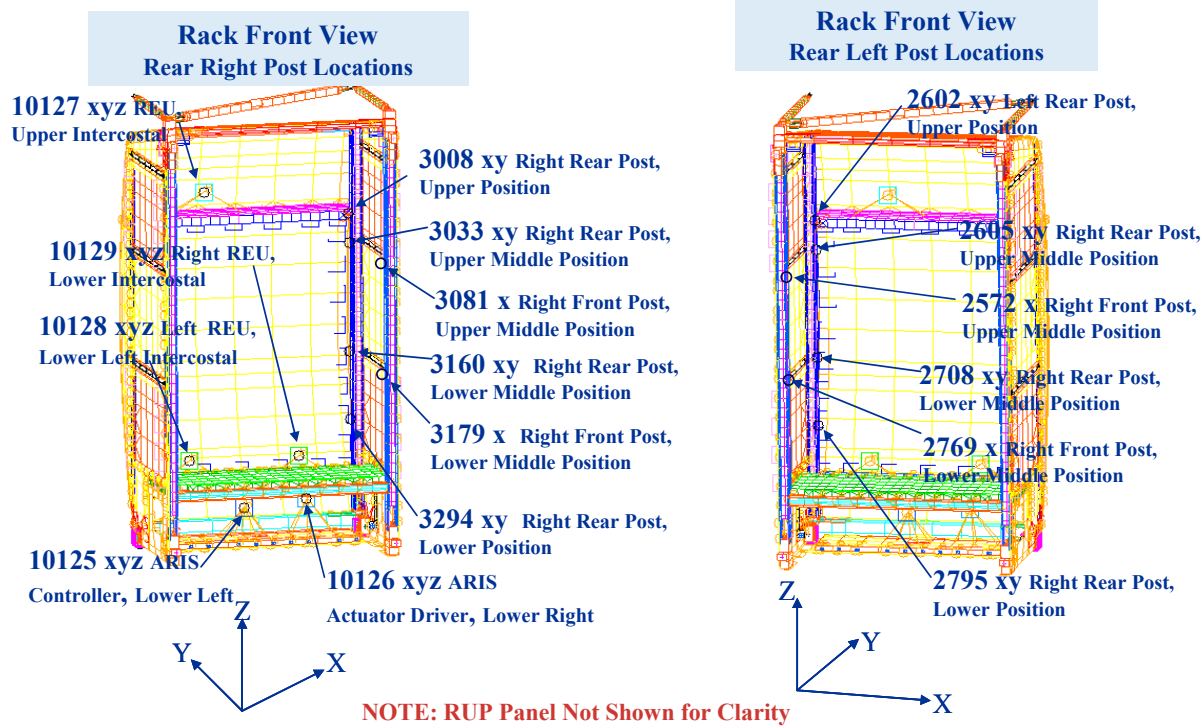
Appendix E

FIR Rack Modal Instrumentation Plan



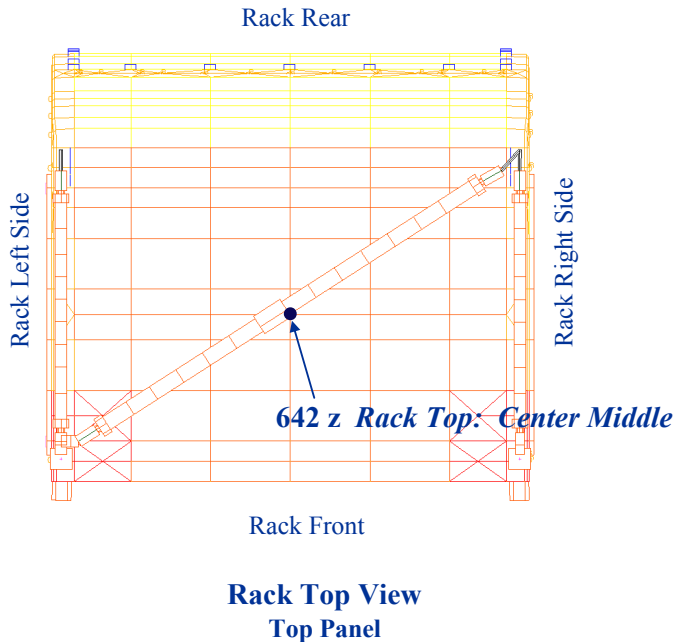
FIR Modal Rack Instrumentation Plan

ISPR (13 locations, 31 accels)



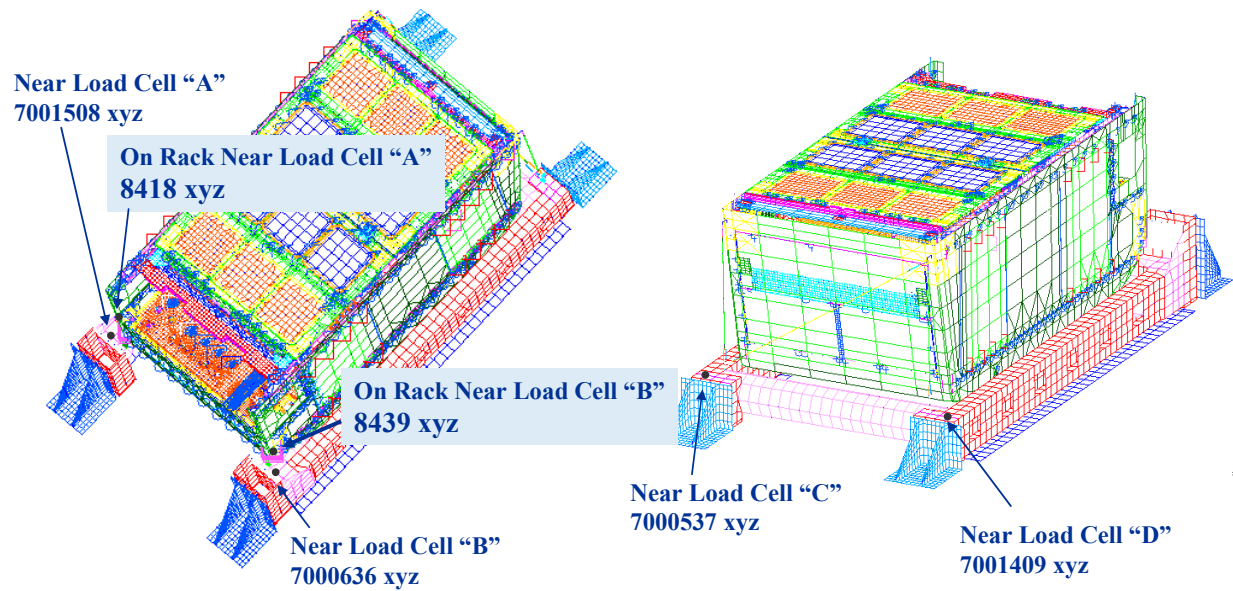
FIR Modal Rack Instrumentation Plan

ISPR (1 locations, 1 accel)



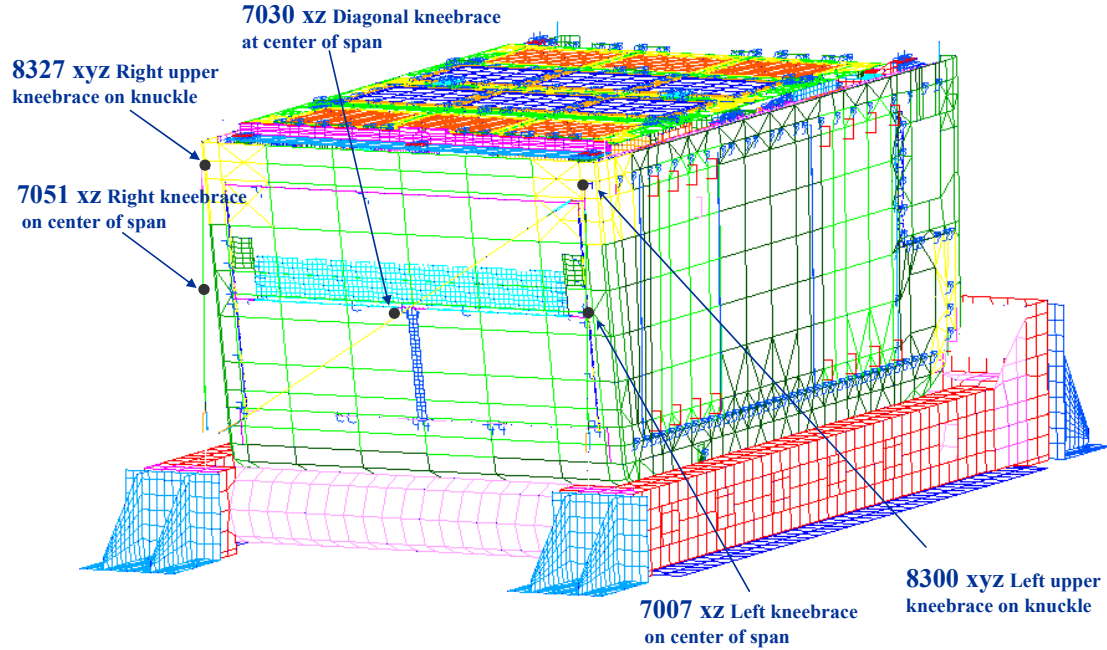
FIR Modal Rack Instrumentation Plan

Blue Boy Control Accelerometers (6 locations, 24 accels)



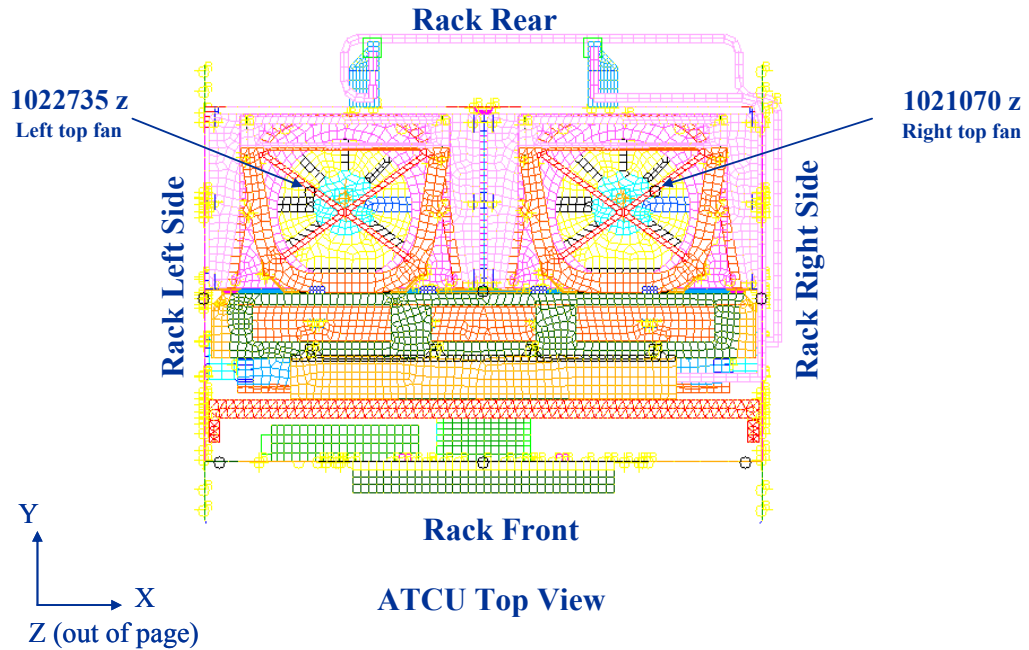
FIR Modal Rack Instrumentation Plan

Strut (5 locations, 12 accels)

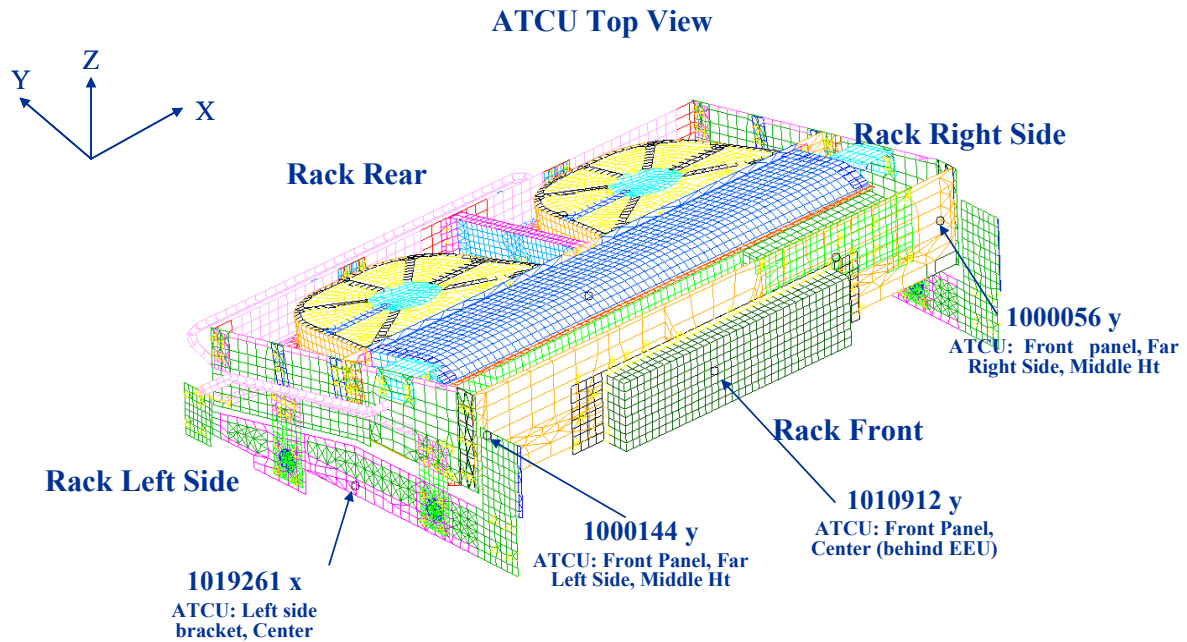


FIR Modal Rack Instrumentation Plan

ATCU (2 locations, 2 accels)

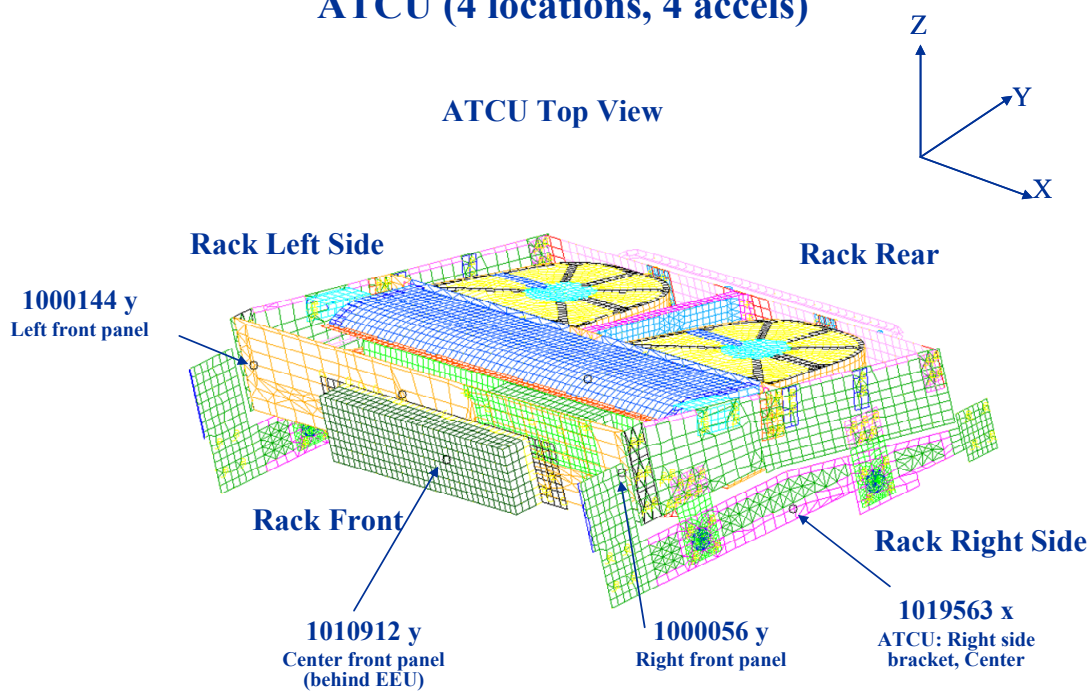


FIR Modal Rack Instrumentation Plan ATCU (4 locations, 4 accels)



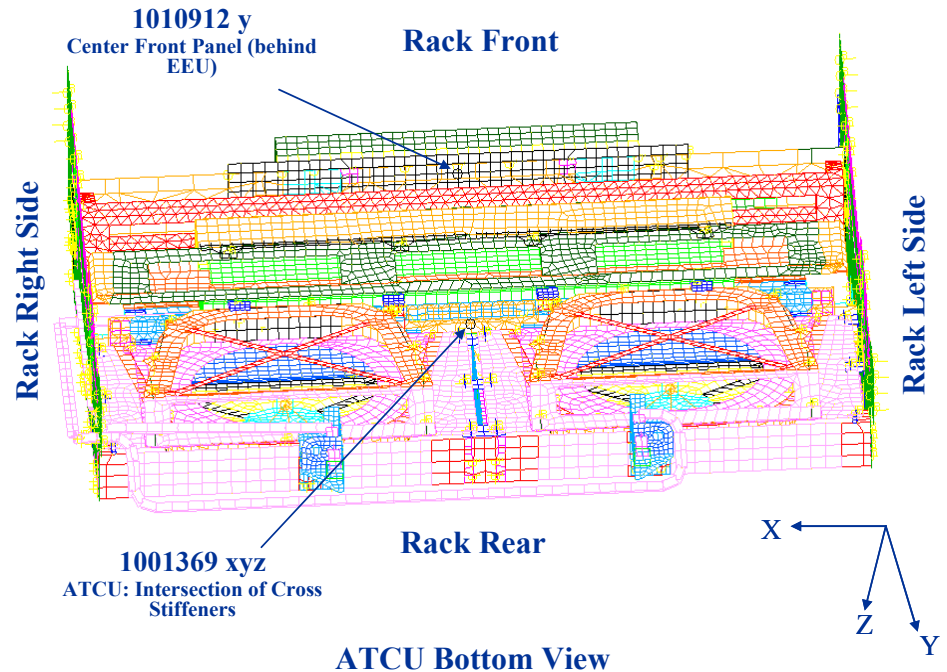
FIR Modal Rack Instrumentation Plan

ATCU (4 locations, 4 accels)



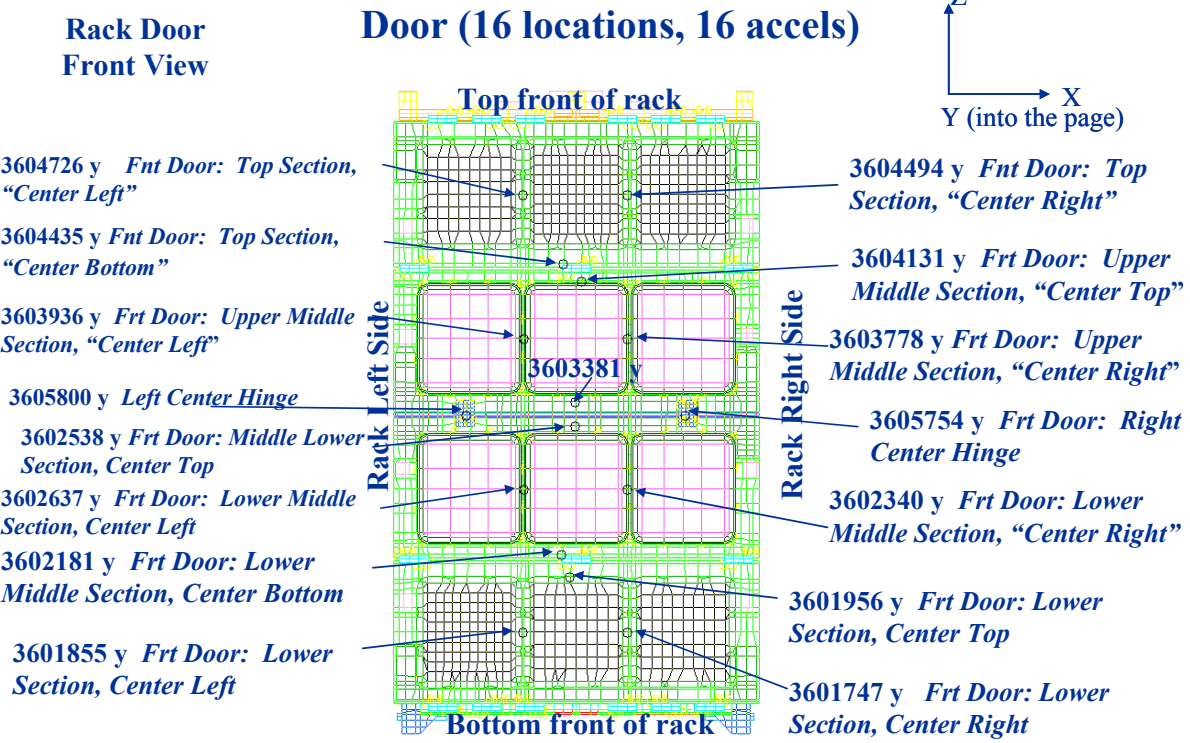
FIR Modal Rack Instrumentation Plan

ATCU (2 locations, 4 accels)



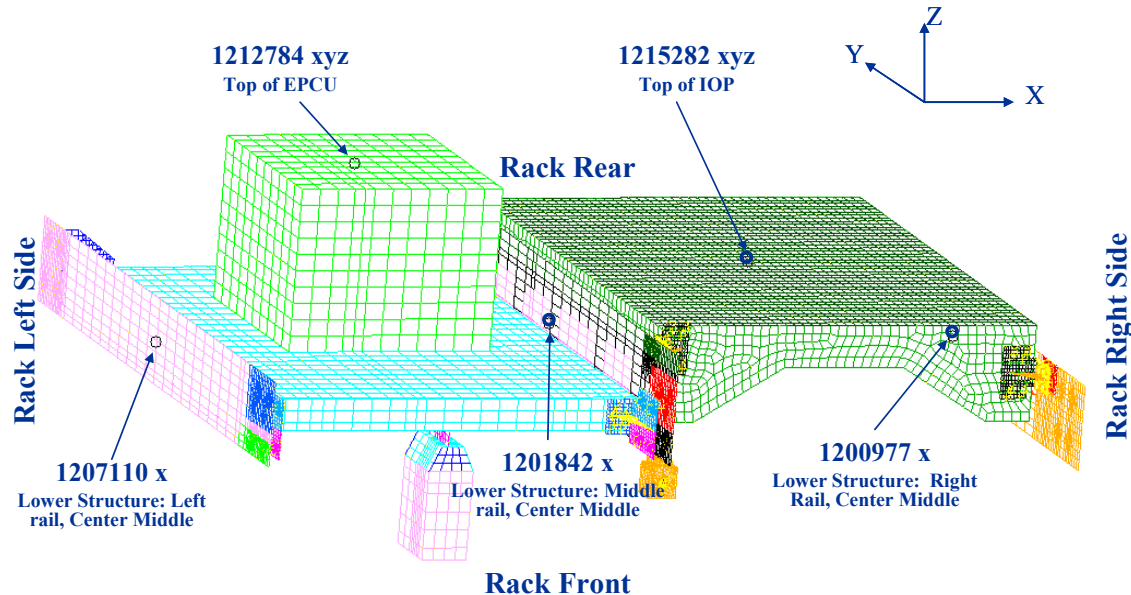
FIR Modal Rack Instrumentation Plan

Door (16 locations, 16 accels)



FIR Modal Rack Instrumentation Plan

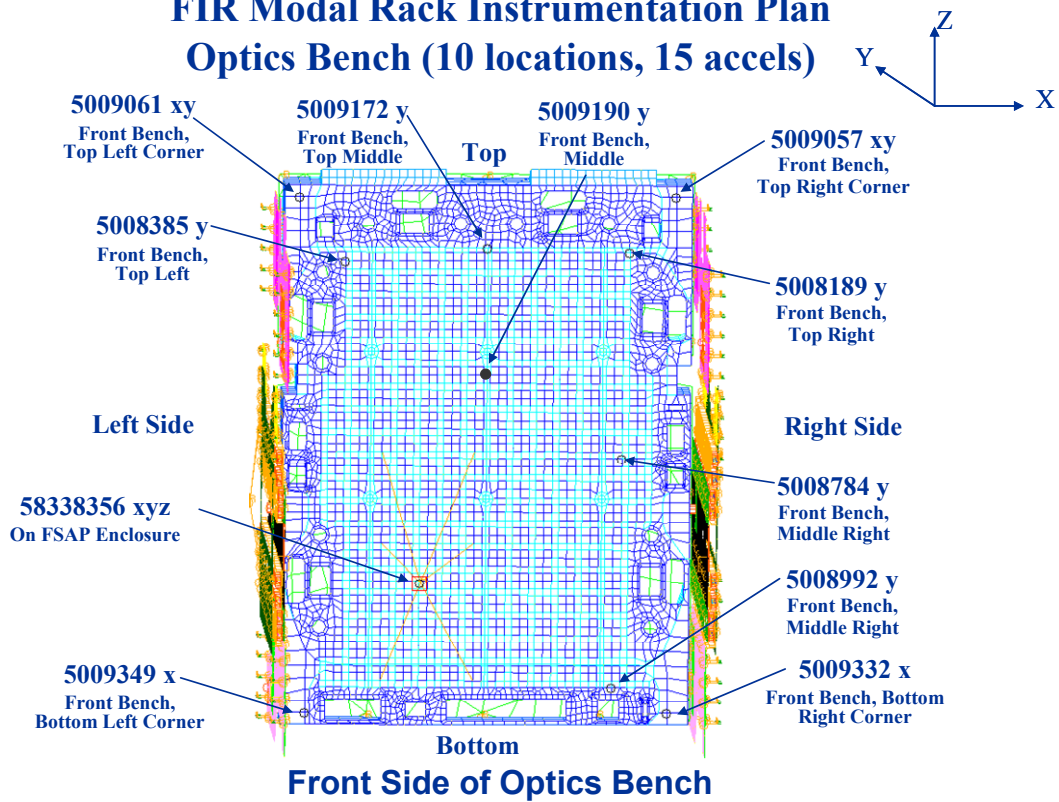
Lower Structure Assembly (5 locations, 9 accels)



Front Perspective View of Lower Structure Assembly

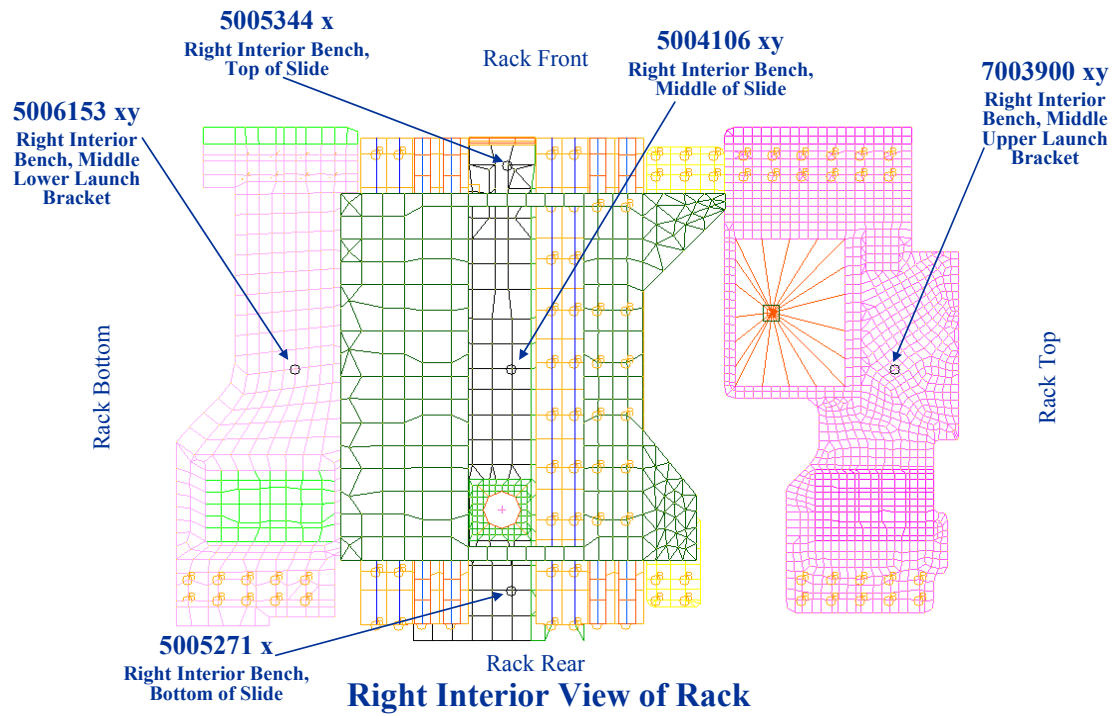
FIR Modal Rack Instrumentation Plan

Optics Bench (10 locations, 15 accels)



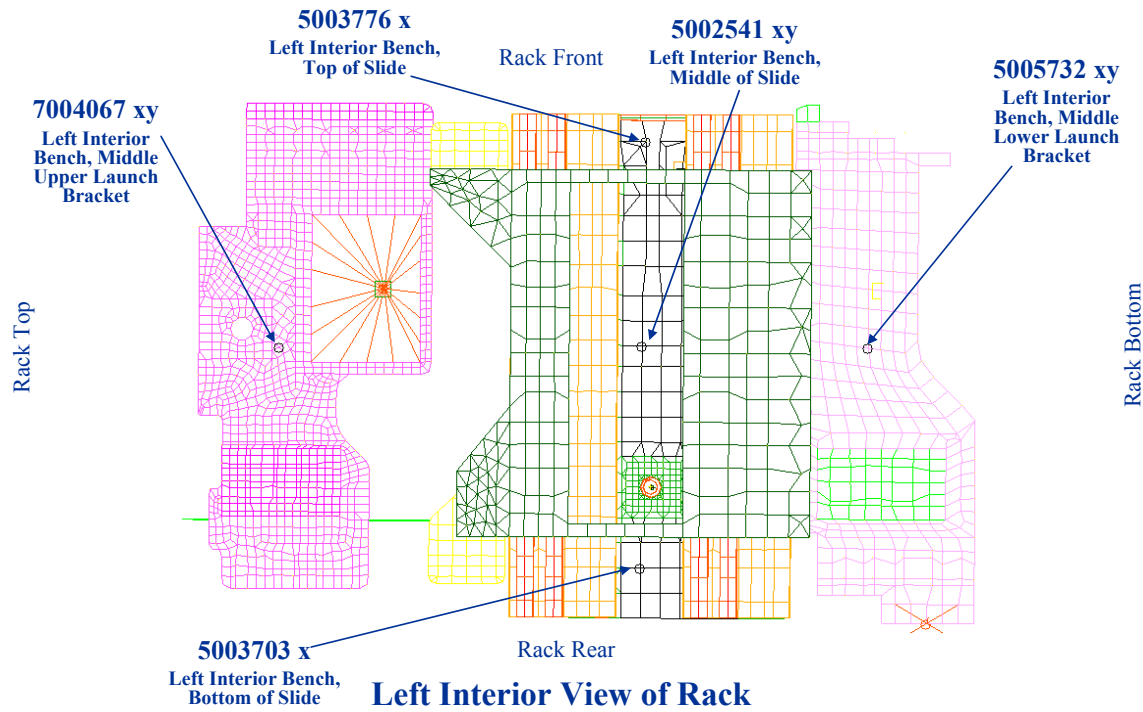
FIR Modal Rack Instrumentation Plan

Slide and Launch Brackets (5 locations, 8 accels)



FIR Modal Rack Instrumentation Plan

Slide and Launch Brackets (5 locations, 8 accels)



Appendix F

FIR Rack Correlated Model Comparison of Frequency and Cross-Orthogonality

TABLE F.1 – COMPARISON OF FLIGHT FEM (IN RIGID BOUNDARY CONDITIONS) AND TAM (IN RIGID BOUNDARY CONDITIONS) TARGET MODE FREQUENCY DIFFERENCE AND CROSS-ORTHOGONALITY

Mode		FLIGHT ASET Rigid BC			Delta Freq	Mode Shape Description
	Mode	1	5	6		
TAM Rigid BC	1	27.2	0.966	0	-10.2%	Rack X-axis Translation
	5	46.7	0	-0.948	-2.5%	Rack Y-axis Translation
	6	51.1	0	0	-3.6%	Rack Z-axis Translation

TABLE F.2 – COMPARISON OF TEST FEM (IN RIGID BOUNDARY CONDITIONS) AND TEST FEM (IN FIXTURE) TARGET MODE FREQUENCY DIFFERENCE AND CROSS-ORTHOGONALITY

Mode		Test FEM Rigid BC			Delta Freq	Mode Shape Description
	Mode	1	7	8		
Test FEM w/Fixture	1	26.8	-0.988	0.000	-10.1%	Rack X-axis Translation
	5	41.1	0	0.700	-10.8%	Rack Y-axis Translation
	8	47.9	0	0.403	-5.7%	Rack Z-axis Translation

TABLE F.3 – COMPARISON OF TEST AND TAM TARGET MODE FREQUENCY DIFFERENCE AND CROSS-ORTHOGONALITY

Mode		TAM			Delta Freq	Mode Shape Description
	Mode	1	2	6		
Test FEM w/Fixture	1	27.2	41.0	48.6	-1.5%	Rack X-axis Translation
	5	26.8	-0.963	0	0.2%	Rack Y-axis Translation
	8	41.1	0	0.914	-1.5%	Rack Z-axis Translation

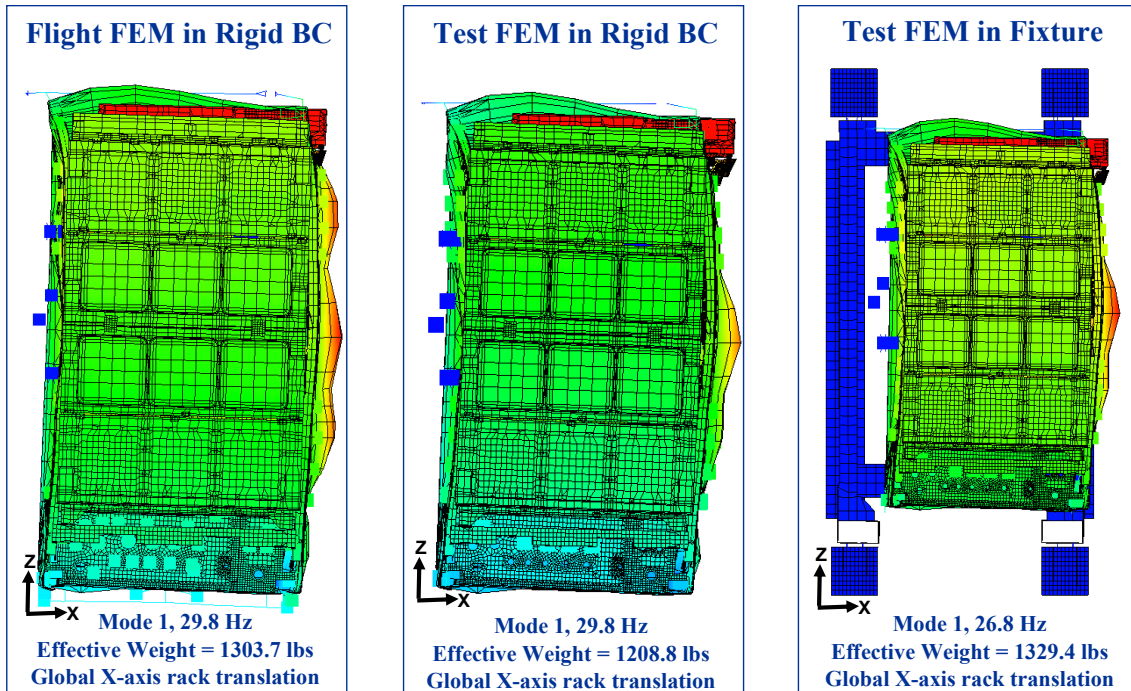


FIGURE F.1 – X-AXIS PRIMARY TARGET MODE

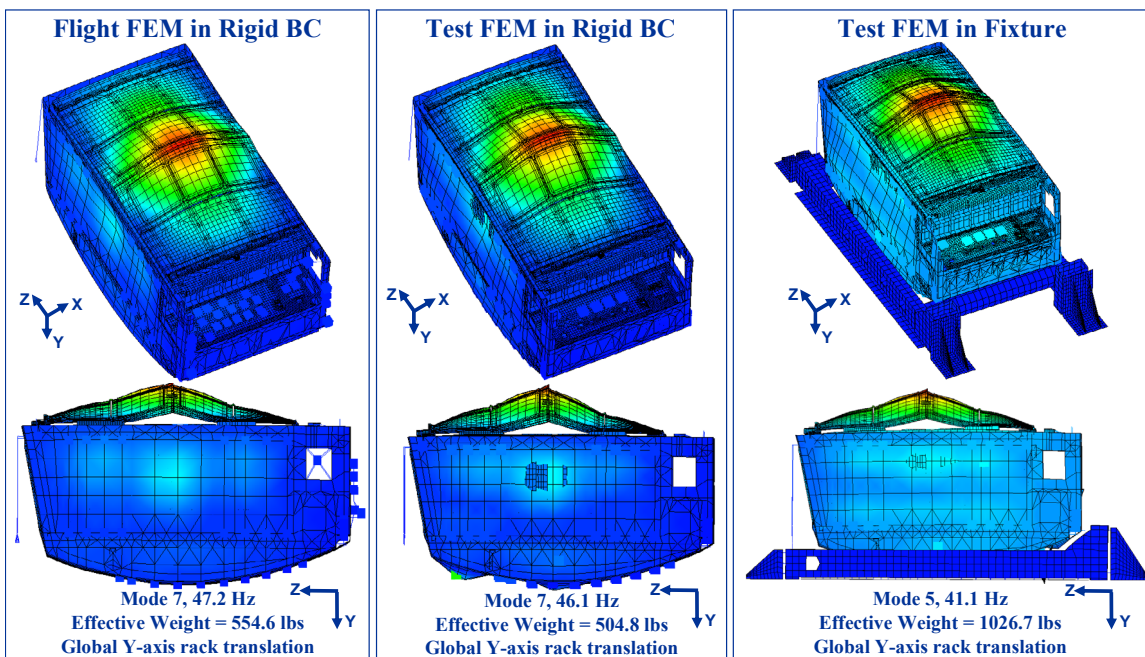


FIGURE F.2 – Y-AXIS PRIMARY TARGET MODE

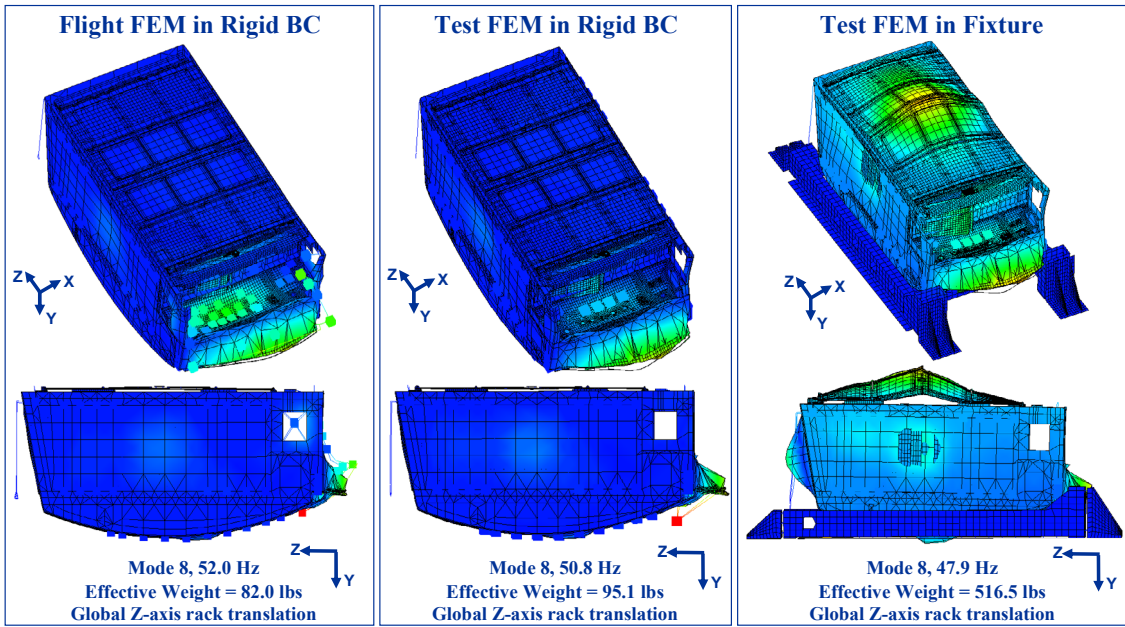


FIGURE F.3 – Z-AXIS SECONDARY TARGET MODE

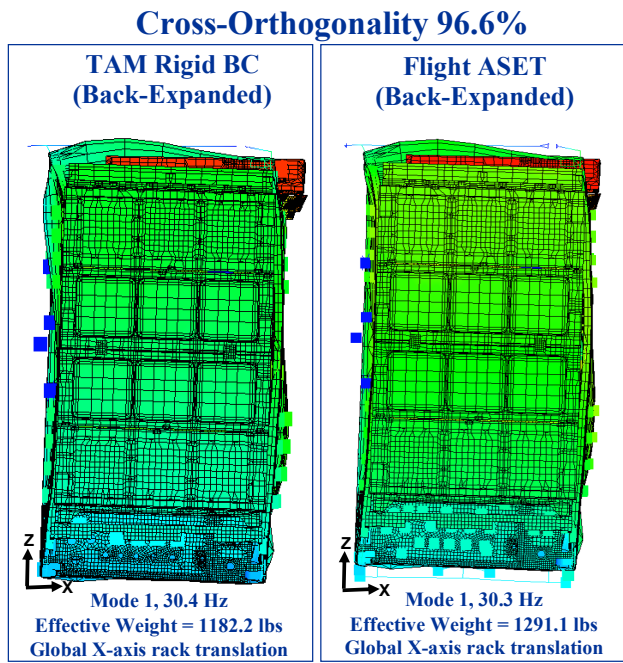


FIGURE F.4 – COMPARISON OF TEST FEM TO TAM FOR THE X-AXIS TARGET MODE

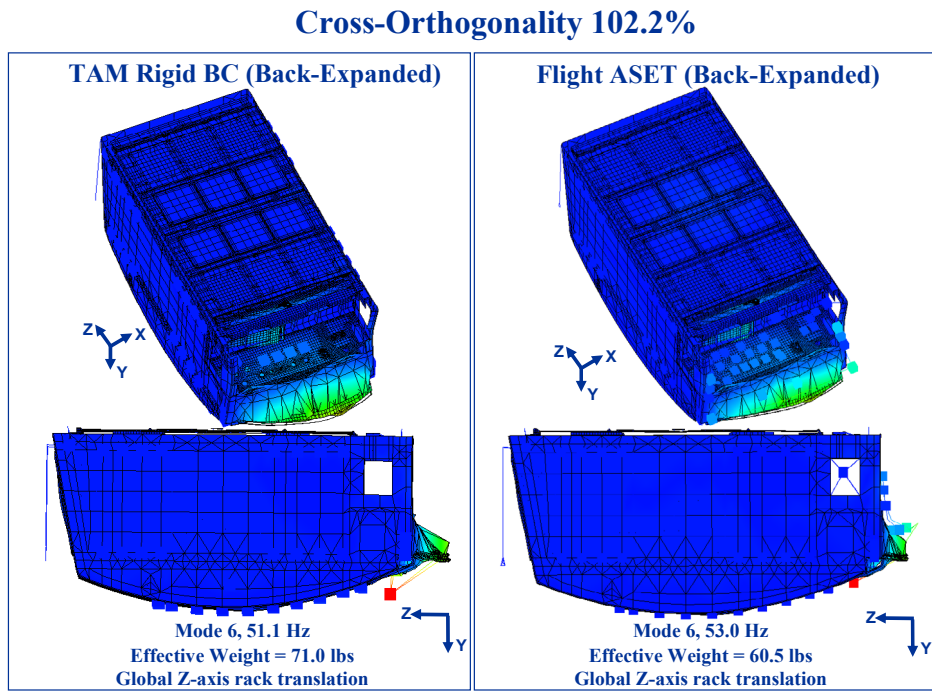


FIGURE F.5 – COMPARISON OF TEST FEM TO TAM FOR THE Y-AXIS TARGET MODE

Cross-Orthogonality 102.2%

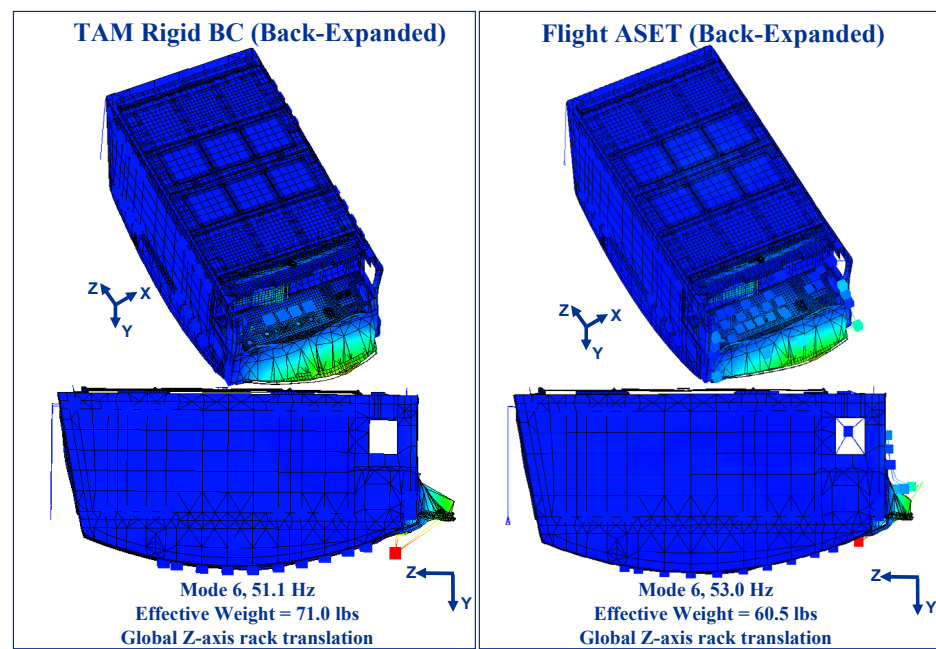


FIGURE F.6 – COMPARISON OF TEST FEM TO TAM FOR THE Z-AXIS TARGET MODE

REPORT DOCUMENTATION PAGE			<i>Form Approved OMB No. 0704-0188</i>
Public reporting burden for this collection of information is estimated to average 1 hour per response, including the time for reviewing instructions, searching existing data sources, gathering and maintaining the data needed, and completing and reviewing the collection of information. Send comments regarding this burden estimate or any other aspect of this collection of information, including suggestions for reducing this burden, to Washington Headquarters Services, Directorate for Information Operations and Reports, 1215 Jefferson Davis Highway, Suite 1204, Arlington, VA 22202-4302, and to the Office of Management and Budget, Paperwork Reduction Project (0704-0188), Washington, DC 20503.			
1. AGENCY USE ONLY (Leave blank)	2. REPORT DATE	3. REPORT TYPE AND DATES COVERED	
	December 2005	Technical Memorandum	
4. TITLE AND SUBTITLE		5. FUNDING NUMBERS	
Fluids and Combustion Facility: Fluids Integrated Rack Modal Model Correlation		WBS 825080.04.02	
6. AUTHOR(S)		8. PERFORMING ORGANIZATION REPORT NUMBER	
Mark E. McNelis, Vicente J. Suarez, Timothy L. Sullivan, Kim D. Otten, and James C. Akers		E-15413	
7. PERFORMING ORGANIZATION NAME(S) AND ADDRESS(ES)		10. SPONSORING/MONITORING AGENCY REPORT NUMBER	
National Aeronautics and Space Administration John H. Glenn Research Center at Lewis Field Cleveland, Ohio 44135-3191		NASA TM—2005-214056 GRC-DEV-FCF-2005-002	
9. SPONSORING/MONITORING AGENCY NAME(S) AND ADDRESS(ES)			
National Aeronautics and Space Administration Washington, DC 20546-0001			
11. SUPPLEMENTARY NOTES			
Mark E. McNelis and Vicente J. Suarez, NASA Glenn Research Center; Timothy L. Sullivan (Retired), Kim D. Otten, and James C. Akers, Analex Corporation, 1100 Apollo Drive, Brook Park, Ohio 44142. Responsible person, Mark E. McNelis, organization code DEV, 216-433-8395.			
12a. DISTRIBUTION/AVAILABILITY STATEMENT		12b. DISTRIBUTION CODE	
Unclassified - Unlimited Subject Category: 39 Available electronically at http://gltrs.grc.nasa.gov This publication is available from the NASA Center for AeroSpace Information, 301-621-0390.			
13. ABSTRACT (Maximum 200 words)			
The Fluids Integrated Rack (FIR) is one of two racks in the Fluids and Combustion Facility on the International Space Station. The FIR is dedicated to the scientific investigation of space system fluids management supporting NASA's Exploration of Space Initiative. The FIR hardware was modal tested and FIR finite element model updated to satisfy the International Space Station model correlation criteria. The final cross-orthogonality results between the correlated model and test mode shapes was greater than 90 percent for all primary target modes.			
14. SUBJECT TERMS			15. NUMBER OF PAGES
Structural dynamics; Modal testing			102
			16. PRICE CODE
17. SECURITY CLASSIFICATION OF REPORT	18. SECURITY CLASSIFICATION OF THIS PAGE	19. SECURITY CLASSIFICATION OF ABSTRACT	20. LIMITATION OF ABSTRACT
Unclassified	Unclassified	Unclassified	

